Congestion Control and Resource Allocation in Emerging Wireless Networks

by

Kefan Xiao

A dissertation submitted to the Graduate Faculty of
Auburn University
in partial fulfillment of the
requirements for the Degree of
Doctor of Philosophy

Auburn, Alabama
May 4, 2018

Keywords: Congestion control, Video streaming, Wireless networks, Deep reinforcement learning

Abstract

With the fast growth of wireless technologies, such as 4G-LTE, cognitive radio networks, and 5G and beyond, data transportation in the wireless environment is dramatically increasing and has taken the dominant role over wired networks. The advantage of wireless networks are obvious: easier deployment, ubiquitous access, etc. However, the traditional transportation layer protocols, such as Transmission Control Protocol (TCP), are well known to perform poorly in wireless environments. This is because packets might be dropped due to transmission errors or broken connection, in addition to congestion caused buffer overflow. Furthermore, the capacity variation of wireless links also affect the TCP performance.

One of the key applications of TCP nowadays, is video streaming. It has now dominated the mobile data traffic, i.e., over 60 percent, in 2016, and is expected to account for over 75 percent of the mobile data in 2021. At the same time, rapidly growing overall mobile traffic (which has increased 18-fold since 2011) and the large number of mobile devices (429 millions were added in 2016) have made it a great challenge for mobile video streaming. The instability nature of wireless link capacity will make the situation even worse. There is a compelling need now to deal with the problem: how to achieve efficiency and robustness for video delivery over emerging wireless networks. This problem should be studied from both the wireless infrastructure and user equipment aspects.

In this thesis, we first conduct research on how to enhance the performance of TCP in wireless environment, specifically, for cognitive radio networks (CRNs). We investigate the problem of robust congestion control in infrastructure based cognitive radio networks (CRN). We develop an active queue management (AQM) algorithm, termed MAQ, which is based on multiple model predictive control (MMPC). The goal is to stabilize the TCP queue at the base station (BS) under disturbances from the time-varying service capacity for secondary users (SU). The proposed MAQ scheme is validated with extensive simulation studies under various types of background traffic and system/network configurations. It outperforms two benchmark schemes with considerable gains in all the scenarios considered.

We then further investigate the dynamics of nowadays complicated networking systems and propose a smart congestion control algorithm based on recent progress of Artificial Intelligence (i.e., Deep reinforcement learning (DRL)). In order to accommodate the wide range of different types of networks and goals, the general framework of congestion control based on DRL is first proposed. With the understanding of the congestion control problem, the states, actions, and reward of the DRL framework are defined. The new progress in deep learning such as convolutional neural network (CNN) and long short term memory (LSTM) are also utilized to deal with the challenges in congestion control problem. Extensive NS3 simulation studies are conducted, which validate the superior of this method over all scenarios.

Finally, the problem of effective and robust delivery of video over orthogonal frequency-division multiplexing access (OFDMA) wireless network is studied. The measurement of real network capacity and request interval time is presented as the motivation for the consideration of the estimation of capacity and request interval. The offline cross-layer optimization is first formulated. Then the online transformation is proposed and proved to be asymptotically converge to the offline solution. After analyzing the structure of the optimization problem, we proposed an primal decomposition (DORA) for this DASH bit rate adaption and OFDM Resource Allocation problem. Further, we introduce the stochastic model predictive control (SMPC) to achieve better Robustness on bit rate adaption and consider the request Interval time at resource allocation (DORA-RI). Simulations are conducted and the efficacy and robustness of the proposed scheme are validated.

Acknowledgments

I would like to express my sincere appreciation to my major advisor Prof. Shiwen Mao and co-advisor Prof. Tugnait. They provided me the continuous guidance of my Ph.D research with their excellent expertise and superior research ideology. Prof. Mao spent precious time and effort to polish my writing of publications and this dissertation. Moreover, with the communication and interaction in the past four and half years, their research methodology, integrity and curiosity to the world enlightened me how to become a researcher, and most importantly, how to be a better human-being.

I also would like to thank my dissertation committee:Prof. Mark Nelms, and Prof. Xiaowen Gong, for their insightful comments and suggestions to my research works. I am also indebted to Prof. Tao Shu for serving as the university reader, who reviewed my work.

My sincere thanks also goes to my friends at Auburn University: Dr. Yi Xu, Dr. Zhifeng He, Dr. Zhefeng Jiang, Dr. Yu Wang, Dr. Xuyu Wang, Dr. Mingjie Feng, Yu Wang, Ningkai Tang, Lingjun Gao, Wei Sun, Blake A. Jacobs and Brett E. Todd, Chao Yang, Ticao Zhang, for the support, friendship, happiness and tears we shared these years.

Last but certainly not the least, I would like to give my deep appreciation to my parents. Their selflessly love and support provide me the courage along the journey.

This work is supported in part by the US NSF under Grants CNS-1320664, CNS-1702957, and CNS-1822055, and through the Wireless Engineering Research and Education Center (WEREC) at Auburn University.

Table of Contents

List of Figures

List of Tables

List of Abbreviations

Auburn	Auburn University
LoA	List of Abbreviations

Chapter 1

Introduction

The boom of wireless technologies has driven the prosper of mobile data transmission and applications. The mobile data has grown 16 folds in the last five years in which the OFDMA based 4G-LTE traffic accounts for over 60 percent [1]. In the meantime, the mobile video traffic has experienced a tremendous increasing as well. It has now dominated the mobile data traffic for over 60 percent in 2016, and is expected to account for over 75 percent in 2021. However, these dramatic increasings over the mobile usage bring unprecedented challenges to current wireless networking protocols and applications.

First, the widely adopted mobile applications such as video streaming are in constant demand of wireless capacity. And the demand is predicted to increase drastically in the near future. Cognitive radio networking (CRN) is a promising solution for more capacity by exploiting underutilized licensed spectrum [2, 3, 4]. In CRNs, licensed users (or, Primary User (PU)) are the main users for specific spectrum. When they are silence, they share spectrum with CRN users (or, Secondary User (SU)). With the dynamic spectrum access (DSA) approach, SUs detect and access unused licensed channels, where the tension between PU protection and SU capacity gain should be carefully balanced [5, 6]. In particular, the SUs have a lower priority for channel access and their service capacity usually varies over time as affected by the PU transmission behavior. Although CRN has been well-studied in the past decade, the mainstream research effort has been focused on spectrum sensing, access, leasing, and policy related aspects. The upper layer, such as transportation layer, in the networking of CRN, has not received much attention. Some important network-level problems, such as TCP congestion control, have not been well studied. Since most network applications (e.g., video streaming) are based on TCP, supporting TCP in CRNs is critical for enabling such applications in CRNs, which is also crucial for the success of CRNs.

The Transportation Control Protocol (TCP) provides applications with an end-to-end and connection-oriented packet transport mechanism that ensures the reliable and ordered delivery of data. It is an important protocol in transport layer based on which many applications are built. The HyperText Transfer Protocol (HTTP) for the web and the popular video streaming protocol, Dynamic streaming over HTTP (DASH), are all built upon TCP. On the other hand, TCP still has poor performance in wireless environments. Wireless links generally have larger bit error rate (BER) than their wired counterparts. Also, the disconnection due to handoffs, obstacles and out-of-coverage is common in wireless networks. It would cause considerable packet drops. The current TCP lacks the ability to differentiate the packet drops due to congestion from those due to broken connection or transmission errors. In addition, the constant variation of capacity of wireless connection would hurt the efficiency of the TCP algorithms. How to design a TCP variant that works efficiently in different types of emerging wireless networks is still an open problem.

In this dissertation, we aim to further study the applications such as video streaming that based on TCP in the wireless environment. The problem is how to achieve efficiency and robustness for video delivery over emerging wireless networks. It is a problem that should be studied from the perspectives of both wireless infrastructure and user control algorithms due to the popularity of video streaming.

Video streaming has drawn great research attention for decades. The early works are mainly based on User Datagram Protocol (UDP) which can provide timely transmission compared with TCP that is designed for strengthening reliability over timeliness. However, the deployment of UDP based algorithms is challenging due to the incompatibility with firewalls and other type of middleboxes. On the other hand, data flows of TCP are supported by most middleboxes for its reliability and security. The congestion control algorithms facilitate the timeliness of transmission as well. Therefore, the Hypertext Transfer Protocol (HTTP) based on video streaming is now the mainstream technique. In particular, Dynamic video streaming over HTTP (DASH), which can adapt to variation of network conditions, is proposed as a promising technique to enhance the user's quality of experince (QoE). YouTube and Netflix, which are all based on DASH, have accounted for more than half of the total Internet traffic in North America in 2016 [7].

Among different generations of mobile transmission techniques, the 3GPP-Long Term Evolution (LTE) and Wi-Fi (802.11 standard) are the most popular. The Orthogonal frequency-division multiplexing (OFDM) is the common method of both standards that encode digital data into different subcarriers of the broadband channel. OFDM is expected to continue serve the next generation wireless networks for its ability on tackling narrowband interference and frequency-selective fading, etc. with a low complexity. The broadband is divided into several subcarriers, which are modulated with conventional modulation schemes. OFDM also introduces flexibility by dynamically assigning subcarriers, time, and power to each user in order to accommodate their customized QoS requirements.

With the development of different wireless technology and networking algorithms, the complexity of the entire system is increasing. Now, it is hard to use the simplified mathematical models to capture the dynamics of the system and then build the corresponding solutions. With the recent progress of AI technologies, the computer can now achieve super-human performance in video games [8], and even beats top human players in Go [9]. To deal with this problem, we proposed a smart congestion control framework that is based on deep reinforcement learning (DRL) [8]. The framework is focused on the general congestion control problem in different kinds of networks and provides the flexibility to accommodate different design goals.

Motivated by these interesting problems, we investigate the problems of robust congestion control in CRNs, in general wireless networks, and efficient video streaming in the wireless environment. The contributions of this thesis are summarized as follows:

1. We exploit active queue management (AQM) to deal with the CRN congestion control problem. AQM is a class of packet dropping/marking mechanisms implemented at the router queue to support end-to-end congestion control. We develop a robust AQM mechanism to stabilize the queue length at the CRN BS, which can not only yield a relative stable queueing delay, but also absorb the disturbances caused by busty background

traffic or capacity variation. The proposed scheme, termed MAQ, is based on multiple model predictive control (MMPC) that integrates the estimation and prediction of multiple models with different weights, which can significantly enhance the robustness of the controller to reject disturbances from the environment [10]. We evaluate the performance of the proposed scheme with extensive NS2 simulations, such as under responsive and non-responsive background traffic, varying number of TCP connections, various propagation delays, and various reference queue lengths. The simulation study shows that MAQ can effectively stabilize the TCP buffer in all the scenarios we simulated, and outperforms two benchmark schemes with considerable gains.

2. The congestion control problem is further studied in a general network setting. As wired/wireless networks become more and more complex, the fundamental assumptions made by many existing TCP variants may not hold true anymore. In this dissertation, we develop a model free congestion control algorithm based on deep reinforcement learning (DRL), which has a high potential in dealing with the complex and varying network environment. We present *TCP-Drinc*, acronym for *D*eep *R*e*I*nforcement lear*N*ing based *C*ongestion Control, which learns from past experience and a set of measured features to decide the next action on adjusting the congestion window size. We present the TCP-Drinc design and validate its performance with extensive NS3 simulations and comparison with five benchmark schemes.

3. We investigate the problem of effective and robust delivery of DASH videos over an orthogonal frequency-division multiplexing access (OFDMA) network. Motivated by a measurement study, we propose to explore the request interval and robust rate prediction for DASH over OFDMA. We first formulate an offline cross-layer optimization problem based on a novel QoE model. Then the online reformulation is derived and proved to be asymptotically optimal. After analyzing the structure of the online problem, we propose a decomposition approach to obtain a UE rate adaptation problem and a BS resource allocation problem. We introduce stochastic model predictive control (SMPC) to achieve high robustness on video rate adaption and consider the request interval for more efficient

resource allocation. The efficacy of the proposed DORA-RI scheme is validated with simulations.

Chapter 2

MAQ: A Multiple Model Predictive Congestion Control Scheme for Cognitive Radio Networks

In this chapter, we investigate the problem of robust congestion control in infrastructure based cognitive radio networks (CRN). We develop an active queue management (AQM) algorithm, termed MAQ, which is based on multiple model predictive control (MMPC). The goal is to stabilize the TCP queue at the base station (BS) under disturbances from the time-varying service capacity for secondary users (SU). The proposed MAQ scheme is validated with extensive simulation studies under various types of background traffic and system/network configurations. It outperforms two benchmark schemes with considerable gains in all the scenarios considered.

2.1 Introduction

The wide availability of mobile devices and services has triggered unprecedented demand for wireless capacity, and the demand is predicted to increase drastically in the near future. In addition, the emerging wireless sensing techniques [11, 12, 13, 14, 15, 16, 17, 18, 19] requres. Cognitive radio network (CRN) is a promising solution for more capacity by exploiting underutilized licensed spectrum [2]. In CRNs, licensed users (or, Primary User (PU)) share spectrum with CRN users (or, Secondary User (SU)). With the dynamic spectrum access (DSA) approach, SUs detect and access unused licensed channels, where the tension between PU protection and SU capacity gain should be carefully balanced [5, 20, 21, 22, 23]. In particular, the SUs have a lower priority for channel access and their service capacity usually varies over time as affected by the PU transmission behavior.

Although CRN has been well-studied in the past decade, the mainstream research effort has been focused on spectrum sensing, access, leasing, and policy related aspects. Some other important network-level problems, such as congestion control, have not been well studied. Since most network applications (e.g., even video streaming from many commercial video-sharing websites) are based on TCP, supporting TCP in CRNs is critical for enabling such applications in CRNs, which is also crucial for the success of CRNs. However, this problem has only been investigated in a few prior works [24, 25, 26]. In [24, 25, 27, 28], the TCP congestion control mechanism is modified for the CRN environment, while in [26], a partially observable Markov decision process (POMDP) based approach is proposed to maximize the SU throughput by jointly adjusting spectrum sensing, access, and the physical-layer modulation and coding scheme. Although interesting results are derived, the existing schemes are either offline [26] or based on heuristics [24, 25].

Motivated by these interesting works, we investigate the problem of robust congestion control in CRNs. It is well-known that TCP does not work well in wireless networks, largely due to the fact that it does not distinguish between packet loss due to congestion or transmission errors. Many effective solutions have been proposed in the literature, such as split-TCP or making the wireless link more reliable [29]. In CRNs, the additional challenge is the time-varying capacity for SU TCP sessions, which may even be zero during sensing periods when all the SUs stop transmission to sense the channels. During the transmission period, the capacity that is available for SU TCP sessions also varies over time due to PU transmissions, and the variation could be large and occur at various timescales from session to packet levels. These pose considerable disturbance to the TCP feedback control mechanism. There is a critical need for robust congestion control mechanisms in such a highly dynamic network environment.

In this chapter, we consider an infrastructure-based CRN, where multiple SUs maintain TCP connections with various TCP servers in the Internet. The TCP sessions share a buffer at the CRN base station (BS) and the last hop, and bottleneck, of the TCP connections is the downlink of the CRN. The BS advertises a zero-size receive window on behalf of the SUs to inform the TCP senders of the sensing period and to freeze the TCP servers during the sensing period [24]. Since the classic additive-increase-multiple-decrease (AIMD) algorithm incorporated in TCP does not deal well with the frozen period and capacity variations, we aim to develop a new congestion control mechanism that is robust to such disturbances.

Specifically, we exploit active queue management (AQM) to deal with the CRN congestion control problem. AQM is a class of packet dropping/marking mechanisms implemented at the router queue to support end-to-end congestion control. We develop a robust AQM mechanism to stabilize the queue length at the CRN BS, which can not only yield a relative stable queueing delay, but also absorb the disturbances caused by busty background traffic or capacity variation. The proposed scheme, termed MAQ, is based on multiple model predictive control (MMPC) that integrates the estimation and prediction of multiple models with different weights, which can significantly enhance the robustness of the controller to reject disturbances from the environment [10]. We evaluate the performance of the proposed scheme with extensive NS2 simulations, such as under responsive and non-responsive background traffic, varying number of TCP connections, various propagation delays, and various reference queue lengths. The simulation study shows that MAQ can effectively stabilize the TCP buffer in all the scenarios we simulated, and outperforms two benchmark schemes with considerable gains.

The remainder of this chapter is organized as follows. We present the system model and problem formulation in Section 2.2. We discuss the MAQ design in Section 2.3 and validate its performance in Section 4.5. Related work is reviewed in Section 4.6 and Section 4.7 concludes this chapter.

2.2 System Model and Problem Formulation

2.2.1 Network Model

We consider a primary network with M licensed channels. The primary users transmit on the licensed channels from time to time, and the availability of each channel (i.e., transmission opportunities for SUs) follows a certain on-off process [5]. There is a CRN collocated with the primary network, consisting of a CRN base station (BS) and N active SUs. The CRN BS and SUs cooperatively sense the licensed channels to identify transmission opportunities for SUs. Since spectrum sensing is a well-studied problem, we assume that an effective spectrum

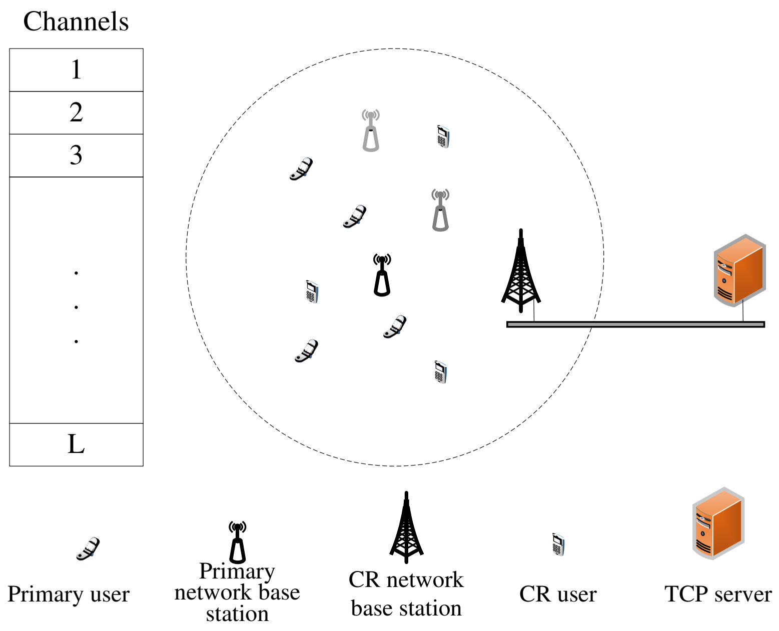

Figure 2.1: Network model of CR network

sensing scheme is in force and the sensing results are accurate with a high probability. The infrastructure-based CRN network model is illustrated in Fig. 2.1.

In the CRN, each active SU maintains a TCP connection with a TCP server in the Internet cloud (e.g., downloading a large file). We assume the channel bonding/aggregation technique is used, such that the BS and SUs can transmit and receive on multiple assigned channels simultaneously to make use of all the available spectrum [30]. Let the aggregated usable capacity be $C(t)$, which is time-varying as availability of the licensed channels vary over time. All the TCP connections share the downlink capacity of the BS with time division multiplexing (TDM), assuming negligible uplink feedback. Due to the mismatch of capacity between wired and wireless links, it is reasonable to assume that the CRN BS is the bottleneck of the TCP connections.

We aim to develop a congestion control mechanism to stabilize the bottleneck queue at the CRN BS for the TCP connections under time-varying capacity $C(t)$. In addition to the time-varying capacity $C(t)$, the sensing period of the CRN also poses a challenge for congestion control, during which $C(t) = 0$ since the BS and all the SUs stop transmission to sense the licensed channels. We follow the approach in [24] to freeze the TCP senders during the sensing period, assuming that the TCP servers obtain the sensing schedule of the CRN during the session setup phase and the zero-size receive window mechanism is used [24]. Thus the sensing period only has a negligible impact on the congestion control except for a fixed small cost to the overall throughput.

2.2.2 Fluid Flow Model for TCP Sessions

Ignoring the sensing period of the CRN, during the transmission period, the dynamics of the multiple-TCP system can be modeled by a fluid flow model [31]. Different from many existing AQM algorithms, we adopt the *drop-from-front* mechanism [32], i.e., when there is incipient congestion, the head-of-line (HOL) packet in the bottleneck queue will be dropped (instead of the packet at the tail). This way, the TCP server can infer congestion more quickly (i.e., without the queueing delay) and react faster to congestion as well as the changing capacity in the CRN.

The dynamics of the TCP connections sharing a queue at the CRN BS can be derived by slightly modifying the model in [31] as follows.

$$\dot{W}(t) = \frac{1}{R(t)} - \beta W(t)\frac{W(t-T_p)}{R(t-T_p)}p(t-T_p) \tag{2.1}$$

$$\dot{q}(t) = \begin{cases} N(t)\frac{W(t)}{R(t)} - C(t), & q > 0 \\ \max\left\{0, N(t)\frac{W(t)}{R(t)} - C(t)\right\}, & q = 0, \end{cases} \tag{2.2}$$

where $\dot{f}(t)$ donates the time-derivative of a function $f(t)$. The other functions are defined as follows.

- $q(t)$: the queue length at the CRN BS and $q(t) \in [0, B]$, where B is the maximum buffer size.
- $C(t)$: the downlink capacity of the CRN BS in packets/s.
- $R(t)$: the round trip time (RTT) of a TCP connection.
- $p(t)$: the packet drop probability of AQM.
- T_p: the propagation delay of a TCP connection, i.e., RTT minus queueing delay at the CRN BS.

- $N(t)$: the number of active TCP connections going through the CRN BS.
- $W(t)$: the congestion window size of the TCP source.
- β: the window multiplicative decrease parameter, which a constant and is usually set to $1/2$ (sometimes as $\ln(2)$) [33].

This model is based on the fluid flow traffic model and is a system of delayed stochastic differential equations. It ignores the TCP time out mechanism to make the problem manageable. Since drop-from-front is adopted, the drop probability p is actually delayed by a propagation delay T_p to take effect at the TCP server.

2.2.3 Linearization and Discretization

Linearization

We first build the model bank for the proposed MMPC scheme by choosing *multiple* operating points (each corresponding to a model) and linearizing the system around them. It's obvious that the more models, the more accurate the representation will be. However, the computational complexity will also be higher. For practical systems, usually three to five models should be sufficient. We choose π different reference capacity values denoted as C_i, $i = 1, 2, \ldots, \pi$, in descending order as follows.

- When $\pi = 3$: $\bar{C}$, $\bar{C} \pm \sigma_C$;
- When $\pi = 5$: $\bar{C}$, $\bar{C} \pm 0.75 \times \sigma_C$, $\bar{C} \pm 1.5 \times \sigma_C$,

where $\bar{C} = \mathrm{E}[C(t)]$ is the average link capacity and σ_C is the standard deviation of $C(t)$, which can be obtained from historical data.

A change in the capacity will cause immediate change of the queue length. The magnitude depends on how quickly the TCP source can react to the changing capacity. Given an expected queuing delay D_q and considering the chosen reference capacities, we choose the corresponding π reference queue lengths as q_i, $i = 1, 2, \ldots, \pi$, in ascending order as follows.

- When $\pi = 3$: $q_1 = \bar{C}D_q$, $q_1 \pm \sigma_C D_q$;

- When $\pi = 5$: $q_1 = \bar{C}D_q$, $q_1 \pm 0.75 \times \sigma_C D_q$, $q_1 \pm 1.5 \times \sigma_C D_q$.

The operating point i of the system, denoted as five-tuples $(W_i, q_i, p_i, C_i, R_i)$, can be solved from the system equations (2.1) and (2.2) by setting $\dot{W} = 0$ and $\dot{q} = 0$, for $i = 1, 2, \ldots, \pi$. Assuming the system is stabilized at operating point i, we have $W(t) = W(t - T_p)$ and $R(t) = R(t - T_p)$. It follows that

$$\beta W_i^2 p_i = 1; \;\; W_i = \frac{R_i C_i}{N}; \;\; R_i = T_p + \frac{q_i}{C_i}. \tag{2.3}$$

Denote the deviations from operating point i as $\delta W_i = W(t) - W_i$, $\delta q_i = q(t) - q_i$, $\delta p_i = p(t) - p_i$, and $\delta C_i = C(t) - C_i$. Further denote model i state as $x_i = [\delta q_i, \delta W_i]^T$ and output as $y_i = \delta q_i$, and define $\delta p_i(t - T_p)$ as $u_i(t - T_p)$. The linearized system around operating point i can be obtained as follows.

$$\dot{x}_i(t) = A_i x_i(t) + B_i u_i(t - T_p) + D_i \delta C_i(t) \tag{2.4}$$

$$y_i(t) = Q_i x_i(t) + v(t). \tag{2.5}$$

Equation (2.4) is the state equation and (2.5) is the output equation, where $v(t)$ accounts for the disturbance from the uncertainty nature of control input $u_i(t - T_p)$. The coefficient matrices are given below. The details are omitted for brevity.

$$A_i = \begin{bmatrix} -\frac{1}{R_i} & \frac{N}{R_i} \\ 0 & -R_i^2 \end{bmatrix}, \quad B_i = \begin{bmatrix} 0 \\ -\frac{\beta R_i C_i^2}{N^2} \end{bmatrix},$$

$$D_i = \begin{bmatrix} -\frac{T_p}{R_i} & 0 \end{bmatrix}^T, \qquad Q_i = \begin{bmatrix} 1 & 0 \end{bmatrix}.$$

Discretization

Since packets arriving and departing in a discrete manner, the entire system can be viewed as sampling from the continuous-time model with a finite sampling rate. Denote the sampling period as T_s, which is a constant and is sufficiently small, such that every propagation delay T_p is an integer multiple of T_s as $T_p = n_0 T_s$.

Let $x[k]$ represent the kth sample $x(kT_s)$. Then the ith linear model (around operating point i) can be discretized as

$$x_i[k+1] = \Phi_i x_i[k] + \Gamma_i u_i[k-n_0] + \Delta_i \delta C_i(k) \tag{2.6}$$

$$y_i[k] = Q_i x_i[k] + v_i[k]. \tag{2.7}$$

The new coefficients Φ_i, Γ_i, and Δ_i are derived with the standard discretization algorithm and are given below.

$$\Phi_i = e^{A_i T_s} = \begin{bmatrix} e^{-\frac{T_s}{R_i}} & \frac{C_i N R_i}{C_i R_i - 2N}\left(e^{-\frac{2NT_s}{R_i^2 C_i}} - e^{-\frac{T_s}{R_i}}\right) \\ 0 & e^{-\frac{2NT_s}{R_i^2 C_i}} \end{bmatrix},$$

$$\Gamma_i = \left(\int_0^{T_s} e^{A_i\tau} d\tau\right) B = \beta \frac{C_i^3 R_i^3}{N} \times \begin{bmatrix} \frac{C_i R_i}{2N(C_i R_i - 2N)} e^{-\frac{2NT_s}{R_i^2 C_i}} - \frac{1}{C_i R_i - 2N} e^{-\frac{T_s}{R_i}} - \frac{1}{2N} \\ \frac{1}{2N^2}\left(e^{-\frac{2NT_s}{R_i^2 C_i}} - 1\right) \end{bmatrix},$$

$$\Delta_i = \left(\int_0^{T_s} e^{A_i\tau} d\tau\right) D_i = \begin{bmatrix} T_p\left(e^{-\frac{T_s}{R_i}} - 1\right) \\ 0 \end{bmatrix}.$$

The above derivation assumes $C_0 R_i - 2N \neq 0$. Otherwise, when $C_0 R_i = 2N$, the coefficients become

$$\Phi_i = \begin{bmatrix} e^{-\frac{T_s}{R_i}} & \frac{NT_s}{R_i}\left(e^{-\frac{T_s}{R_i}}\right) \\ 0 & e^{\frac{T_s}{R_i}} \end{bmatrix}$$

$$\Gamma_i = 4\beta N \begin{bmatrix} -\left(1 + \frac{T_s}{R_i}\right) e^{-\frac{T_s}{R_i}} - 1 \\ e^{-\frac{T_s}{R_i}} - 1 \end{bmatrix}.$$

We also consider $\delta C[k]$, the variation of link capacity, as a state variable, which accounts for both capacity variations and other disturbances. $\delta C[k]$ evolves as follows.

$$\delta C[k+1] = \delta C[k] + \omega[k], \tag{2.8}$$

where $\omega[\cdot]$ is the external disturbance. Due to the uncertainty such as modeling error or unknown disturbance, it is usually hard, if not impossible, to drive the system to converge to the operating point without an offset. In order to ensure convergence, augmenting the system state with the disturbance is a feasible approach, since it would be possible to estimate the disturbance and then suppress its impact. The augmented state is $x_i^a[k] = [\delta q_i, \delta W_i, \delta C_i]^T$. Finally, the discretized system can be rewritten as

$$x_i^a[k+1] = \Phi_i^a x_i^a[k] + \Gamma_i^a u[k-n_0] + \Theta_i^a w[k] \tag{2.9}$$

$$y_i[k] = Q_i^a x_i^a[k] + v_i[k], \tag{2.10}$$

where the coefficient matrices are

$$\Phi_i^a = \begin{bmatrix} \Phi_i & \Delta_i \\ 0 & I \end{bmatrix}, \ \Gamma_i^a = \begin{bmatrix} \Gamma_i \\ 0 \end{bmatrix}, \ \Theta_i^a = \begin{bmatrix} 0 \\ I \end{bmatrix}, \ Q_i^a = [Q_i, 0].$$

2.3 MAQ Design

In the previous section, we obtain multiple models for the CRN congestion control system by linearization at several operating points, discretization, and state augmentation. Although it is possible to design one controller for each model respectively, it is hard to determine which controller should be active. Instead, we use the entire set of models as a *model bank* to estimate the system state and output. The estimation part is crucial in our control algorithm design. Due to the propagation delay, the control output, i.e., the dropping probability p, will take effect at the TCP server after the propagation delay T_p.

The entire control system is shown in Fig. 2.2. When there is incipient congestion, packets are dropped from front with a certain probability at the CRN BS. It's worth noting that we calculate dropping probability $p[k]$ based on the measurement $q[k]$ at time step k, as shown in Fig. 2.2. However, the probability $p[k]$ will take effect on the queue length after a propagation delay. For the control loop, we have discussed the model bank in the previous section but we

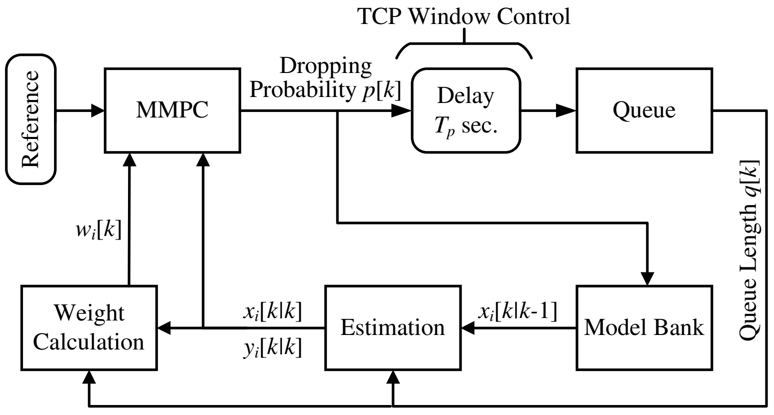

Figure 2.2: The control system structure.

still need to briefly restate it in the control context. We present the design of the MAQ scheme in rest of this section.

2.3.1 Estimation

In the model bank we developed, the noise is usually not known in advance in practice. It is necessary to utilize the previous information to estimate both the augmented state and output. Let $q[k]$ be the measured queue length at step k. We use Kalman Filter to perform state and output estimation as follows.

$$\hat{x}_i^a[k|k-1] = \Phi_i^a \hat{x}_i^a[k-1|k-1] + \Gamma_i^a u_i[k-n_0-1] \tag{2.11}$$

$$\hat{x}_i^a[k|k] = \hat{x}_i^a[k|k-1] + L_i[k](q[k] - q_i - Q_i^a \hat{x}_i^a[k|k-1]) \tag{2.12}$$

$$\hat{y}_i^a[k|k] = Q_i^a \hat{x}_i^a[k|k], \tag{2.13}$$

where $\hat{x}_i^a[k|k-1]$ is the estimation of step k based on step $(k-1)$ information, $\hat{x}_i^a[k|k]$ represents the updated state at step k based on the measurement $q[k]$ at time step k, and $L_i[k]$ is the Kalman gain of model i. The "hat" notation indicates that they are estimations. Eq. (2.13) is the output estimation. The Kalman gain $L_i[k]$ can be derived from the following process.

$$L_i[k] = P_i[k](Q_i^a)^T(Q_i^a P_i[k-1](Q_i^a)^T + G_i)^{-1} \tag{2.14}$$

$$\begin{aligned} P_i[k] = {} & \Phi_i^a P_i[k-1](\Phi_i^a)^T + \Theta_i^a O_i(\Theta_i^a)^T - \Phi_i^a P_i[k-1](Q_i^a)^T \\ & (Q_i^a P_i[k-1](Q_i^a)^T + G_i)^{-1} Q_i^a P_i[k-1](\Phi_i^a)^T, \end{aligned} \tag{2.15}$$

where $P_i[k]$ is the estimation error covariance of model i at step k.

This algorithm works in an iterative manner. Parameters O_i and G_i in (2.15) are stochastic terms that account for the variance of state interference and output, respectively. Since usually the variance is unknown, O_i and G_i are the parameters to be tuned. In the MAQ design, both O_i and G_i are scalar and are tuned for each of the models.

2.3.2 Weight Calculation

Given the estimations of the state and output of each model, a more accurate approximation to the real system dynamics can be obtained by probabilistically integrating the models. We first derive the weight for each model based on their *residual* at time step k, denoted as $\xi_i[k]$, which is the difference between the real measurement and estimation output of each model. Noticing that the measurement $q[k]$ is the queue length while the estimation $\hat{y}_i[k|k]$ is the deviation from the operating point, we have

$$\xi_i[k] = q[k] - q_i - \hat{y}_i[k|k]. \tag{2.16}$$

Under the general assumption that the weights are Gaussian, the probability that model i represents the system at step k can be derived with the Bayesian theorem as

$$\rho_i[k] = \frac{\exp(-0.5\lambda\xi_i^2[k])\rho_i[k-1]}{\sum_{j=1}^{\pi}\exp\big(-0.5\lambda\xi_j^2[k]\big)\rho_j[k-1]}. \tag{2.17}$$

In (2.17), the exponential term is due to the Gaussian distribution of the weights. It would be beneficial that the rejecting speed of the unsuitable models is exponential. The coefficient λ determines the sensitivity to the residual. Furthermore, the formula is recursive; once $\rho_i[k]$ is 0 at some step k, it will remain at 0 even if the model is more accurate than others. We thus set a lower limit $\mu > 0$, such that if $\rho_i[k]$ is lower than μ, it will be set to μ.

The weights are then calculated by normalizing the probabilities, as

$$w_i[k] = \begin{cases} \frac{\rho_i[k]}{\sum_{j=1}^{\pi} \rho_j[k]}, & \rho_i[k] > \mu \\ 0, & \rho_i[k] \leq \mu. \end{cases} \tag{2.18}$$

In the initialization phase, all the weights are set to $1/\pi$ since there is no a priori information about the system.

2.3.3 MMPC Control Law

We are now ready to derive the MMPC control law. Due to the propagation delay, the control signal $u_i[k]$ affects the queue length at time $(k+n_0)$. It is thus necessary to estimate the n_0-step ahead state and output, i.e., at time $(k+n_0)$. We estimate state $x_i^a[k+n_0]$ as

$$\begin{aligned} \hat{x}_i^a[k+n_0|k] &= \Phi_i^a \hat{x}_i^a[k+n_0-1|k] + \Gamma_i^a u_i[k-1] \\ &= (\Phi_i^a)^{n_0} \hat{x}[k|k] + \sum_{j=1}^{n_0} (\Phi_i^a)^{j-1} \Gamma_i^a u_i[k-j]. \end{aligned} \tag{2.19}$$

The output of each model at time $(k+n_0)$ can also be estimated. A more accurate estimation, $\bar{y}$, can be obtained as the weighted average of the estimated outputs. It follows that

$$\bar{y}[k+n_0|k] = \sum_{i=1}^{\pi} w_i[k] \hat{y}_i[k+n_0|k], \tag{2.20}$$

where $\hat{y}_i[k+n_0|k]$ is derived with the estimation precess. Recall that output $\hat{y}_i[k+n_0|k]$ is the difference between the estimated queue length and the ith operating point q_i. Substituting $\hat{y}_i[k+n_0|k] = \hat{q}[k+n_0] - q_i$ into (2.20), we have

$$\bar{y}[k+n_0|k] = \hat{q}[k+n_0] - \sum_{i=1}^{\pi} w_i[k] q_i. \tag{2.21}$$

Furthermore, the control signal $u_i[k]$ is the difference between the dropping probability and its operating point value, i.e., $u_i[k] = p[k] - p_i$, while $p[k]$ is to be derived. The control objective function is formed with a prediction horizon of s time steps and a control horizon of m time steps. As discussed, the prediction horizon starts from time step $(k+n_0)$. By solving the optimization problem with this objective function at every time step, a series of optimal control signals $\{\Delta p[k], \Delta p[k+1], \ldots, \Delta p[k+s]\}$ can be derived, where $\Delta p[k] = p[k+1] - p[k]$. The first control signal is then chosen as our result. The $(k + n_0 + j)$th step prediction is the weighted average of all the model outputs at the same time step, i.e.,

$$\bar{y}[k+n_0+j|k] = \sum_{i=1}^{\pi} w_i[k]\hat{y}_i[k+n_0+j|k]. \tag{2.22}$$

The design objective is to stabilize the queue length around the set point while keeping the difference between each control move as small as possible. The first goal is obvious, and the reason for the second one would be explained in the later section. With the relation given in (2.21), we define the objective function as

$$\min \ (Y_{ref} - \bar{Y})^T W_y (Y_{ref} - \bar{Y}) + \Delta U^T W_u \Delta U, \tag{2.23}$$

where Y_{ref} is the modified reference output based on the reference queue length. The reference queue length is given as q_{ref} and the estimated queue length is $\hat{q}[k+n_0+j]$. It follows that

$$Y_{ref} = \begin{bmatrix} q_{ref} - \sum_{i=1}^{\pi} w_i[k]q_i \\ q_{ref} - \sum_{i=1}^{\pi} w_i[k]q_i \\ \vdots \\ q_{ref} - \sum_{i=1}^{\pi} w_i[k]q_i \end{bmatrix}. \tag{2.24}$$

Furthermore, $\bar{Y}$ is a vector of the weight estimations of the model outputs over the prediction horizon, while ΔU is a vector of dropping probability increments over the control horizon, i.e.,

$$\bar{Y} = \begin{bmatrix} \bar{y}[k+n_0+1|k] \\ \bar{y}[k+n_0+2|k] \\ \vdots \\ \bar{y}[k+n_0+s|k] \end{bmatrix}, \quad \Delta U = \begin{bmatrix} \Delta p[k] \\ \Delta p[k+1] \\ \vdots \\ \Delta p[k+m] \end{bmatrix}. \tag{2.25}$$

Finally, W_y and W_u are diagonal weight matrices of queue length differences and control moves, respectively, which can be used to trade-off between the dual objectives of stabilizing the queue and minimizing the control moves.

In (2.23), the first term minimizes the difference between the real queue length and reference queue length. The second term in the objective function is the penalty for changing the dropping probability. To solve this problem, we need to derive $\bar{y}$ from $\bar{y}[k+n_0+1|k]$ to $\bar{y}[k+n_0+s|k]$. To facilitate this process, the propagation matrix is given as follows.

$$\bar{Y} = M_x^a + M_c^a M_e \Delta U + M_c^a U_0 - M_{cp}. \tag{2.26}$$

The matrices in (2.26) are given as

$$M_x^a = \sum_{j=1}^{\pi} w_j[k] \begin{bmatrix} Q_j^a(\Phi_j^a) \\ \vdots \\ Q_j^a(\Phi_j^a)^m \end{bmatrix} \hat{x}_j^a[k+n_0|k]$$

$$M_e = \begin{pmatrix} 1 & & 0 \\ \vdots & \ddots & \\ 1 & \cdots & 1 \end{pmatrix}, \quad U_0 = \begin{bmatrix} p[k-1] \\ \vdots \\ p[k-1] \end{bmatrix}$$

$$M_c^a = \sum_{j=1}^{\pi} w_j[k] \begin{bmatrix} Q_j^a\Gamma_j^a & & 0 \\ \vdots & \ddots & \\ Q_j^a(\Phi_j^a)^{m-1}\Gamma_j^a & \cdots & Q_j^a\Gamma_j^a \end{bmatrix}$$

$$M_{cp}^a = \sum_{j=1}^{\pi} w_j[k] \begin{bmatrix} Q_j^a\Gamma_j^a & & 0 \\ \vdots & \ddots & \\ Q_j^a(\Phi_j^a)^{m-1}\Gamma_j^a & \cdots & Q_j^a\Gamma_j^a \end{bmatrix} \begin{bmatrix} p_j \\ \vdots \\ p_j \end{bmatrix},$$

where M_{cp} is the compensation for the deviation from operating point p_i of each model i. The optimization variables of problem (2.23) is ΔU, which can be solved as

$$\begin{aligned} \Delta U = {} & (M_e^T M_c^{aT} W_y M_c^a M_e + W_u)^{-1} M_e^T M_c^{aT} \\ & W_y(\tilde{Y}_{ref} - M_x^a - M_c^a U_0), \end{aligned} \tag{2.27}$$

where $\tilde{Y}_{ref} = Y_{ref} + M_{cp}$.

2.3.4 Parameter Tuning

The proposed CRN congestion control algorithm is presented in Algorithm 1. In the proposed MAQ scheme, there are several parameters that need to be tuned to achieve good performance. First, the two weight matrices W_y and W_u in the objective function (2.23) are directly related to the optimal control signal. The control move is the dropping probability in the range of $[0, 1]$.

Algorithm 1: The Proposed MAQ Algorithm

```
Data: Average and variance of service capacity ($\bar{C}$ and $\sigma_C$), queue length at each time $k$
Result: The drop/mark probability $p[k]$ at time $k$
1  Choose the model number $\pi$;
2  Assign the weight of each model as $\frac{1}{\pi}$;
3  Define the Kalman Gain matrix $L_i$ and estimation error covariance $P_i$;
4  while System is running do
5      for $i = 1 : \pi$ do
6          Calculate the estimation $\hat{y}_i^a[k|k]$;
7          Update the Kalman gain $L_i$ and estimation error covariance $P_i$;
8      for $i = 1 : \pi$ do
9          Update probability $\rho_i[k]$ based on (2.17);
10         Calculate weight $w_i$;
11     for $j = 1 : n_0$ do
12         Estimate feature state information $\hat{x}_i^a[k + j|k]$;
13     Minimize the objective function (2.23) and obtain the analytical solution (2.27);
14     Use the first element of the result to obtain $p[k]$;
15     Generate uniformly distributed random number $u(0, 1)$;
16     if $u < p[k]$ then
17         Drop the head-of-line packet at CRN BS queue;
```

We can use the saturation function to enforce this range, i.e.,

$$p[k] = \max\{0, \min\{1, p[k-1] + \Delta p[k]\}\}. \tag{2.28}$$

However, to avoid offset or unstability, it is necessary to choose a large W_u. Usually, the larger the ratio W_y/W_u, the more aggressive the control move. For the CRN congestion control system, we recommend $W_y = \text{diag}(1, 1, \ldots, 1)$ and $W_u = \text{diag}(10^6, 10^6, \ldots, 10^6)$, which work well in our simulation study.

Second, in the estimation procedure, the matrix $P_i[0]$ should be initialized with large and diagonal values if we do not know the covariance of the state variable. Moreover, as the capacity variations may be large and the estimation error may not be zero due to the uncertain nature of the flow model, the disturbance variance O_i is set to be the standard deviation of capacity σ_C and the output variance G_i is set to a small but non-zero value. According to [10], the larger the ratio O_i/G_i, the smaller the response time, but the larger the overshoot (even leading to oscillation). We choose $G_i \in [0.4, 1]$ in this chapter based on our simulation study.

Third, for weight calculation, the coefficient λ determines the sensitivity of weights to estimation error. Consider the potentially large network parameter variation, which leads to estimation error, we would not recommend a large λ since it will easily drive the model probability $\rho_i[k]$ to 0. Given such a system with large variations of parameters and conditions, we set $\lambda = 1$ in this chapter.

2.4 Simulation Study

In this section, we evaluate the performance of MAQ with NS2 simulations. We extend the NS2 simulator with the multiple-channel extension, TDM module, and the channel bonding/aggregation module. We assume 10 licensed channels: five of them with a capacity of 500 Kb/s and the other five with a 1 Mb/s capacity. As in prior work [5, 25], each channel is modeled as an on-off process. Both the on and off periods are exponentially distributed with mean $\eta(\text{on}) = 4$ seconds and $\eta(\text{off}) = 5$ seconds, respectively. The sensing phase of the CRN is 20ms and the transmission phase is 200ms. If there is no channel available after the sensing period, the frozen state will continue until an idle channel is found.

The CRN maintains a large number of TCP connections. The RTT and propagation delay are a key factor influencing the performance of congestion control. In real networks, different users may have different propagation delays. So we choose propagation delays uniformly distributed in $(100, 150)$ ms (unless stated otherwise). The capacity of the wireline link between the BS to a TCP server is 20 Mb/s. The average capacity for the CRN downlink is $\bar{C} = 3.2$ Mb/s with variance $\sigma_C = 1.3$ Mb/s. The capacity $C(t)$ used in one of the simulations is shown as a function of time in Fig. 2.3. The packet size is 540 Bytes with 500 Bytes data and 40 Bytes header. The reference queue length is set to 90 packets, corresponding to a queueing delay around 100 ms. The queue size B is set to 500 packets (about 2Mb).

For comparison purpose, we also simulated two existing control-theoretic schemes: (i) the proportional integral (PI) controller, which is canonical and has been shown to be effective on

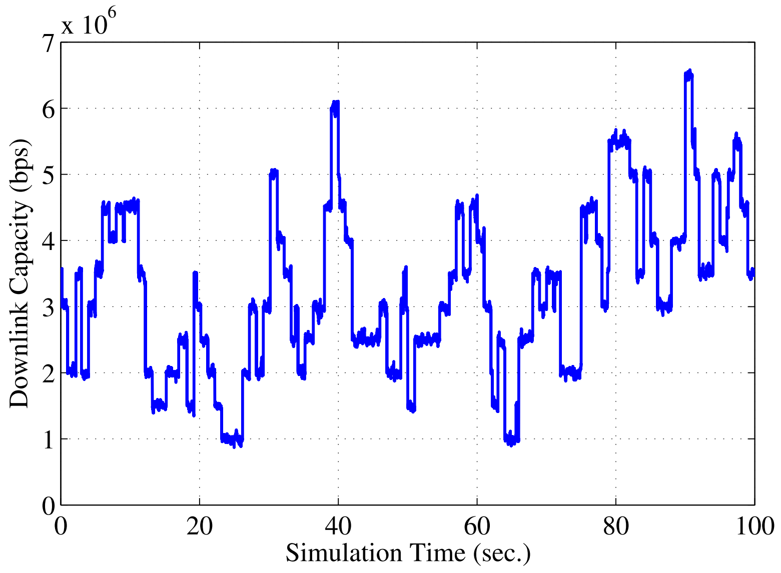

Figure 2.3: The CRN downlink capacity over time used in one of the simulations.

dealing with varying capacities [34]; (ii) the discrete sliding modes (DSM) controller, which is a most recent advance that is based on the principles of discrete sliding-mode control [35]. We set the PI parameters as: 4.839×10^{-5} and 4.346×10^{-5}, as recommended in [34]. The DSM parameter is set as recommended in [35], with $\gamma = 0.01$, and a sigmoid function with $\delta = 10$ is used. We test the proposed scheme under responsive and non-responsive background traffic and under various parameter settings.

2.4.1 Responsive Background Traffic

We first conduct simulations with a fixed number of long-lived FTP sessions and HTTP background flows. The HTTP flows are generated using PACKMIME-HTTP in NS2 with a rate of 10, i.e., on average 10 HTTP connections are generated in every second. The transport agent in each source node is set to be TCP/Reno. The number of SUs is $N = 60$. For MAQ, the parameters are set as: $q_i \in \{30, 60, 90, 120, 150\}$ packets, $C_i \in \{1.2, 2.1, 3, 3.9, 4.8\}$Mb/s, $T_p = 100$ms, $W_y = \mathbf{I}$, $W_u = 10^6\mathbf{I}$, where $\mathbf{I}$ is the identity matrix. The covariance parameters are set as $O_i = 300$ and $G_i = 1$, for $i = 1, 2, \ldots, 5$.

Figure 2.4 presents the queue length dynamics of MAQ and PI. The sudden variation of capacity would cause the queue length change immediately. We find that MAQ can stabilize the queue around the reference point of 90 packets with almost no underflow (i.e., an empty queue),

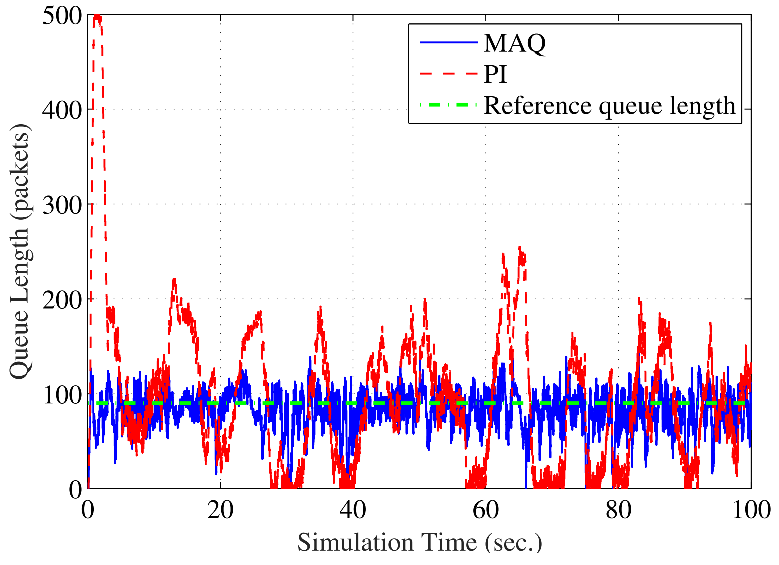

Figure 2.4: Queue length dynamics under responsive background traffic.

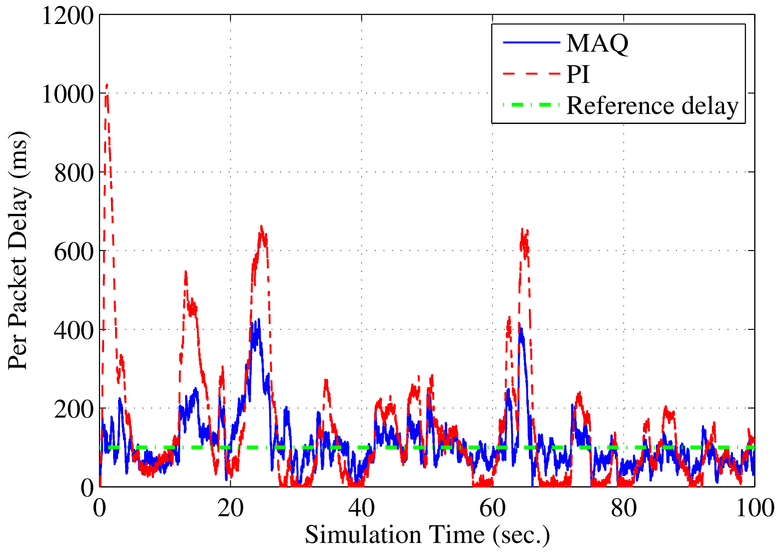

Figure 2.5: Packet queuing delay dynamics under responsive background traffic.

while the PI queue exhibits much larger variations with a lot of underflows. Fig. 2.5 presents the packet queuing delay dynamics. PI cannot adjust its drop probability quickly enough to adapt to the capacity variations, while MAQ is able to reject the influence of capacity variation and hence achieves lower and more stable queueing delays.

We also present the queue length, delay, and link utilization statistics in Table 2.1. The average queue length of MAQ is closer to the reference point and its standard deviation is about

Table 2.1: Queue Length, Queueing Delay, and Link Utilization Statistics

	Average queue length (packets)	STD queue length (packets)	Mean delay (ms)	STD delay (ms)	Average Utilization (%)
Responsive Background Traffic					
MAQ	82	20	87.5	51.9	99.73
PI	98	81	107.4	138.4	96.79
Non-responsive Background Traffic					
MAQ	78	33	72.3	39.8	97.14
PI	140	201	193.5	203.5	41.23

a quarter of that of PI. The average delay of MAQ is also about 20ms lower than that of PI, and its delay standard deviation is 87ms lower than that of PI. It is worth noting that MAQ achieves both lower and more stable queueing delay than PI.

2.4.2 Non-responsive Background Traffic

We next consider a more realistic setting by introducing a non-responsive traffic generator for background traffic. The non-responsive sources would act like disturbance by constantly injecting packets to the queue with exponentially distributed burst time and idle time. We use User Data Protocol (UDP), which does not perform congestion control, for the non-responsive flows. There are 60 FTP flows and 5 non-responsive flows. The burst data rate is 1Mb for each non-responsive flow with packet size 500 Bytes. The non-responsive flows are activated in the following two time intervals: [10s, 30s] and [60s, 80s].

The queue length dynamics with non-responsive background traffic are presented in Fig. 2.6. Both queues oscillate with a larger range due to the unexpected background traffic bursts. The PI queue overflows (i.e., buffer becomes full) for almost the entire non-responsive traffic transmission period, and then its buffer underflows in the following period when the burst transmissions are off. The MAQ queue, on the other hand, remains relatively stable and takes less time to recover when the bursts are off. We find that since PI has too much overflow and packets drop, the sender's TCP window size would drop to 1, which greatly affects the TCP transmission rate. The dropping probability of PI is also kept high even after the burst transmission period. This is the reason of its long recover time. MAQ, however, can stabilize the queue

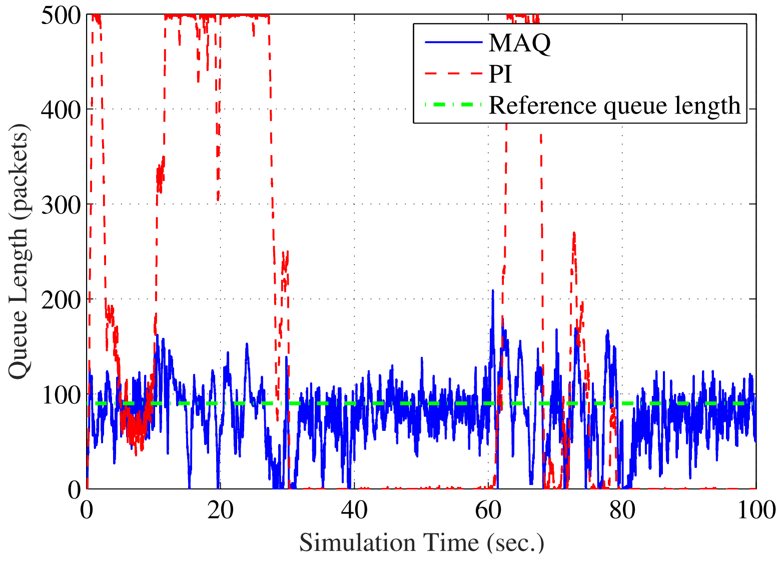

Figure 2.6: Queue length dynamics under non-responsive background traffic.

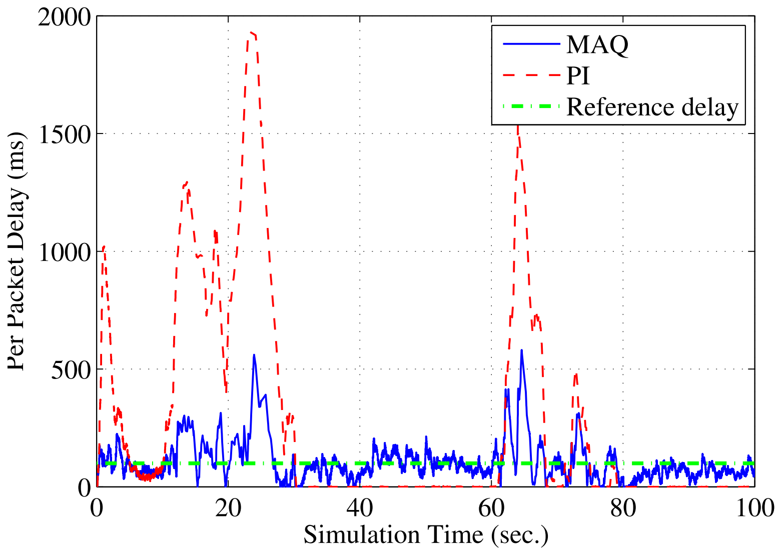

Figure 2.7: Packet queuing delay dynamics under non-responsive background traffic.

length around the reference point even with large variations in both the service capacity and background traffic, thus avoiding both buffer underflow and overflow and high link utilization. Another benefit of MAQ is the much lower and more stable packet queuing delay in such highly dynamic situation, as shown in Fig. 2.7.

The statistics for the non-responsive background traffic simulations are also presented in Table 2.1. Clearly, MAQ is more robust to strong disturbances in both background traffic and

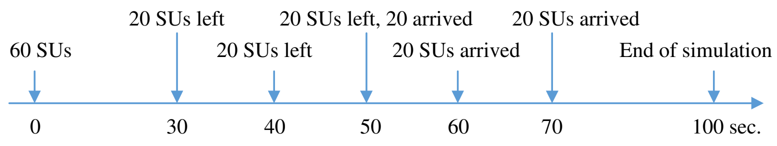

Figure 2.8: Change of the number of FTP connections during the simulation period.

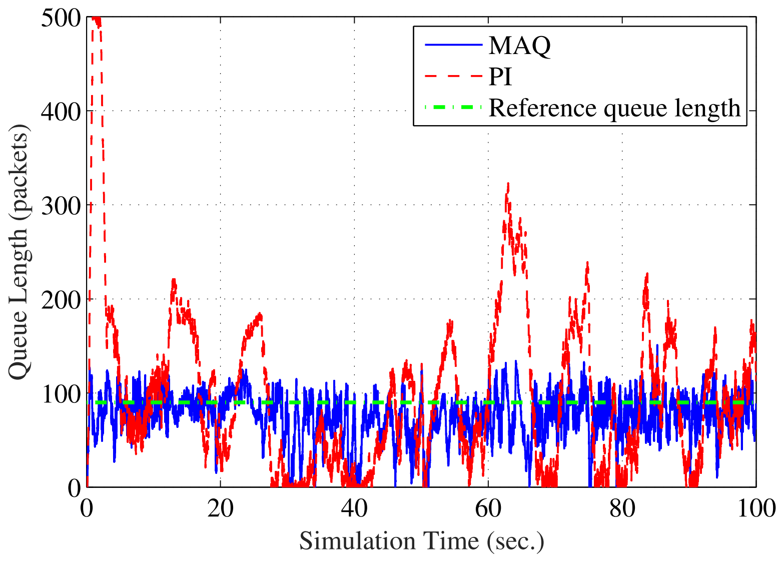

Figure 2.9: Queue length dynamics under varying number of connections.

service capacity. In this scenario, the MAQ average delay is only 37.36% of that of PI, and MAQ achieves a 56% gain on link utilization over PI.

2.4.3 Varying Number of FTP Connections

We also examine the case when the number of FTP connections varies over time. In this experiment, the simulation starts with 60 FTP connections. The changes of the number of FTP connections during the simulation period are shown in Fig. 2.8.

The queue length and delay dynamics for this simulation are presented in Figs. 2.11 and 2.12. When the connection number goes down, there are fewer TCP flows, which lead to an empty queue. MAQ can act quickly to adjust the dropping probability to allow the source congestion window to grow, which will stabilize the queue length again at the reference point. However, the PI queue length will become empty when the connection number goes down, due to its conservative adjustment policy, leading to low link utilization. The superior delay performance of MAQ can also be observed in Fig. 2.12.

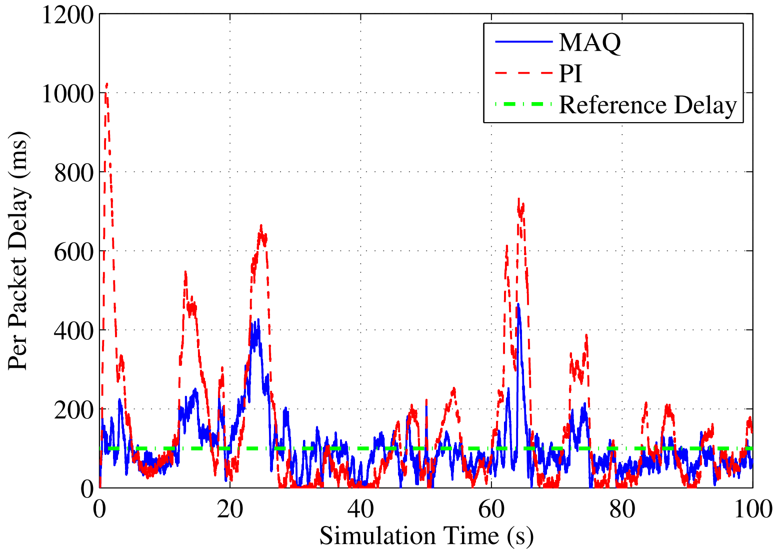

Figure 2.10: Packet queuing delay dynamics under varying number of connections.

2.4.4 Different Propagation Delay and Reference Queue Length

Finally, we analyze the impact of different propagation delay and reference queue length on the congestion control performance. We vary the average propagation delay from 30 ms to 450 ms in steps of 20 ms in a series of simulations. In each simulation, the propagation delay of each SU is the average plus a disturbance uniformly chosen from $[0, 50]$ ms. We also set different reference queue length in the range of $[10, 115]$ packets, which is indicative of different queueing delays. In the simulations, we compare the link utilization and delay of MAQ with that of PI and DSM, which is shown to be robust against system condition variations [35].

Figure 2.13 shows the link utilization of each scheme under different propagation delays. A large propagation delay has a negative impact on all the three algorithms, since it is harder to accurately predict future states and outputs. When the RTT is larger than the average capacity changing period, it will be impossible to properly control the queue. This is because when a control signal takes effect on the queue, the service capacity may have already changed to some other value. We find that MAQ can still maintain a considerably higher throughput than both PI and DSM, and the DSM performance degrades more quickly than MAQ and PI under increased propagation delays.

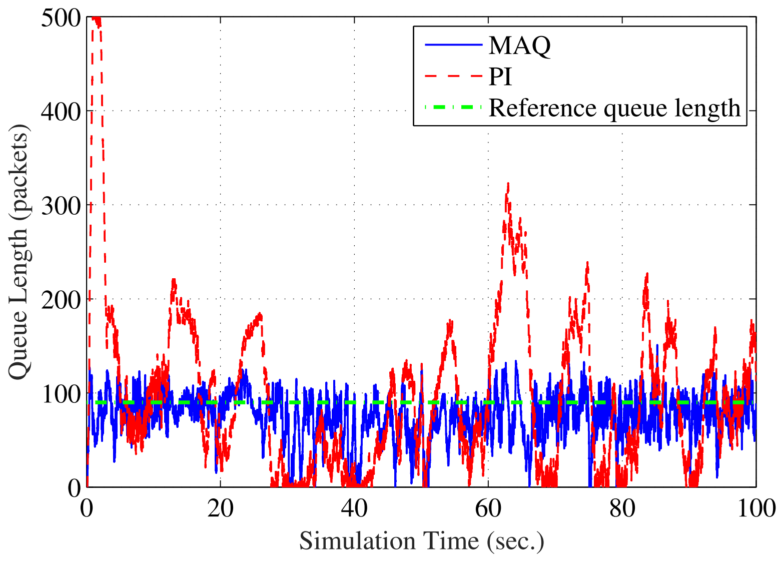

Figure 2.11: Queue length dynamics under varying number of connections.

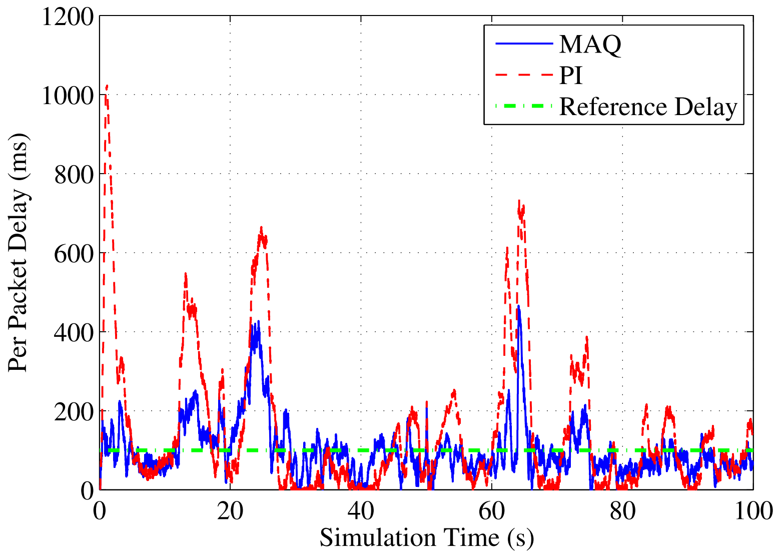

Figure 2.12: Packet queuing delay dynamics under varying number of connections.

Reference queue length is also critical for congestion control, since a large buffer could mitigate the effect of capacity variation. The link utilization of the three schemes for increased reference queue lengths are presented in Fig. 2.14. Again, MAQ achieves considerably higher link utilization than the other two schemes, especially when the reference queue length is small. For example, when the reference queue length is 10 packets, the MAQ link utilization is about

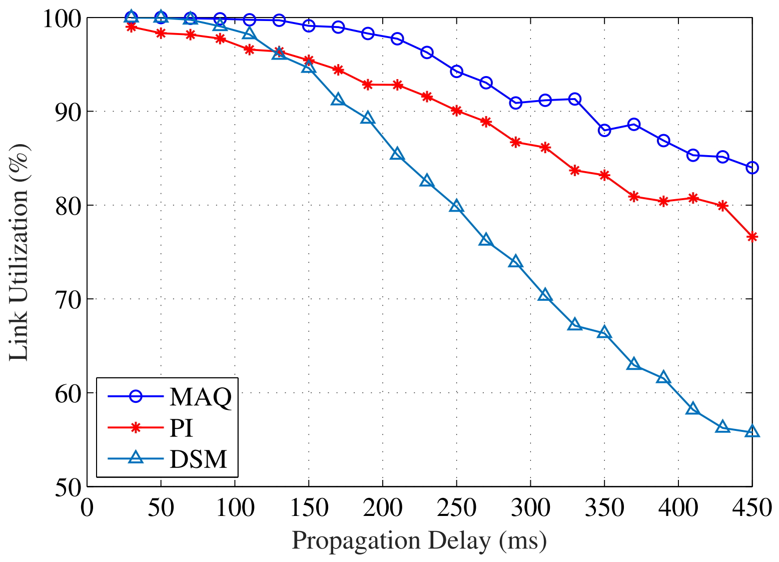

Figure 2.13: Average link utilization under increased propagation delays.

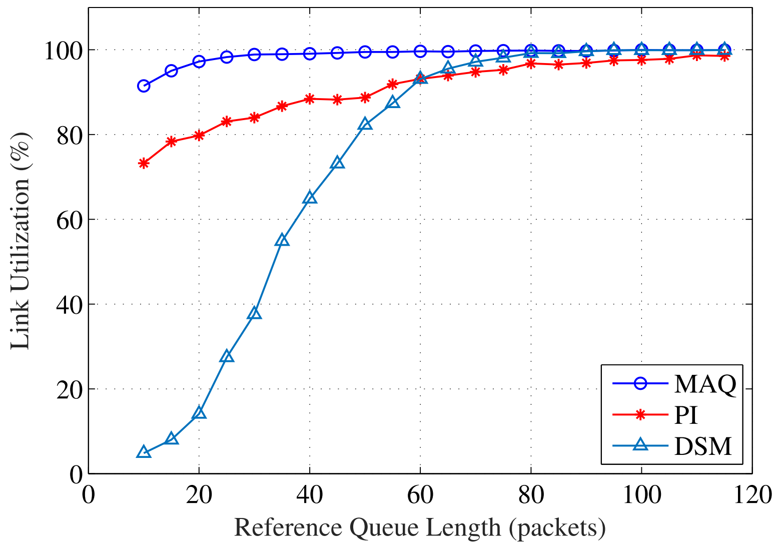

Figure 2.14: Link utilization under under increasing reference queue lengths.

20% higher than that of PI and 70% higher than that of DSM. When the reference queue length becomes large, all the three schemes achieve a high link utilization. However, as can be seen later in Fig. 2.16, PI and DSM achieve the high link utilization at the cost of higher delay and large delay variation than MAQ.

The queueing delay performance under different propagation delay and reference queue length are plotted in Fig. 2.15 and 2.16, respectively. We find that the average delay of MAQ is not only much smaller than PI (e.g., around 50% of that of PI), but also much stable over the entire range of propagation delay values. DSM exhibits better performance on controlling

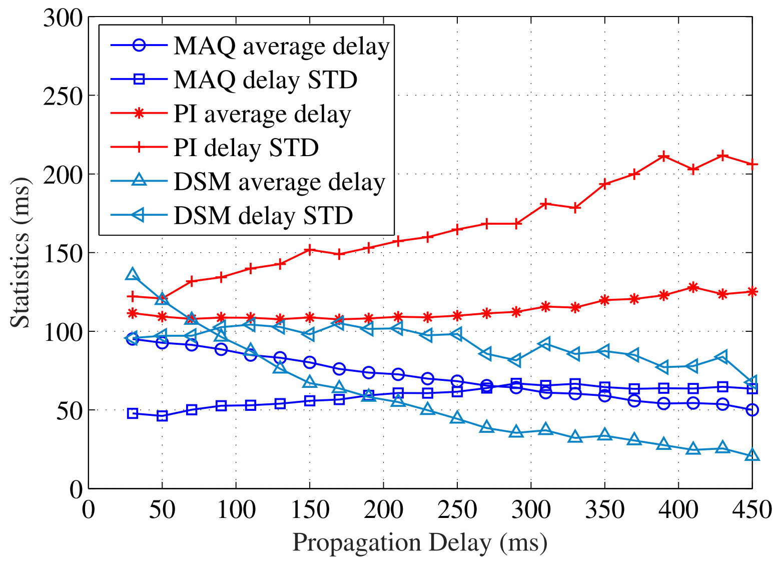

Figure 2.15: Average delay and delay STD under increasing propagation delays.

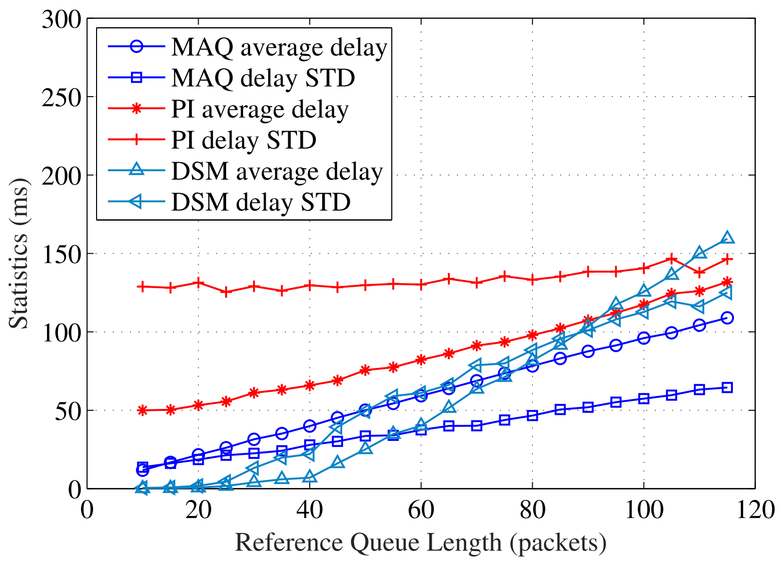

Figure 2.16: Average delay and delay STD under increasing reference queue lengths.

queuing delay than PI. Although its queueing delay is low when propagation delay is large, this is achieved at the cost of a low throughput, since its queue is empty more often than the other two schemes.

Under different reference queue lengths, the average queuing delay goes up roughly linearly since it is around $q_{ref}/\bar{C}$, as shown in Fig. 2.16. The DSM has very small average delay when the reference queue length is lower than 40 packets. As discussed, this is achieved at the cost of very low link utilization (see Fig. 2.14). MAQ not only achieves low queueing delay and delay variation, the two MAQ curves are also less sensitive to the increased reference queue lengths than the other two schemes.

2.5 Related Work

In this section, we briefly review related work on congestion control, which can be classified as end-to-end solutions and router-based solutions. We then discuss the several closely related work on congestion control in CRNs.

2.5.1 End-to-End Solutions

In the early age, congestion control algorithms are mostly based on the assumption that all packet losses are caused by buffer overflow at the bottleneck router. TCP Reno [36], TCP Tahoe [37], and TCP NewReno [38] are the several most popular algorithms based on such an idea. On the other hand, protocols were proposed, e.g., TCP Vegas [39], which are delay based. The mainstream protocols that most computer system use are TCP Cubic [40] and Compound TCP [41]. These protocols are mainly based the classical AIMD algorithm and combined with various modifications. However, none of the existing protocols are suitable for congestion control in CRNs, where the service capacity usually has frequent, large variations. In addition, none of the existing schemes consider the frozen transmissions during the spectrum sensing period.

Most recent congestion control proposals are mainly focusing on cellular networks, which also have varying link capacity due to fading and shadowing [42, 43]. The basic idea of [42] is to use a stochastic model: Poisson process with rate that follows a Brownian motion to predict the capacity of the wireless link. This model may not work well in CRN because the variation of capacity is mainly caused by the activity of primary users, in addition to fading and shadowing effects. Yasir et al. in [43] propose a method based on the training model between packet delay and window size. However, the most significant difference between cellular network and CRN studied in this chapter is, the cellular BS maintains a separate queue for each user (e.g., each user with a dedicate channel), but the CRN BS maintains a shared queue for all users in our model. Thus the basic assumption in such protocols does not hold and the application of such protocols in CRN would be hard, if not impossible. Also the spectrum sensing period will have a big effect on congestion control, which calls for a new CRN specific protocol design.

2.5.2 Router-based Solutions

Our work is closely related to the literature on AQM design in the context of the Internet. Instead of actually dropping packets, the authors in [44] proposed a method with Explicit Congestion Notification (ECN), to provide a feedback from the bottleneck router. The authors in [45] present a control theoretic analysis of random early detection (RED) [46] and find that RED is sensitive to its parameter setting and it is hard to stabilize if the delay is taken into consideration. In [34], a Proportional-Integral (PI) AQM scheme is developed. However, the PI scheme may react slowly to outside disturbances. Model predictive control (MPC) is an important industry control method, which predicts future system states and computes the optimal control input at each sampling time slot. Generalized predictive control has been used in network congestion control [47] and an MPC based AQM method (MPAQM) is proposed in [48]. These methods can compensate the impact of RTT with the model predictor. However, they do not explicitly take disturbance (e.g., varying service capacity) into consideration.

Chavan, et al. in [49] propose a solution to address the capacity variation due to a fading wireless channel based on the H_∞ technique. However, its conservative policy makes it unsuitable for CRNs where the capacity may change at various/fast timescales. In [50], the authors propose a latency control algorithm, termed CoDel, which provides a solution to the *bufferbloat* problem; but the design does not directly apply to CRNs. In [35], the authors propose an AQM algorithm, termed DSM, based on the discrete sliding mode control (DSMC) theory. Although it deals with high frequency oscillation of link capacity, DSMC suffers from the over control problem and it is hard to choose a proper control gain for this algorithm.

2.5.3 CRN Congestion Control Schemes

The problem of enhancing TCP performance in CRNs has been addressed in only a few papers [24, 26, 25]. In [24], the authors propose a new network management framework, termed DSASync, for DSA based WLANs. This work uses a zero-size receive window to freeze the

TCP sender and smooth the ACKs from the BS during the sensing period. Its design is largely based on heuristic methods, while smoothing ACKs would slow down the growth of window size during the valuable transmission period.

In [26], a cross-layer approach is proposed to maximize throughput by jointly adjusting spectrum sensing, access decision, and modulation and coding scheme in the physical layer. The problem is formulated based on a POMDP framework and solved by dynamic programming. This is an offline scheme that requires full prior knowledge of all system statistics, due to the complex POMDP approach. In [25], the impact of channel sensing and spectrum opportunity change on TCP performance is analyzed and a window based transport control protocol for CR Ad Hoc Networks is proposed. The proposed protocol is mainly based on heuristics rather than a rigorous theoretic analysis, and the enhancements may not be backward compatible with existing TCP protocols that have already been widely used in both wireless and wireline networks.

2.6 Conclusion

In this chapter, we designed a congestion control scheme for infrastructure-base CRNs. The goal was to stabilize the TCP buffer at the CRN BS under a wide range of system/network parameters and dynamics. The proposed scheme, termed MAQ, was based on MMPC with enhanced state and output estimation. The proposed scheme was evaluated with extensive NS2 simulations under various background traffic types and network/system parameter settings. It was shown to achieve superior performance over two benchmark schemes.

Chapter 3

Model Free Congestion Control for Mobile Network based on Deep Reinforcement Learning

As wired/wireline networks become more and more complex, the fundamental assumptions made by many existing TCP variants may not hold true anymore. In this chapter, we develop a model free congestion control algorithm based on deep reinforcement learning (DRL), which has a high potential in dealing with the complex and varying network environment. We present *TCP-Drinc*, acronym for *D*eep *R*e*I*nforcement lear*N*ing based *C*ongestion Control, which learns from past experience and a set of measured features to decide the next action on adjusting the congestion window size. We present the TCP-Drinc design and validate its performance with extensive NS3 simulations and comparison with five benchmark schemes.

3.1 Introduction

The unprecedented growth of network traffic, in particular, mobile traffic, has greatly stressed today's Internet. Although the capacities of wired and wireless links have been greatly increased, the gap between user demand and what the Internet can offer is actually getting wider. Furthermore, many emerging applications not only require high throughput and reliability, but also low delay. Although the brute-force approach of deploying wired and wireless links with higher capacity helps to mitigate the problem, a more viable approach is to revisit the higher layer protocol design, to make more efficient use of the increased physical layer capacity. Some works such as [51, 52, 53, 54, **?**] are inspiring.

Congestion control is the most important networking function of the transport layer, which ensures reliable delivery of application data. However, the design of a congestion control protocol is highly challenging. First, the transport network is an extremely complex network of queues. The TCP end host itself consists of various interconnected queues. When the TCP flow gets into the Internet, it traverses various queues at routers/switches along the end-to-end path, each shared by cross-traffic and other TCP flows and served with some scheduling discipline. Significant efforts are still needed to gain good understanding of such a complex network to develop the queueing network theory that can guide the design of a congestion control protocol. Second, if following the end-to-end principle, agents at end hosts have to probe the network status and make independent decisions without coordination. The detected network state is usually error-prone and delayed, and the delayed effect of an action also depends on the actions of other competing hosts. Third, if to involve the routers, the algorithm must be extremely simple (e.g., stateless) to ensure scalability, since the router may handle a huge amount of flows. Finally, as more wireless devices are connected, the lossy and capacity-varying wireless links also pose great challenges to congestion control design.

Many effective congestion control protocols have been developed in the past three decades since the pioneering work [37] (see Section II). However, many existing schemes are based on some fundamental assumptions. For example, early generation of TCP variants assume that all losses are due to buffer overflow, and uses loss as indicator of congestion. Since such assumption does not hold true for wireless networks, many heuristics are proposed for TCP over wireless to distinguish the losses due to congestion from that incurred by link errors. Moreover, many existing schemes assume a single bottleneck link in the end-to-end path, and the wireless last hop (if there is one) is always the bottleneck. Given the high capacity wireless links and the complex network topology/traffic conditions we have today, such assumptions are less likely to be true. The bottleneck could be at either the wired or wireless segment, it could move around, and there could be more than one bottlenecks. Finally, when there is a wireless last hop, some existing work [42] assumes no competition among the flows at the base station (BS), which, as shown in [43], may not be true due to coupled wireless transmission scheduling at the BS.

In this chapter, we aim to develop an effective congestion control algorithm that does not rely on the above assumptions. Motivated by the recent success of applying machine learning to wireless networking problems [55], and based on our experience of applying deep learning

(DR)/deep reinforcement learning (DRL) to 5G mmWave networks [56], edge computing and caching [57, 58, 59], and RF sensing and indoor localization [12, 18, 11], we propose to develop a model free congestion control algorithm based on DRL. The original methods that treat the network as a white box have been shown to have many limitations. To this end, machine learning, in particular, DRL, has a high potential in dealing with the complex network and traffic conditions by learning from past experience and extracting useful features. A DRL based approach also relieves the burden on training data, and has the unique advantages of being adaptive to varying network conditions.

In particular, we present **TCP-Drinc**, acronym for **D**eep **R**e**I**nforcement lear**N**ing based **C**ongestion Control. TCP-Drinc is a DRL based agent that is executed at the sender side. The agent estimates features such as congestion window change, round trip time (RTT), the minimum RTT over RTT ratio, the difference between RTT and the minimum RTT, and the inter-arrival time of ACKs, and stores historical data in an experience buffer. Then the agent uses a DRL with a deep convolutional neural network (DCNN) concatenated with a long short term memory (LSTM) network to learn from the historical data and select the next action to adjust the congestion window size. The contributions of this work are summarized as follows.

1. To the best of our knowledge, this is the first work that applies DRL to the congestion control problem. Specifically, we propose a DRL based framework on (i) how to build the experience buffer to deal with the delayed environment, where an action will take effect after a delay and feedbacks are also delayed, (ii) how to handle the multi-agent competition problem, and (iii) how to compute each components including states, action, and reward. We believe this framework could help to boost the future research on smart congestion control protocols.

2. The proposed TCP-Drinc framework also offers solutions for long-existing problems in congestion control: delayed environment, partial observable information, and measurement variations. The LSTM is utilized to handle the autocorrelation within the time-series introduced by delay and partial information that one agent senses. Moreover, we

applied CNN as a filter to extract the stable features from the rich but noisy measurements, instead of using EWMA as a coarse filter as in previous works.

3. We develop a realistic implementation of TCP-Drinc on the NS3 and Tensorflow platforms. The DRL agent is developed on Tensorflow and the training and inference interfaces are built in NS3 using Tensorflow C++. We conduct extensive simulations with TCP-Drinc and compare with five representative benchmark schemes, including both loss based and latency based schemes. TCP-Drinc achives superior performance in throughput and RTT in all the simulations, and exhibits high adaptiveness and robustness under dynamic network environments.

The remainder of this chapter is organized as follows. We first review related work in Section 3.2. In Section 3.3, we discuss preliminaries of deep reinforcement learning. The system model and problem statement are presented in Section 4.2. The proposed TCP-Drinc is presented in Section 3.5, and validated with simulation in Section 4.5. We conclude this chapter in Section 3.7. The math notation is summarized in Table 4.1.

3.2 Related Work

Congestion control is a fundamental networking problem, which has drawn extensive attention and has been studies over the past three decades. In this section, we review key related work and recent progress in this area. We classify existing congestion control techniques into three categories, end-to-end, router based, and smart schemes, as discussed below.

3.2.1 End-to-End Schemes

This class of work can be further classified into loss-based or delay-based schemes. TCP Reno [36], TCP Tahoe [37] and TCP NewReno [38] were early protocols that are loss-based. TCP Vegas was the first delay-based protocol. Currently, most computer operation systems adopt TCP Cubic [40] or Compound TCP [41], which mainly deal with the situation with large capacity RTT products.

Table 3.1: Notation

Symbol	Description
$\mathbf{s}_t$	the state tensor at time t
$\mathbf{a}_t$	the action tensor at time t
$r(\mathbf{s}_t, \mathbf{a}_t)$	the reward function scalar given the state and action at time t
$V(\mathbf{s}_t, \mathbf{a}_t)$	the value function
$Q^\pi(\boldsymbol{s}_t, \boldsymbol{a}_t)$	the Q function for discounted accumulated reward
R_t	the discounted summation reward
$\pi(t)$	the policy at time t
$\boldsymbol{\omega}$	the DQN weights
$J(\boldsymbol{\omega})$	the loss function for weight training
y_t	the target value in the loss function
τ_{RTT}	the round trip time
$\hat{\tau}_p$	the minimum RTT
τ_p	the propagation delay
τ_q	the queuing delay
L	the length of historical states taken into account
Δw	cWnd difference
v_{RTT}	the minimum RTT over RTT ratio
δ_{RTT}	the difference between RTT and the minimum RTT
τ_{ACK}	inter-arrival time of ACKs
M	number of time slots in a state
$\mathcal{S}$	the state space
$\mathcal{A}$	the action space
$x(t)$	the sending rate at time t
$w(t)$	the congestion window size at time t
$z(t)$	the impact of an action at time t on future goodput
$U(\cdot)$	the utility function
N_{pre}	the duration of the pre training process
N_{dis}	the duration of the distributed training process

These protocols are designed for the wired Internet. However, recent measurements on 3G and 4G LTE networks reveals fast oscillation of channel capacity [42]. In addition, the authors in [43] shows that burst scheduling and competing traffic will also influence the RTT and capacity utilization of the network. The authors then propose new end-to-end protocols that observes the packet arrival times to infer the uncertain dynamics of the network path (Sprout [42]) and utilizes delay measurement (i.e., Verus [43]) to cope with these challenges.

Another recent progress on congestion control is on data center networks. Compare with normal networks, the capacity in data center networks is larger (Gigbits or 10s Gigbits) but stable and the latency is much smaller (in μs). And acknowledge is not sent for every packets. The Data Center TCP (DCTCP) [60] exploits the ECN feedback from switches. Performance-oriented Congestion Control (PCC) proposes to continuously observe the connection between it actions and experienced performance, and to adopt actions that lead to good performance [61]. The authors in [62] leverages sliding mode control theory to analyze and fix the stability issue of quantized congestion notification (QCN) in data center Ethernet networks.

3.2.2 Router based Schemes

This class of work involves switch or routers in congestion control. Explicit Congestion Notification (ECN) [44] is introduced as a substitution of loss as a congetion signal. Active queue management (AQM) such as RED [46], CoDel [50], and MAQ [63, 64] are all proposed to let routers to mark or drop packets on incipient congestion. These approaches require modification of the routers and intermediate devices, which may not be practical or may not scale to large number of TCP flows.

3.2.3 Smart Schemes

With the recent success of machine learning/deep learning on image recognition, video analytics, and natural language processing, there is strong interest on apply machine learning to solving networking problems [55]. Interesting results in [65, 66] provide insight into machine generated congestion protocols. However, these learning algorithms require offline training based on prior knowledge of the network and can only be adopted for limited situations. In [67], the authors propose an algorithm based on deep reinforcement learning (DRL) to deal with the traffic engineer problem at intermediate nodes. This is the first work that applies DRL to the traffic engineering problem in the Internet protocol (IP) layer. In [68], the authors incorporate Q-learning into congestion control design, termed QTCP. It is based on limited feature scales (discretized states) and uses Kanerva Coding instead of a deep neural network to handle Q-function approximation. The authors show considerable gains achieved by QTCP over the classical TCP NewReno.

3.3 Preliminaries of DRL

In this section, we present the preliminaries of deep reinforcement learning, which form the foundation of the proposed TCP-Drinc design to be presented in the next sections.

The general reinforcement learning consists of two entities: the agent and the environment, as shown in Fig. 3.1. The interactions between the environment and the agent constantly influences the environment and trains the agent. The typical problem studied in deep reinforcement learning is the Markov decision problem (MDP). At each episode, the agent receives the *state* tensor $\mathbf{s}_t$, takes an action $\mathbf{a}_t$ based on the *policy* $\pi(\mathbf{s_t})$, and receives a scalar value *reward* $r(\mathbf{s}_t, \mathbf{a}_t)$. There may be a delay τ_1 before the action $\mathbf{a}_t$ starts to influence the environment, and there may also be a delay τ_2 for the reward $r(\mathbf{s}_t, \mathbf{a}_t)$ to be sensed by the agent. Howver, in most RL designs, these delays are neglected. However, for congestion control, such delays play an important role on the stability of the system as will be demonstrated in the following sections.

The value function $V(\mathbf{s}_t, \mathbf{a}_t)$ could be represented as the discounted, accumulated reward, which is calculated as

$$R_t = \sum_{i=t}^{T} \gamma^{i-t} \cdot r(\mathbf{s}_t, \mathbf{a}_t), \tag{3.1}$$

where $\gamma \in [0, 1]$ is the discount factor and T is the end of the episode. With the Bellman-Ford equation, (3.1) can be rewritten as

$$R_t = r(\mathbf{s}_t, \mathbf{a}_t) + \gamma R_{t+1}. \tag{3.2}$$

In general settings, the policy $\pi(\mathbf{a}|\mathbf{s_t})$ or $\pi(\mathbf{s_t})$ generates the target action by mapping the state space to the action space: $\mathcal{S} \to \mathcal{A}$, stochastically or deterministically. For example, we could model the output action as a probability distribution over a discrete action space $\mathbf{p}(\mathbf{a})$. And the action that is to be taken could be either sampled with this distribution or the one with the largest probability. It is natural to use neural networks (NN) to approximate these policy and value functions. However, the approximation is unstable, due to the strong correlation between sequential samples. In addition, the nonstationary target values could further degrade the stability. The shallow NN has a limited ability to extract important features.

Deep reinforcement learning (DRL) algorithms, first introduced in [8], are based on a similar structure but incorporate a deep neural network (DNN) as to approximate the value function and/ or the policy function. In other words, DRL extends the idea of Q-learning with DNN. The raw sensory data is applied as state $\boldsymbol{s}_t$ and directly treated as input to the DNN. The DNN is utilized to approximate the Q-function $Q(\boldsymbol{s}_t, \boldsymbol{a}_t)$, which calculates the optimal value for each possible action given state $\boldsymbol{s}_t$. This method is called Deep Q-Network (DQN). The Q value function $Q^{\pi}(\boldsymbol{s}_t, \boldsymbol{a}_t)$ for given policy π is defined as

$$Q^{\pi}(\boldsymbol{s}_t, \boldsymbol{a}_t) = \mathbb{E}\left[R_t | \boldsymbol{s}_t, \boldsymbol{a}_t\right], \tag{3.3}$$

where $R_t = \sum_{i=t}^{T} \gamma^{i-t} \cdot r(\mathrm{s}_t, \mathbf{a}_t)$. The equation can be unrolled as

$$Q^{\pi}(\boldsymbol{s}_t, \boldsymbol{a}_t) = \mathbb{E}_{s_{t+1}}\left[r_t + \gamma Q^{\pi}(\boldsymbol{s}_{t+1}, \boldsymbol{a}_{t+1}) | \boldsymbol{s}_t, \boldsymbol{a}_t\right]. \tag{3.4}$$

Let $\boldsymbol{\omega}$ represent the weights in the DQN. Suppose the DQN $Q(\mathrm{s}_t, \mathbf{a}_t, \boldsymbol{\omega}) \approx Q^{\pi}(\mathrm{s}_t, \mathbf{a}_t)$. We can define a loss function as

$$J(\boldsymbol{\omega}) = \mathbb{E}\left[\left(r_t + \gamma Q(\mathrm{s}_{t+1}, \mathbf{a}_{t+1}, \boldsymbol{\omega}) - Q(\mathrm{s}_t, \mathbf{a}_t, \boldsymbol{\omega})\right)^2\right]. \tag{3.5}$$

The sum of the first two terms on the right-hand-side is defined as the target value, i.e., $y_t = r_t + \gamma Q(\mathrm{s}_{t+1}, \mathbf{a}_{t+1}, \boldsymbol{\omega})$.

In order to solve the instability problem during the training, the authors in [8] adopted two key strategies: *experience replay* and *target networks*. First, the history of the transitional states and actions is stored as *experience*. The DQN is trained with batches of data that are sampled randomly from the experience, so as to break the correlation between sequential data samples. In fact, mini-batches are randomly drawn from the experience in order to apply stochastic gradient decent (SGD) to further reduce the correlation. Second, an additional target network is introduced to calculate the target value $y_t = r_t + \gamma Q(\mathrm{s}_{t+1}, \mathbf{a}_{t+1}, \boldsymbol{\omega}')$ in the training process,

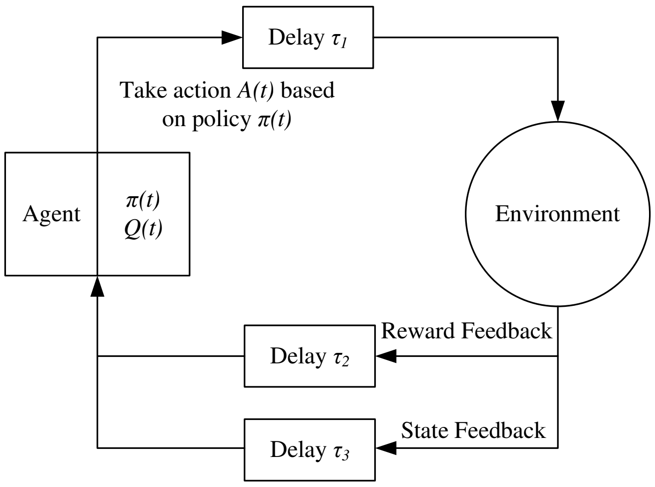

Figure 3.1: Reinforcement learning design for congestion control.

whose weights ω' are updated periodically with the running weights. The target value will become stable after certain amount of steps in the training process.

3.4 System Model, Assumptions and Problem Statement

3.4.1 Network Architecture

In this chapter, a general setting of congestion control is considered, as shown in Fig. 3.2, where a set of remote hosts serving a set of mobile users (the last hop could also be wired). Each end-to-end path, from a remote host to a mobile user, consists of multiple hops. The remote hosts apply a TCP congestion window (cWnd) based protocol. The base station (e.g., eNodeB) maintains separate queues for different mobile users it serves. The two features of the general setting are: competitions among different flows at bottleneck links and potentially multiple bottlenecks along the end-to-end path.

Most prior works assume that the last wireless hop is the single bottleneck. Under this assumption, the round-trip time (RTT) of a user, $\tau_{RTT}(t) = \tau_p + \tau_q(t)$, where τ_p is the *propagation delay* and $\tau_q(t)$ is the *queuing delay*, seems independent to other users, since the eNodeB maintains separate queues for different users. However, even in this case, the multiple queues at the eNodeB are still coupled due to the transmission scheduling algorithm used at the base station [43]. Furthermore, the flows may still compete with each other for transmission resources and buffer storage along the multihop path if they share common nodes.

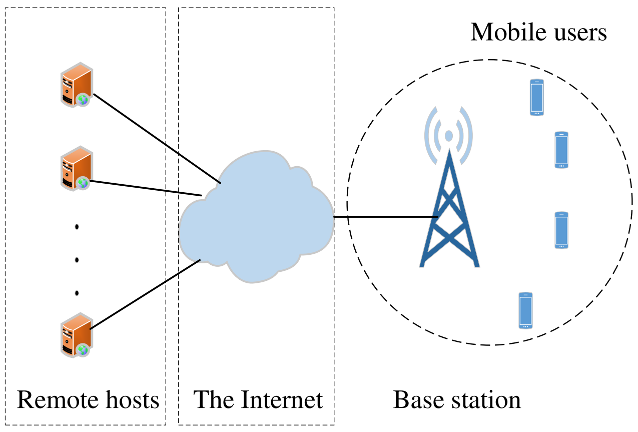

Figure 3.2: System architecture for TCP over wireless.

The general problem of congestion control should be treated as a *delayed, distributed decision making problem*. Each sender needs to decide the congestion window size (cWnd) and/or the sending rate. We focus on cWnd since it can be implicitly translated into the sending rate according to the TCP clocking phenomenon [69]. The "delayed" feature means the feedback from the receiver about the network condition is usually received a round trip time (RTT) later; and the action senders takes will influence the bottleneck queue after a forward propagation delay. If the global information on each user's strategy, the network topology, and traffic condition were known, one could have made perfect decision. But the global information is usually unavailable and the users do not cooperate on congestion control, which entails "distributed" decision making. Although these features have been considered in prior work, e.g., modeling TCP throughput as delayed differential equations, they all pose great challenges to a DRL based congestion control design.

3.4.2 Partially Observable Information

In the congestion control process, the information each sender can acquire is partial and delayed. The measured RTT can only tell the total delay, but lacks the details of the delay on each hop, on forward and backward delays, and on propagation and queueing delays. One popular approach is to approximate the propagation delay by the minimal RTT. In addition, as discussed, the acquisition of RTT and the effect of action are both delayed. Therefore, congestion control is actually a partially observable Markov decision process (POMDP).

The problem of congestion control could be interpreted as a sender algorithm that explores the network environment and exploits the cWnd to properly transport data. This process is conducted by many other senders as well due to shared networking resources. Therefore, the environment one sender sensed could be also affected by other users' decisions and constantly changing. In this chapter, we proposed integrated solution to deal with the "multi-agent" feature of the congestion control problem.

For the POMDP problem, it helps to utilize historical information to exploit the momentum and correlations in the process. However, utilizing the historical information is non-trivial for the associated time and space complexity. In DNN, a promising solution is recurrent neural network (RNN), which is effective to capture the temporal, dynamic behavior from a time series.

3.4.3 Basic Assumptions

To make the design general, we do not assume the system is Markovian. In the past, most of the TCP variants, such as [70, 40], make control decisions based only on the current state, since they have a basic assumption that the next state only depends on the current state, no matter what congestion signal they use: delay or loss. In the recent work [65], the exponential average over the historical delay is utilized. This an intuitive solution to the problem of congestion control because the current state alone is delayed and partial. As discussed, not only the sending rate is determined by the states of one RTT before, but also the states of queues and latency depend on the state one propagation delay ago. In short, the Markovian assumption may be too simplistic and it is helpful to exploit historical information for better decision making.

In real network environments, received signals are usually noisy, which can be mitigated by an exponential window moving average to acquire the stable information. We thus utilize a convolutional neural network (CNN) as an automatically tuned filter to extract stable information. To make the model mathematically tractable, the amount of previous states to be considered is limited to a window size of L.

We make no assumption on how the users compete for resources. The information senders could acquire is very limited in practice. Many existing algorithms are based on certain assumptions of network conditions. For example, Sprout [42] assumes that the only dynamic component of delay is queuing delay, and more important, it is self-inflicted, meaning that it is solely determined by the sending rate and channel capacity. This assumption may be strong since the traffic flows are coupled by the transmission scheduling at the BS, and cross-traffic may also affect the propagation delay when queues and transmission capacity are shared in the wired hops. For a scheme to be practical, the server should not need to know if the physical network is wired or wireless, how many bottlenecks are out there, and what scheduling algorithms are used at each hop. Therefore, it is better to make no extra assumptions the physical network. We thus assume the information a sender could acquire is its own sending rate, congestion window cWnd, and its measured RTT.

3.4.4 Network Modeling

Without loss of generality, suppose there are M hosts serving M mobile users. The traffic model adopted in this chapter is based on TCP clocking [69]; the sending rate can be implicitly determined by the cWnd and RTT. The congestion window cWnd is the maximum amount of TCP segments the server can inject into the network without ACK. Thus the network and receiver can control the sending pace by delaying or withholding ACKs. The benefit of focusing on cWnd is the reduced control action dimension.

To simplify notation, we omit the subscript i for server i in the following presentation. Let the sender cWnd be $w(t)$. Recall the RTT is $\tau_{RTT}(t) = \tau_p + \tau_q(t)$, where τ_p is the propagation delay, and $\tau_q(t)$ is the total queuing delay incurred at one or more bottleneck links along the end-to-end path. The τ_p can be estimated by the minimum RTT within a time window. The instantaneous sending rate, $x(t)$, and its relationship with cWnd $w(t)$ at time t, is given by [69]

$$\int_{t-\tau_{RTT}(t)}^{t} x(\iota)d\iota = w(t). \tag{3.6}$$

Differentiating (3.6) and rearranging terms, we have [69]

$$x(t) = \frac{x(t - \tau_{RTT}(\tilde{t}))}{1 + \dot{\tau}_{RTT}(t - \tau_{RTT}(\tilde{t}))} + \dot{w}(t), \tag{3.7}$$

where $\tilde{t} = t - \tau_{RTT}(t)$. Notice that the instantaneous sending rate at time t not only depends on the sending rate one RTT ago, but also the derivative of the window size and the derivative of RTT one RTT ago.

Therefore, the congestion control process can be viewed as a "combined" sparse reward process. Combined means it is not a complete sparse process, since the current action can still be rewarded, while the previous actions would also influence the reward of the current step as well. Moreover, the window size $w(t)$ is an integer, and the influence of additive increase (AI) or additive decrease (AD) of $\frac{1}{w(t)}$ will be delayed until $w(t)$ packets are received.

3.4.5 Utility Function

We next define a utility function for training and evaluation of the proposed algorithm. For resource allocation/traffic engineering, the α fairness function is widely adopted [65]. In this model, the utility function is defined as

$$U_\alpha(\iota) = \begin{cases} \log(\iota), & \text{if } \alpha = 1 \\ \frac{\iota^{1-\alpha}}{1-\alpha}, & \text{otherwise.} \end{cases} \tag{3.8}$$

where parameter α determines different types of fairness. For example, if $\alpha \to \infty$, maximizing the sum utility becomes a max-min problem. If $\alpha = 1$, maximizing the sum utility would achieve proportional fairness. In FAST TCP [71], the authors adopt this utility function and prove the fairness of the proposed congestion control algorithm.

In this chapter, the goal is to trade-off between throughput and latency. For high throughput, the sending rate (i.e., the cWnd) should be set high, to ensure the bottleneck queue be nonempty (so the bottleneck capacity can be fully utilized). On the other hand, for low latency, the sending rate should be small to ensure low occupancy level at the bottleneck queue (so the queueing delay is low). We adopt the following utility function to trade-off the two design goals [65]

$$U(x(t), \tau_{RTT}(t)) = U_\alpha(x(t)) - \beta U_\alpha(\tau_{RTT}(t)). \tag{3.9}$$

where coefficient β indicates the relative importance of latency and throughput. *The goal of the congestion control algorithm is to optimize the expectation of* (4.7) *by properly setting cWnd.*

3.5 TCP-Drinc Design

In this section, we present the design of Deep ReInforcement learNing based Congestion control (TCP-Drinc). We first present the feature engineering process, which are some necessary transformation and statistics of the given information that can provide additional features. The state and action space and the reward function are then defined as the cornerstone for the proposed algorithm. Finally, the proposed TCP-Drinc algorithm is presented.

3.5.1 Approach for Multi-agent Situation

As discussed, we are dealing with a multi-agent competition problem. At a bottleneck, multiple flows compete for network resources such as buffer and capacity. In addition, the exploration strategy of other users could be sensed as dynamics of the environment, which could lead to misinformed state feedback and result in an unstable training process and poor performance. We tackle this problem by integrating three methods: (i) feature selection, (ii) clipped rewards, and (iii) a modified training process. The feature selection method is presented in Section 3.5.2. By hand picking the features that are indicative of the system state, we can deal with abnormal system dynamics caused by other users unknown strategies. Reward clipping can reduce the reward variation in different environments and increase the learning stability, which is discussed in detail in Section 3.5.4.

For the training process, we combine the suggestion from [72, 73, 74] to have: (i) a relatively small experience replay buffer, and (ii) concurrent experience replay trajectories (CERTs) for sampling. The first method can mitigate the non-stationary nature of the local experience sensed by single agent. The normal experience replay buffer size is multiples of 10K. In this work, we set the buffer size to 1600, meaning the algorithm only keeps the most recent 1600

samples. For CERTs, each time the agent takes the same samples for training. To ensure this, the only synchronization needed is to assign the same random seed to each agent at the beginning of training. It requires no synchronization afterward, while guaranteeing the independent operation of each agent.

3.5.2 Feature Engineering

During the TCP session, the sender acquires the following information: (i) inter-arrival time of ACKs, (ii) congestion window size, and (iii) the RTT. It is necessary to pre-process the data. The benefits are two-fold: accelerating the training process and better explanation of the model. From (3.6) and (3.7), the current sending rate is determined by the cWnd difference and the sending rate one RTT ago. Therefore, cWnd difference, as measured by the difference in two consecutive time slots, and RTT τ_{RTT} should be collected as features.

In the transportation process, the minimum RTT for a certain period of time provides an estimation of the propagation delay. The reason why not using the minimum RTT of the entire transmission process is to take into account the possibility of change of routing. Denote the minimum RTT as $\hat{\tau}_p$. When cWnd is smaller than the product of capacity and $\hat{\tau}_p$, the measured RTT will always converge to $\hat{\tau}_p$. The minimum RTT $\hat{\tau}_p$ can also be treated as state information, since it helps to differentiate the different conditions of the system. We thus take the ratio $v_{RTT} = \hat{\tau}_p/\tau_{RTT}$ as a feature, which is indicative of the relative portions of the propagation delay in the RTT. Furthermore, the difference between RTT and the minimum RTT, i.e., $\delta_{RTT} = \tau_{RTT} - \hat{\tau}_p$, is indicative of the network congestion level. This value provides an estimate of the overall queuing delay. To track the minimum RTT, the estimation will be updated at 10 RTT intervals. The last feature we take is the inter-arrival time of ACKs, which partially indicates the goodput of the network.

3.5.3 Definitions of States and Actions

We next define the state and action space of the TCP-Drinc system. The non-Markovian nature of the problem makes it necessary to take history into consideration. As discussed, we consider the following features of a TCP connection: (i) cWnd difference Δw, (ii) RTT τ_{RTT}, (iii) the minimum RTT over RTT ratio v_{RTT}, (iv) the difference between RTT and the minimum RTT δ_{RTT}, and (v) inter-arrival time of ACKs τ_{ACK}. The algorithm runs in slotted time (e.g., 10 ms per time slot). In each time slot t, we measure the above features and record them as the state of the time slot s_t. If there is no events (e.g., ACK received or cWnd changed) in a time slot t, we have $\mathrm{s}_t = \mathrm{s}_{t-1}$. We then take the combination of the states of M consecutive time slots as as one system state. Therefore, the state of TCP-Drinc is a two-dimensional tensor, denotes as $\mathcal{S}$ and given by

$$\mathcal{S} = [\mathrm{s}_0, \mathrm{s}_1, ..., \mathrm{s}_{M-1}], \tag{3.10}$$

where $\mathrm{s}_m = [\Delta w(m),\, \tau_{RTT}(m),\, v_{RTT}(m),\, \delta_{RTT}(m),\, \tau_{ACK}(m)]$. The reward value for each time slot is calculated as in (3.15).

The action space consists of 5 actions on cWnd. In order to trade-off between agile and robust adjustment through the process, we adopt actions $w = w \pm 1$ as exponentially increase/decrease and actions $w = w \pm \frac{1}{w}$ as linearly increase/decrease. The exponentially increase/decrease allows the agent to quickly adjust the window to deal with fast variations of the environment. The linearly increase/decrease can enhance the robustness when the agent decides to doodle around a proper operating point. In addition, the *no change* action is also included in the action space. Therefore the action space is defined as

$$\mathcal{A} = \{w = w \pm 1; w = w \pm \frac{1}{w}; \text{no action}\}. \tag{3.11}$$

3.5.4 Reward Calculation

Reward design is also challenging for the congestion control problem. The RTT measurements at the sender side is usually noisy. Factors such as the bursty sending process, the varying processing times at the devices along the path, and recovery from packet losses in the physical layer all contribute to the measurement noise. However, it is important to acquire accurate RTT measurements since a misinformed RTT might result in wrong reward to the agent action, and affect the convergence of the training process. In this chapter, we adopt a low-pass filter with a fixed window size of RTT measurements, which ignores frequent, small latency jitters.

The goodput is measured by calculating the number of ACKs received during a given time window. One of the important benefit of this method is we directly calculate the goodput with consideration of random packet losses. This measurement is constantly varied due to factors such as the bursty sending process and uneven distribution in the intermediate queues, as well as packet losses caused by random link error or congestion. In this chapter, we take the exponential window moving average (EWMA) over sliding window of one RTT.

Recall that the action of sender will take effect after one RTT, and the impact in the future is discounted exponentially. The overall impact of an action (i.e., change of cWnd), Δw, on the future system goodput, denoted as $z(t)$, can be estimated as

$$z(t) = \sum_{\iota=t}^{\infty} \hat{z}(\iota)(1-\eta)\eta^{\iota-t}, \tag{3.12}$$

where $\eta < 1$ is the decay rate of the action's influence in the future, and $\hat{z}(t)$ is the measured goodput at time t. In order to make the calculation tractable in time and storage, we cut off the time to have a horizon of L. The approximation of $z(t)$ for an L horizon is

$$z(t) = \sum_{\iota=t}^{L} \hat{z}(\iota) \cdot \frac{(1-\eta)}{1-\eta^{L+1}} \cdot \eta^{\iota-t} \tag{3.13}$$

This is a critical component for the end-to-end algorithm that can learn about the future.

For fairness, we compute the utility function as

$$U(z(t), \tau_{RTT}(t)) = U_{\alpha}(z(t)) - \beta U_{\alpha}(\tau_{RTT}(t)). \tag{3.14}$$

In the context of Q-learning, the Q-value denotes the expectation of the overall reward. If we only adopt the utility (3.14) in the reward function, the agent may keeps on adopting one action, which returns a positive utility value but does not converge to the optimal operating point. Therefore, we define the reward function as the utility difference, as

$$r(t) = U(t + \tau_{RTT}(\tilde{t})) - U(t), \tag{3.15}$$

where $\tilde{t}$ is one RTT after t and $\tau_{RTT}(\tilde{t})$ is the measured RTT.

Furthermore, for different network environments (e.g., different link capacities and propagation delays), the reward calculated using (3.15) may have a great range of variations. In order to make the TCP-Drinc design more general and adaptable to various network environments, we clip the reward value to the range of $[-1, 1]$. With clipping, although the training process could be relatively longer in some cases, the convergence of the training process could be improved (i.e., by avoiding large oscillations) and the same TCP-Drinc design can be applied to varying network environments (e.g., changing of link capacity).

3.5.5 Experience Buffer Formation

The TCP-Drinc design is shown in Fig. 3.3. We take the specifically designed structure of the training samples to implicitly learn and predict the future. As shown in Fig. 3.1, the feedback of ACKs carry the system state with delay $\tau_2(t)$. Therefore, the currently sensed state $\mathbf{s}(t)$ is actually the system state $\mathbf{s}_s(t - \tau_2(t))$. In addition, the action takes $\tau_1(t)$ to take effect on the queues of intermediate nodes. Therefore, the action that actually works should be $\mathbf{a}_s(t - \tau_1(t))$. To deal with such delays, we could look into the future for $\tau_1(t) + \tau_2(t)$ to predict the system state based on the current state and action, and then generate the next action. However, such prediction is challenging since (i) the delays $\tau_1(t)$ and $\tau_2(t)$ are stochastic; (ii) the predictions are usually noisy and error-prone; and (iii) the computation could be intensive due to the high dimension of the system.

In this chapter, we introduce a new strategy to address this problem. First of all, we use a buffer to store the running dynamics history with $\{$state, action, reward$\}$. Every time when a new tuple $\{\mathbf{s}(t)$, $\mathbf{a}(t)$, $r(t)\}$ is inserted, we looking backward in the buffer to find the older tuple that formed one RTT before. Then we combine these two tuples to obtain a complete training sample as $\{\mathbf{s}(t - \tau_{RTT}(t))$, $\mathbf{a}(t - \tau_{RTT}(t))$, $\mathbf{s}(t)$, $r(t - \tau_{RTT}(t))\}$. This sample is then stored in the experience buffer to be used in the training process. This way, the DRL network can better learn the reward based on the current and future states.

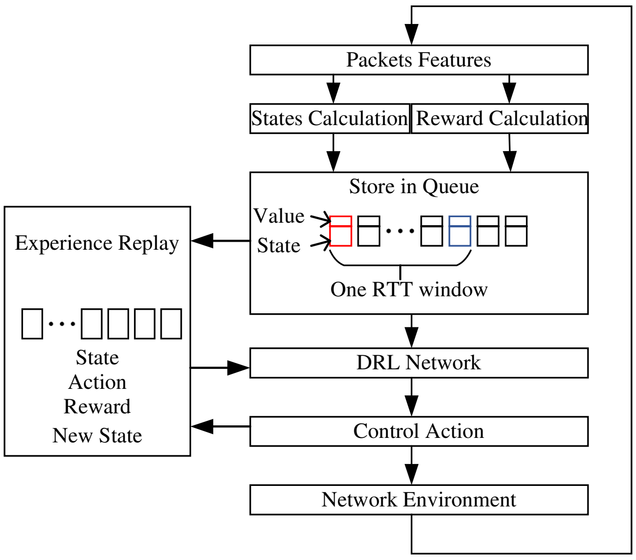

Figure 3.3: The TCP-Drinc system architecture.

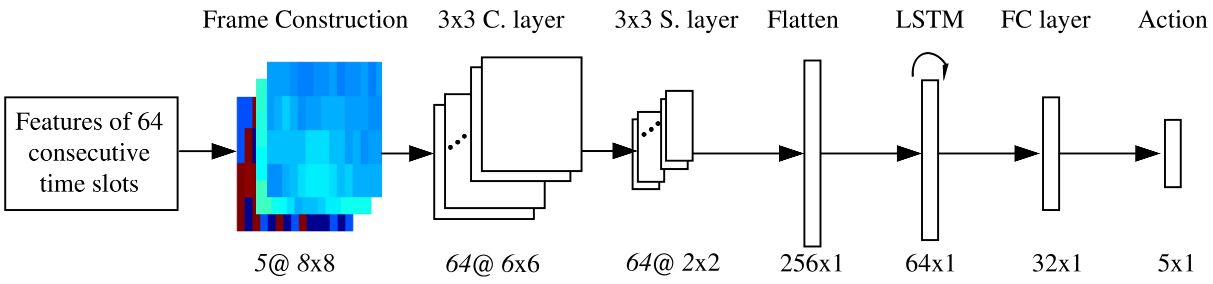

Figure 3.4: Design of the proposed convolutional neural network (in the figure, "C." represents the convolutional layer, "S." represents the down sampling (pooling) layer, "FC" means fully connected).

3.5.6 Agent Design

With proper definitions of space, action, reward calculation, and the experience buffer design, we are now ready to present the DRL network design, which is based on a convolutional neural network model as shown in Fig. 3.4. The DRL network takes features (of 64 consecutive time slots) as input and generate the next action, which is on how to adjust the cWnd.

In prior works such as [65], the EWMA is utilized to handle the noisy state information. However, this method suffers from the long tail effect when acting as a filter, and it could miss the rich information in each feedback. In this chapter, we proposed a new approach to fully utilize the rich feedback information by adopting a convolutional neural network (CNN). In the process, note that the feedback information itself could serve as an indicator of how the system operates. Therefore, we use the combined states of the M consecutive time slots including and before the current time t and divide them in to frames as inputs. For instance, we set $M = 64$ and obtain 5 frames. Each frame has a size 8×8 and consists of data from one of the five features, as shown in Fig. 3.4. With the convolutional layers and pooling layer, the more stable, higher level features can be abstracted from the raw state information.

Furthermore, the non-Markovian nature of the problem should also be addressed, as well as the action taking effect delay τ_1 and feedback delay τ_2 (see Fig. 3.1). A promising approach is to incorporate an LSTM to handle the correlation in a time series [75]. Through the back-propagation through time (BPTT), this structure exploits the memory to extract system features. As in Fig. 3.4, the LSTM layer is placed after the CNN extracts the stable features. In [75], the authors proposed two training methods: Bootstrapped Sequential Updates and Bootstrapped Random Updates. The former executes the training by randomly selecting an episode and then starting from the beginning of the episode. The latter, however, picks a random timestep in an episode and proceeds for a fixed amount of timesteps. In this chapter, we adopt the Bootstrapped Random Updates method to train the network by combining with experience replay.

The fully connected layer is used to calculate the Q-value for each action. Through the entire network, we use the Exponential Linear Unit activation function *ELU*, defined as

$$ELU(\iota) = \begin{cases} \iota, & \iota > 0 \\ \lambda \cdot (e^{\iota} - 1), & \iota \leq 0, \end{cases} \tag{3.16}$$

instead of Rectified Linear Units *ReLU*. Since we have to deal with negative rewards, it is beneficial for not killing the nodes with negative outputs. In the last layer, which is to output the Q-value for actions, no activation function is applied.

3.6 Simulation Study

In this section, we present our extensive simulation study with the NS3 platform over different scenarios and models. The basic configuration of the simulations is first demonstrated. In order to have a comprehensive comparison, we also implement several state-of-the-art congestion control protocols and carry out experiments with them.

3.6.1 Simulation Setup

In this chapter, the deep neural network is generated using Tensorflow [76]. The training is executed with a reasonable speed on a PC with I5-8600k CPU and Nvidia GeForce 1060 3GB GPU. The dropout layer is applied with a 0.2 dropout probability to provide both regularization and ensemble effect. For the DNN, one convolutional layer and one pooling layer are incorporated. The LSTM layer with 64 units is applied after the CNN layers. One fully connected layer is used with the activation function ELU. The output layer is a linear combination of the previous output with 5 outputs, one for each action. The control action is applied every $T = 10ms$. If a time period t does not have any ACK received, we simply copy the the state of the previous time slot $\mathbf{a}_{t-1}$ as input to the DNN (see Section 3.5.3). The minimum RTT is updated every 10 RTTs.

For the simulations, we assume there are N remote-hosts that serve N wired or wireless users. The remote-hosts are cWnd based and running the DRL agent independently, i.e., the DRL agents do not share/exchange information during the TCP sessions. The simulation is based on the classical dumbell topology with two routers in the middle, between the remote hosts and users (see Fig. 3.2).

For fair and comprehensive comparison of congestion control performance, we choose the following set of benchmark schemes that cover most of the existing representative algorithms, including: (i) TCP-NewReno [38], (ii) TCP-Cubic[40], (iii) TCP-Hybla [77], (iv) TCP-Vegas [39], (v) TCP-Illinois [78]. We would mainly focus on their performance in throughput and RTT.

3.6.2 Training Process

The training process is divided into two phases: pre-training and distributed training. In the pre-training phase, we train each agent with the same setup except that only one user is served in order to build the baseline behavior for the agent for N_{pre} episodes. Then the distributed training will further train the competition strategy of each agent independently.

Pre-training

In our simulations, we set $N_{pre} = 20$. The bottleneck capacity is 10 Mbps with 80 ms propagation delay. And one training episode lasts for 500 s. Fig. 3.5 shows the dynamics of cWnd and RTT in the 10th training episode. The learning process is divided into three phases: the exploration probability linear annealing phase, the convergence phase, and the phase of randomly learning of other options. Before the red line is the exploration probability annealing process which involves a large probability of random choice of actions. With the exploration probability decrease to 0.1, which is the end of the first phase, the agent can adjust the action to converge to the *perfect operating condition*, i.e., the cWnd that can fully utilize the bottleneck link capacity without introducing extra queuing delay (the red dashed line in Fig. 3.5(a)). Then with a 0.1 probability, the agent will randomly deviate from the perfect operating point to explore the state space. Then it will repeat this process to train the agent with different network conditions.

Distributed Training

After pre-training, we copy the model to 5 different servers (i.e., there are $N = 5$ servers serving 5 wired users), and let them run the training process independently. We set the random seed to be 17 for all the servers. The basic environment setting is the same and the distributed training runs for $N_{dis} = 100$ episodes. In Fig. 3.6, the average throughput and RTT in the distributed training process are presented. We can see that as the training proceeds, the average throughput is increasing in general. And the average RTT eventually converges toward the minimum RTT of 80 ms.

3.6.3 Congestion Control Performance

In this subsection, we present our experimental results with different network parameters to test the performance of TCP-Drinc, specifically, over situations that deviate from that TCP-Drinc is

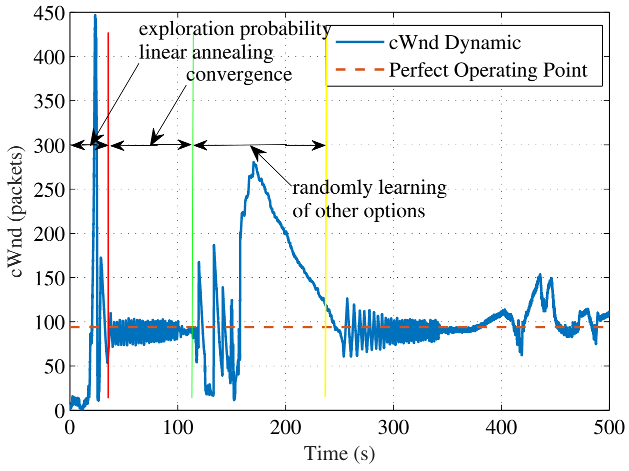

(a) cWnd dynamics

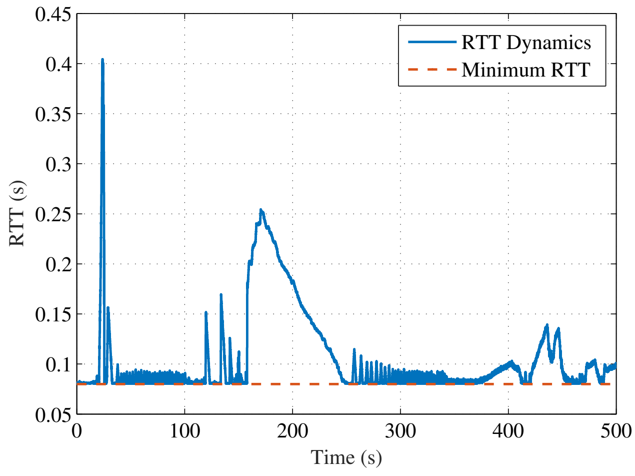

(b) RTT dynamics

Figure 3.5: The dynamics of the single agent pre-training.

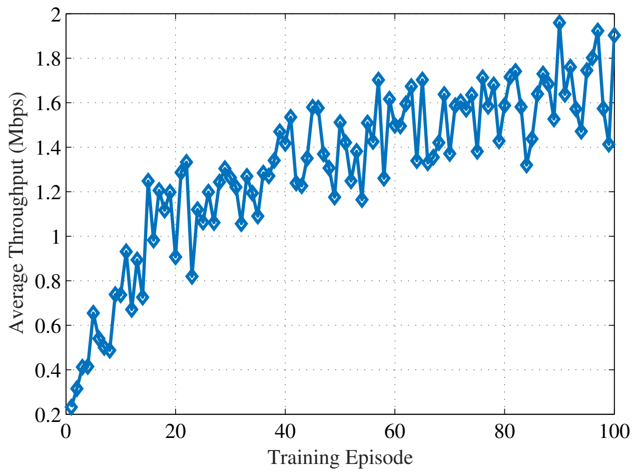

(a) Average throughput

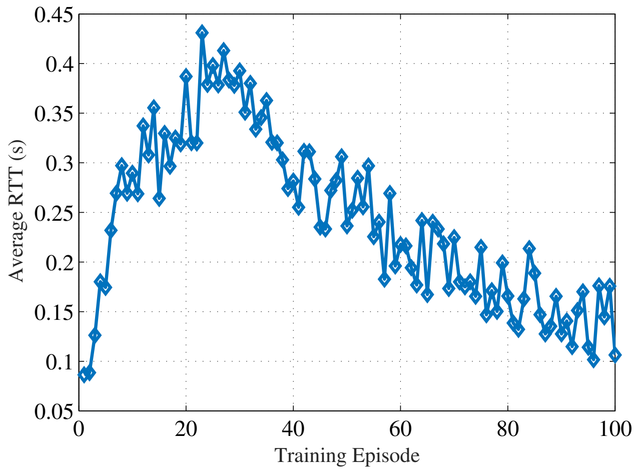

(b) Average RTT

Figure 3.6: The training result of single agent distribute training.

originally trained. As demonstrated above, TCP-Drinc is trained with 5 TCP sessions with 10 Mbps bottleneck capacity and 80 ms propagation delay. Three testing cases are set as follows.

1. 4 users; the propagation delay varies in the range of $[60, 240]$ ms; and the bottleneck bandwidth is 10 Mbps;
2. the number of users varies in the range $[3, 10)$; propagation delay is 80 ms; and the bottleneck bandwidth is 8 Mbps;
3. 4 users; the propagation delay is 100 ms; the bottlneck bandwidth varies in the range of $[5, 20]$ Mbps.

The bottleneck buffer size is chosen as 100 packets. The size of a packet is a 1000-Byte payload plus a 40-Byte header.

As shown in Figs. 3.7, 3.8, and 3.9, the well-trained TCP-Drinc model achieves a promising performance under all the scenarios we simulated. In Fig. 3.7, we present the throughput and delay for increased propagation delay. We can see that all the RTTs increase with propagation delay, while the throughput is relatively stable (except for TCP-Vegas). TCP-Drinc achieves the highest throughput and the second smallest RTT for the entire range of propagation delays. Although TCP-Vegas achieves a lower RTT than TCP-Drinc, its throughput is the lowest, indicating that the low RTT is achieved by keeping the sending rate low and the bottleneck buffer almost empty (i.e., sacrificing the utilization of the bottleneck link capacity). Unlike the loss based protocols, TCP Vegas is a latency based scheme that linearly adjusts its cWnd according to the difference between the current and the minimum RTT. It is effective in keeping RTT low, but is sensitive to network condition changes and suffers from relatively low throughput.

In Fig. 3.8, the throughput and RTT are presented for increased number of users. We can see the capacity for each user decreases with increased number of users. Again, TCP-Drinc achieves the highest throughput and the second lowest RTT. TCP-Vegas outperforms TCP-Drinc with a lower RTT, but at the cost of a low throughput. Fig. 3.9 presents the throughput and RTT achieved under different bottleneck capacity. For increased bottleneck capacity,

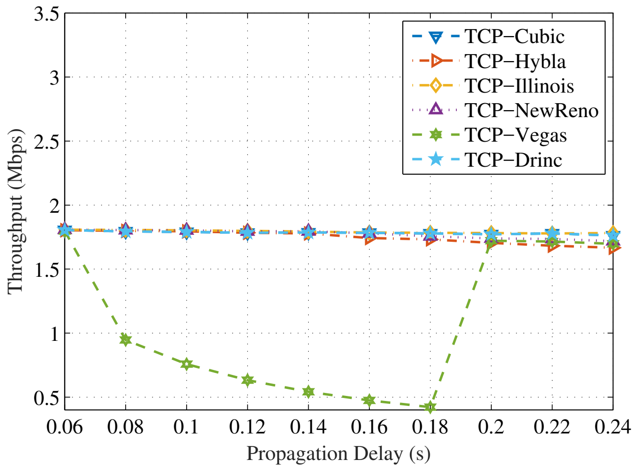

(a) Average throughput

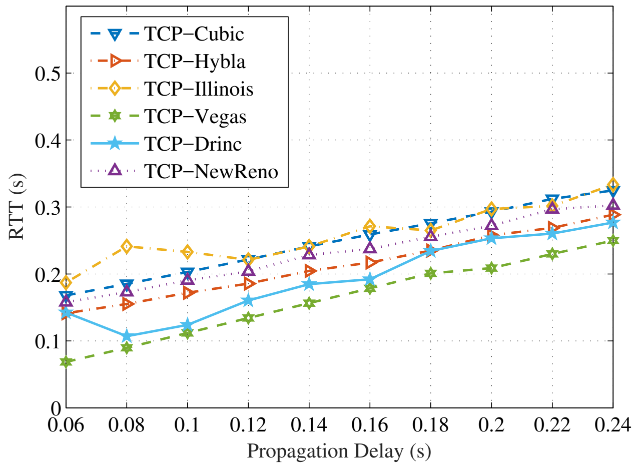

(b) Average RTT

Figure 3.7: Throughput and RTT statistics with different propagation delays.

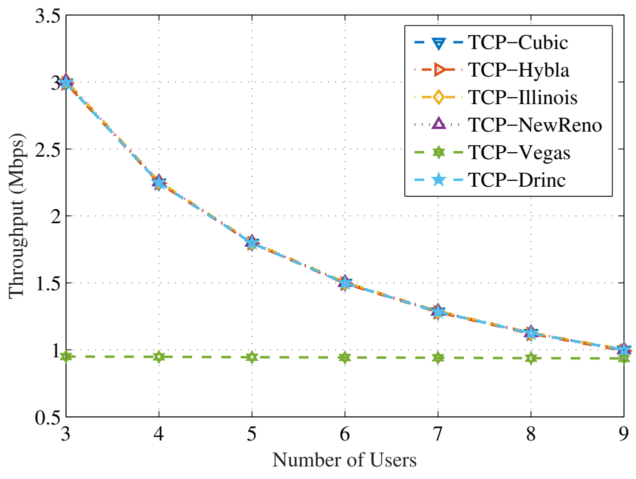

(a) Average throughput

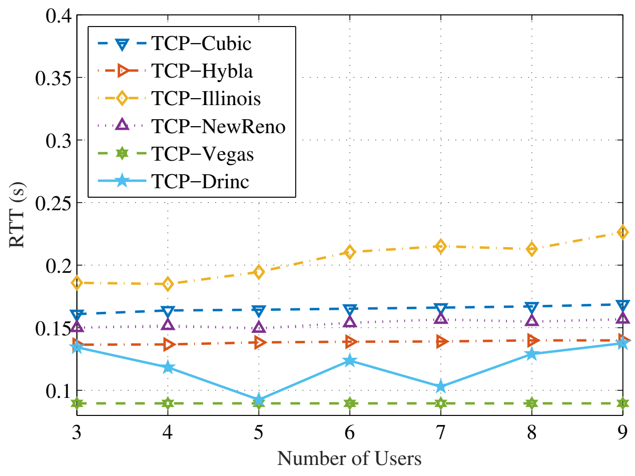

(b) Average RTT

Figure 3.8: Throughput and RTT statistics with different number of users.

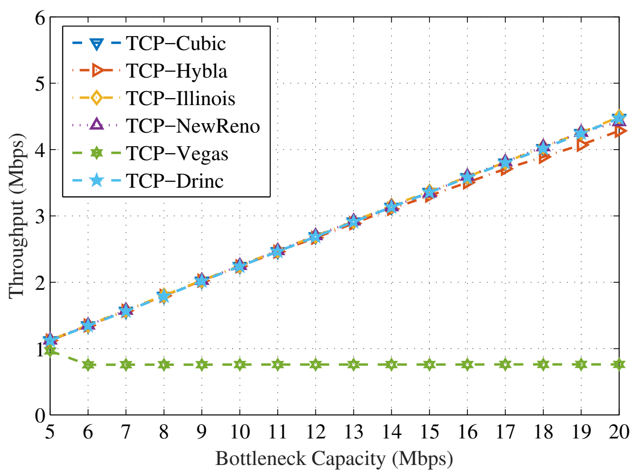

(a) Average throughput

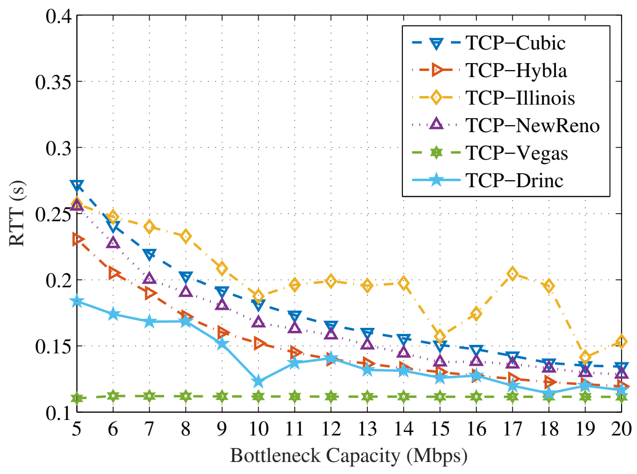

(b) Average RTT

Figure 3.9: Throughput and RTT statistics with different bottleneck capacities.

the throughput increases and the RTT decreases as expected (except for TCP Vegas). Again, TCP-Drinc achieves the highest throughput and the second lowest RTT for the entire range of bottleneck capacity. TCP Vegas can always achieve the lowest RTT, but at the cost of low throughput. TCP-Drinc achieves a comparable throughput as loss based protocols (such as TCP-Cubic or TCP-NewReno), but only introduces a 20% higher RTT than TCP-Vegas. This is because the TCP-Drinc algorithm can always find the operation point that is close to the perfect operating point. We also find that the performance of TCP-Drinc is the best when the network parameters are close to the training scenarios.

We next examine the performance of the schemes under dynamic network settings. In particular, the simulation is executed 100 times, each lasts for 500s. The number of users is 5. The bottleneck capacity is varied at a frequency of 10 Hz; each capacity is randomly drawn from a uniform distribution in $[5, 15]$ Mbps. The propagation delay is also varied at a 10 Hz frequency and each value is randomly draw from a uniform distribution in $[0.06, 0.16]$s. In Fig. 3.10, we plot the combined RTT (x-asix) and throughput (y-axis) results in the form of of 95% confidence intervals. That is, we are 95% confident that the throughput and delay of each scheme are within the corresponding ellipse area. We can see that TCP-Drinc can achieve a comparable throughput performance with the loss based protocols, such TCP-Cubic and TCP-NewReno. Furthermore, TCP-Drinc achieves a much lower RTT performance than the loss based protocols, e.g., at least 46% less than TCP-NewReno and 65% less than TCP-Cubic. TCP-Drinc achieves an over 100% throughput gain over TCP-Vegas at the cost of a 15% higher RTT.

To study the fairness performance of the algorithms, we evaluate the Jain's index they achieve in the simulation. The average fairness index and the corresponding 95% confidence intervals are presented in figure 3.11. The TCP-Vegas and TCP-Illinois achieve the best fairness performance among all the algorithms. TCP-Drinc can still achieve a considerably high fairness index (only 1.9% lower than the best). Note that the best fairness performance of TCP Vegas is achieved at the cost of a poorer throughput performance. It is also worth noting that the 95% confidence interval of TCP-Drinc is the smallest among all the schemes, which is indicative of its robustness under varying network conditions.

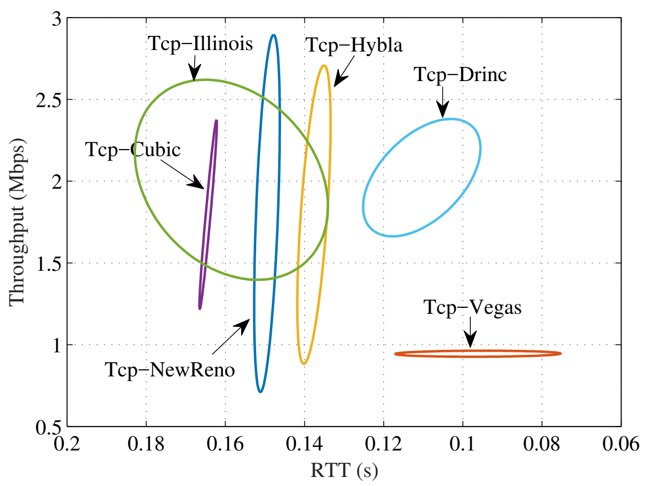

Figure 3.10: Performance of different algorithms over randomly varied parameters.

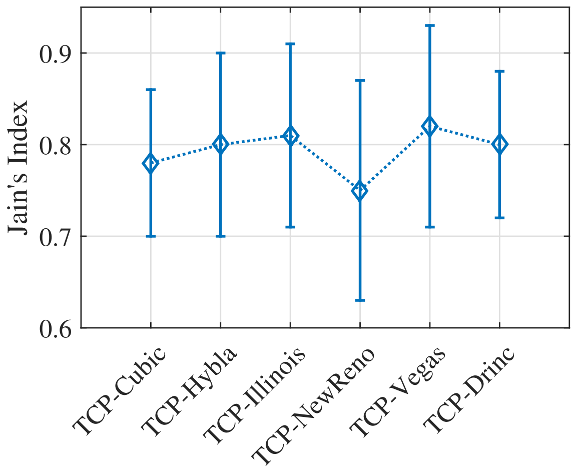

Figure 3.11: Jain's index for each algorithm.

Finally, we evaluate the TCP variants with mobile users. The same network setting is used, except that the last hop is an LTE network with five mobile users. The users move in a disk area of 800 m radius, following a random walk mobility model with 1 m/s speed. The LTE network is simulated using the bulit-in LTE model in NS3 [79]. The wired part has the same configuration as in previous simulations. The simulation results are presented in Fig. 3.12. The LTE base station has a deep and separate queue for each user. Therefore, we do not use TCP-NewReno here since it will introduce a very large RTT in this setting. The proposed algorithm still perform well in the wireless network setting. Its throughput is comparable to the two loss based protocols, with a much reduced RTT. Its throughput is much higher than TCP Vegas while the RTT is only slightly higher.

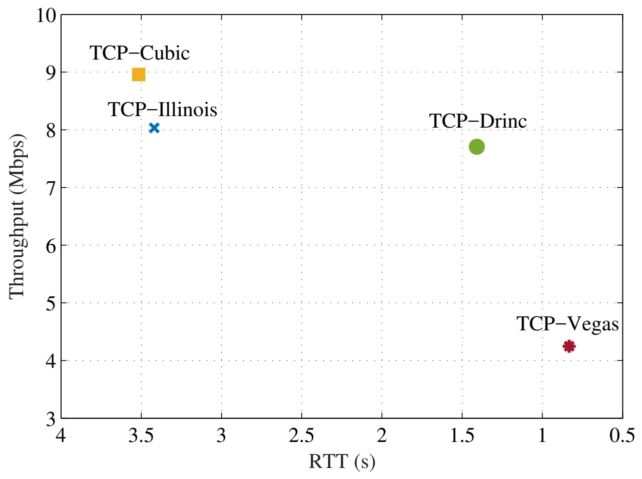

Figure 3.12: LTE network simulation results with the dumbell topology and 5 mobile users.

3.7 Conclusions

In this chapter, we developed a framework for general adaptive congestion control based on deep reinforcement learning techniques. The proposed scheme does not require accurate models for the network, scheduling, and network traffic flow; it also does not require training data. The detailed design of the propoed TCP-Drinc scheme was proposed and the trade-offs were discussed. Extensive simulations with NS3 were conducted to validate the superior performance over several benchmark algorithms.

Chapter 4

DORA: A Cross-layer optimization for Robust QoE-Driven DASH over OFDMA Networks Bit Rate Adaption and Resource Allocation

In this chapter, the problem of effective and robust delivery of DASH videos over an orthogonal frequency-division multiplexing access (OFDMA) network is studied. Motivated by a measurement study, we propose to explore the request interval and robust rate prediction for DASH over OFDMA. We first formulate an offline cross-layer optimization problem based on a novel QoE model. Then the online reformulation is derived and proved to be asymptotically optimal. After analyzing the structure of the online problem, we propose a decomposition approach to obtain a UE rate adaptation problem and a BS resource allocation problem. We introduce stochastic model predictive control (SMPC) to achieve high robustness on video rate adaption and consider the request interval for more efficient resource allocation. The efficacy of the proposed DORA-RI scheme is validated with simulations.

4.1 Introduction

Recent years have witnessed the tremendous increase in mobile video traffic. Video has now dominated the mobile data traffic for over 60 percent in 2016, and is expected to account for over 75 percent in 2021 [1]. At the same time, the rapidly growth in both the overall mobile traffic (which has increased 18-fold since 2011) and the number of mobile devices (429 millions were added in 2016) have made mobile video streaming a great challenge. In addition, the instability nature of wireless links will make the situation even worse. There is a compelling need to achieve high efficiency and robustness of video delivery over wireless networks, while guaranteeing users' Quality of Experience (QoE). This problem should be studied from both the wireless infrastructure and user aspects.

Video streaming has drawn great attention for decades. The early works are mainly based on the User Datagram Protocol (UDP), which can provide timely transmission compared with Transportation Control Protocol (TCP) that is designed for reliability over timeliness. However, the deployment of UDP based algorithms is challenging due to the incompatibility with firewalls and other types of middleboxes. On the other hand, TCP is supported by most middleboxes for its reliability and security. The congestion control algorithms facilitate the timeliness of transmission as well. Therefore, Hypertext Transfer Protocol (HTTP) based on video streaming is now the mainstream technique. In particular, Dynamic video streaming over HTTP (DASH), which can adapt to the variation of network conditions, is recognized as a promising technique to enhance the user QoE. Many commercial video services, e.g., YouTube and Netflix, are all based on DASH, which have accounted for more than half of the total Internet traffic in North America in 2016 [7].

Among different generations of mobile transmission techniques, the 3GPP-Long Term Evolution (LTE) and Wi-Fi (802.11 standard) are the two most popular. The Orthogonal frequency-division multiplexing (OFDM) is the common method of both standards that encode and transmit digital data on multiple subcarriers of a broadband channel. OFDM is expected to continue serving the next generation wireless networks for its ability on tackling narrowband interference and frequency-selective fading with a low complexity. OFDM also introduces great flexibility by allowing dynamically assigning subcarriers, time, and power to each user in order to accommodate customized QoS requirements, such as transmission rate [80, 81, 82] or power efficiency [83]. The similar technique has been applied to smart grid as well [84, 85, 86, 87]. Some cross-layer designed could be found in [88, 89, 90, 91, 92, 93, 94, 95].

Consider a video user equipment (UE) that receives a DASH video through an OFDM network, as shown in Fig 4.1. The two techniques are in different layers in the protocol stack and have different design goals. However, for video streaming, both of them should be designed for the ultimate goal of guaranteeing user QoE. In this chapter, we study the cross-layer, joint design of DASH and OFDM. In DASH, the video consumers take the control of choosing

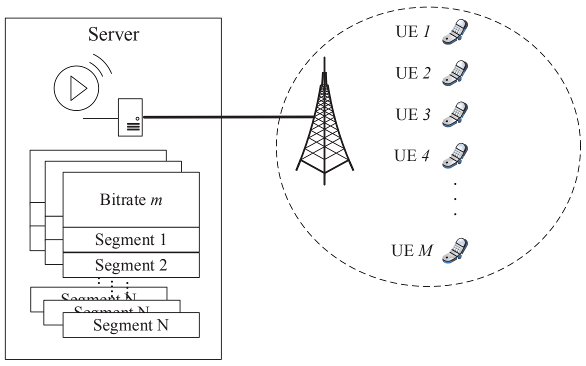

Figure 4.1: DASH mobile video streaming system architecture.

different data rates for future video segments, which are coded (or stored) at the video server. The corresponding information is sent to the consumers at the beginning of video transmission. Resource allocation in OFDMA networks, on the other hand, is executed at the base station, which takes into account various factors such as channel state information (CSI), power budget, and user QoE requirement and determines the optimal resource allocation for multiple video UEs.

4.1.1 Motivation

To provide useful insights into the problem of DASH based video streaming over OFDMA networks, we conducted a measurement study using dash.js [96] in Broun Hall, Auburn University, Auburn, AL, USA over Version LTE. The video source is placed on a remote server and coded into 10 different bit rates ranging from 254 kbps to 14931 kbps. We collected the video playback trace information over LTE in 1 hour daytime and 1 hour night time. Define *request interval* as the period between when the request for the next segment is sent and when the first video byte of the requested segment arrives at the user. In this experiment, we measured the request interval of the DASH video session, as well as the link capacity that can be acquired by measuring the download speed of each video segment.

As shown in Fig. 4.2, the request interval could be as large as 10 s and 80 percent of the intervals are in the range from 0.2 to 0.4 s. However, most of the joint design of DASH and scheduling algorithms do not fully consider this relatively large period of time and still allocate resources to the video users, even though no transmissions are needed during this

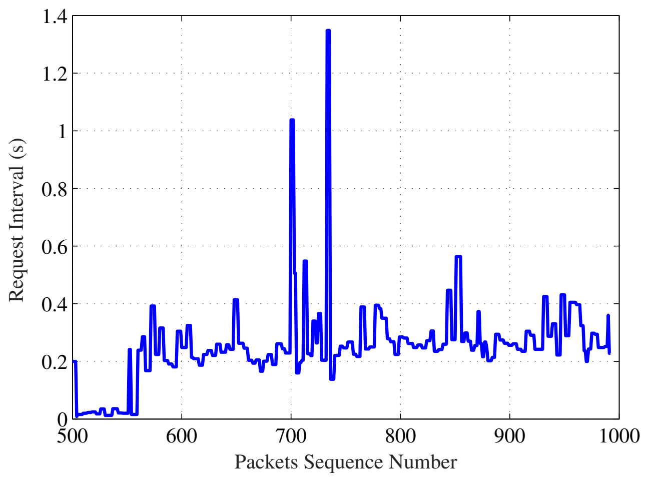

Figure 4.2: The variations of request intervals obtained in our measurement study over an LTE link.

interval (except for the first packet of the requested segment). Motivated by this observation, we propose a new formulation of the resource allocation problem at the BS by exploiting the request intervals (see Section 4.3).

In addition, we measured the capacity of the LTE link during playback. Usually the capacity will be influenced by factors such as fading and shadowing, which will all trigger the capacity variation at small timescales. In DASH, many existing rate adaption schemes are based on the average downloading capacity over one segment, which is assumed to be slowly varying and relatively stable. In Fig. 4.3, we present the average capacity of one segment, which exhibits quite large variations over time. Such large variations could make the existing rate adaptation schemes ineffective. Motivated by this observation, we propose a model predictive control based optimization of the rate adaption at the video user side to achieve better robustness (also see Section 4.3).

4.1.2 Contributions and Organization

We address the cross-layer QoE-driven optimization problem of DASH over OFDMA networks in this chapter. The contribution of this work is three-fold:

1. We develop a new QoE model and formulate an *offline* optimization problem jointly considering the new QoE model as well as the specific resource allocation model in OFDMA networks.

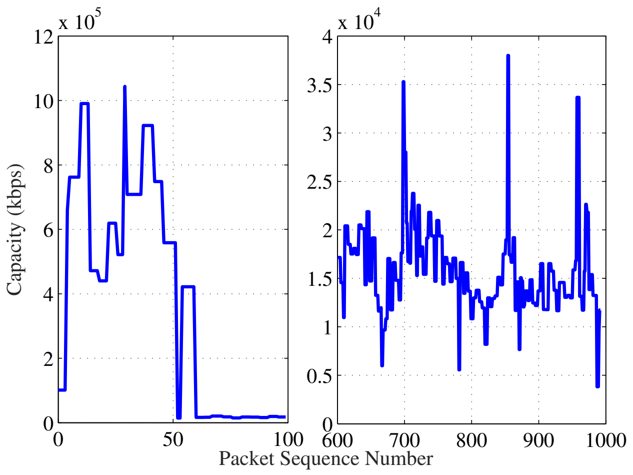

Figure 4.3: The variations in the average capacity of an LTE video link.

2. We then derive an *online* optimization problem to approximate the offline problem. We analyze the online problem and decompose it into a BS resource allocation problem and an UE rate adaptation problem, for each of which effective solution algorithms are developed. More important, we also prove the asymptotic optimality of the online algorithm.

3. Extensive simulations are conducted to validate the performance of the proposed algorithms. The results show that the proposed algorithms can achieve a 40% less rebuffering ratio than the state-of-art MPC based algorithm.

The remainder of this chapter is organized as follow. The System model is presented in Section 4.2. In Section 4.3, we first formulated a globe optimization, offline problem and then transform it to an online optimization problem. The analysis and problem decomposition are presented in Section 4.4. In Section 4.4, we further explicitly take the request interval of the users into consideration for more efficient resource allocation. The rate-adaption process is analyzed and then a robust scheme is proposed. Our simulation study and results are presented in Section 4.5. The related works are discussed in Section 4.6 and we conclude this chapter in Section 4.7. The notation used in this chapter is summarized in Table 4.1.

Table 4.1: Notation

Symbol	Description
N	total number of users
M	total number of subcarriers
W	total bandwidth available
κ	bandwidth per subcarrier
P	total transmission power
g_{im}	channel gain of user i on subcarrier m
v_{im}	user i's time share of subcarrier m
p_{im}	average trans. power allocated to user i on subcarrier m
r_{im}	maximum rate user i can achieve on subcarrier s
r_i	maximum rate user i can achieve
S_i	video length for user i
K_i	number of segments for user i
$R_i[k_i]$	data rate of segment k for user i
$q_i(R_i[k_i])$	quality of segment k to user i given data rate R_k
$q_i[k_i]$	quality at time step k_i
a, b	parameter of quality model
$Q[k_i]$	original definition of QoE
$Q^{fair}[k_i]$	QoE definition with utility function
$m_i[K]$	average video quality of the playback process for user i
$\text{Var}_i[K]$	video quality variation of the playback process for user i
$\text{Reb}_i[K]$	rebuffering ratio of the playback process for user i
T_i^s	Startup delay
θ, λ, η	negative coefficients for QoE
$Q_i^{online}[k_i]$	online definition of QoE
$B_i[k_i]$	buffer occupancy of user i after downloading segment k
$B_{i,max}$	maximum buffer size of user i
$\bar{C}_i[k_i]$	average capacity of downloading segment k_i
α	the Lagrange multiplier for v
β	the Lagrange multiplier for p
$\gamma_{i,min}$	the Lagrange multiplier for $q_{i,min}$
$\gamma_{i,max}$	the Lagrange multiplier for $q_{i,max}$

4.2 System Model

4.2.1 Network Model

We consider a wireless video streaming network as shown in Fig. 4.1, consisting of video servers, the wireline netowrk, a cellular base station (BS), and multiple UEs. The videos are stored in the remote servers. To reduce the delay of transmission, more and more server are deployed closer to end UEs. Generally, the capacity bottleneck in the end-to-end transmission path is the last hop, where a BS serves multiple UEs. The transmission in the Internet before the last hop could be modeled as a *request interval time* since the network conditions such as capacity and congestion level mainly influence the propagation time before the BS.

Assume the BS serves N video streaming UEs with OFDMA, denoted as $\mathbb{N} = \{1, 2, ..., N\}$. Denote the total available bandwidth as W Hz, which consists of M subcarriers denoted as $\mathbb{M} = \{1, 2, ..., M\}$. Each subcarrier $m \in \mathbb{M}$ is assumed to have an equal bandwidth of $\kappa = W/M$ Hz. Since the bandwidth of each subcarrier is sufficiently small, they only experience flat fading. For a resource block in OFDM, the time length of each resource allocation is denoted as τ, the time step is denoted as $t = 1, 2, ...$, and each time slot contains an integer number of OFDM symbols and an integer number of τ.

Denote $g_{im}(t)$ as the channel gain of UE $i \in \mathbb{N}$ on subcarrier $m \in \mathbb{M}$ at time t, and $p_{im}(t)$ accounts for the total transmission power assigned to subcarrier m for UE i at time t. Assume the total power can be assigned is P. Since multiple users can share subcarriers in each time slot, denote the non-overlapping time fraction of user i on subcarrier m in time slot t as $0 \leq v_{im}(t) \leq 1$. Without loss of generality, assume the time slot is unit time. Then we have

$$\sum_{i=1}^{N} v_{im}(t) \leq 1, \;\; \forall m, t. \tag{4.1}$$

The additive white Gaussian noise (AWGN) at the receiver has unit spectrum density. According to Shannon formula, the maximum rate user i can achieve on subcarrier m at time t is

$$\begin{aligned} & r_{im}(t) \\ = & \begin{cases} v_{im}(t)\kappa \log_2 \left(1 + \frac{p_{im}(t) g_{im}^2(t)}{v_{im}(t)\kappa}\right), & \text{if } v_{im}(t) > 0 \\ 0, & \text{otherwise.} \end{cases} \end{aligned} \tag{4.2}$$

The BS will first estimate the CSI on each subcarrier. Then with different targets, e.g., maximizing the total data rate or maximizing the energy efficiency, the BS assigns transmit power $p_{im}(t)$ and time fraction $v_{im}(t)$ to each UE i on each subcarrier m at time t. Naturally, the

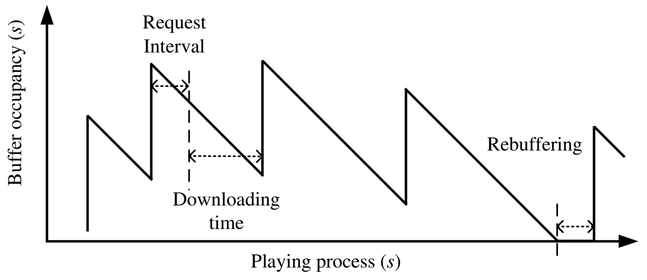

Figure 4.4: Timeline of the discrete time DASH system.

total data rate for UE i at time t is the summation of all the data rate $r_{im}(t)$ on each subcarrier, denoted as $r_i(t) = \sum_{m=1}^{M} r_{im}(t)$.

4.2.2 Streaming Video Model

The video for UE i is S_i s, which has been partitioned into K_i consecutive segments, each coded with different bit rates. Assume each segment of all videos is l s. Without lost of generosity, assume all the coded bit rates R_i are in the same set $\mathbb{R}$. Naturally, the size of segment k_i in bits can be represented as $R_i[k_i] \times l$.

During the video session, the playback buffer dynamic process at a user is illustrated in Fig. 4.4. When a new segment is completely downloaded, the buffer occupancy (in seconds) is immediately increased. The buffer occupancy decreases linearly with time when the segment is played out. When the buffer is empty, the playback process stalls. The time till the next segment arrives is the *rebuffering time* (the interval before the 5th segment in Fig. 4.4). After downloading a segment, the UE estimates the average rate of the segment and sends a request back to the video server for the next segment. The period since the request is sent till the first byte of the next segment arrives at the UE, is the *request interval* (see the 2nd segment in Fig. 4.4). Depends on the computational complexity of the UE algorithm and the server it chooses, the request interval could be as large as several seconds, as shown in Section 4.1.

Denote $B_i[k_i] \in [0, B_{i,max}]$ as the playback buffer occupancy at UE i, which represents the amount of video data stored in the buffer after downloading segment k_i, as measured in playback time. Users may have different buffer sizes $B_{i,max}$, which represents the total amount of storage measured in playback time. The UE can play each video segment only after it is fully downloaded, since the segment itself contains the playback metadata.

Let $s_i[k_i]$ represent the time slot when segment k_i is downloaded at UE i. During playback, the UE calculates the average rate $\bar{C}_i[k_i]$ of downloading segment k_i, as an important indicator of future capacity in most existing algorithms. The request interval is denoted by $\pi_i[k_i]$, which depends on the network parameters and network congestion level. During this period, this UE does not need any resource from the BS for transmission. Since this period could be considerably large, it should be considered in the resource allocation scheme.

The playback buffer process can be modeled as follows. The timeline of the operations and updates is presented in Fig. 4.4.

$$\begin{cases} B_i[k_i] = \min\Big\{\max\Big\{0, B_i[k_i-1] - \pi_i[k_i] - \frac{R_i[k_i]l}{\bar{C}_i[k_i]}\Big\} \\ \qquad\qquad + l, B_{i,max}\} \\ \bar{C}_i[k_i] = \frac{\sum_{t=s_i[k_i-1]+\pi_i[k_i]}^{s_i[k_i]} r_i(t)}{s_i[k_i]-s_i[k_i-1]} \\ s_i[k_i] = s_i[k_i-1] + \pi_i[k_i] + \frac{R_i[k_i]l}{\bar{C}_i[k_i]}. \end{cases} \tag{4.3}$$

The rebuffering time for one segment downloading event is $\max\Big\{0, \pi_i[k_i] + \frac{R_i[k_i]l}{\bar{C}_i[k_i]} - B_i[k_i-1]\Big\}$. Rebuffering event happens when this value is larger than 0, which significantly degrades the user QoE [97].

4.2.3 Quality of Experience (QoE) Model

The QoE is an important indicator of the performance of video communication systems. How to design a QoE model to capture the user assessment has been extensively studied. In the past, the QoE is mainly divided into two parts: objective measures and subjective evaluation. Objective measures, e.g., Peak Signal-to-Noise Ratio (PSNR) represent the quality of video frames, while subjective evaluation, such as Mean Opinion Score (MOS) [98], reflects users assessment of the viewing experience [99].

In [100], the authors study how the factors, such as playback buffer and average bit rate, influence the user engagement. It suggests that new QoE model should be developed that considers both video quality and user experience, which could be represented coarsely as user engagement. The authors in [97] suggest that the main factors of a QoE model should include buffering ratio, video starting time, average bit rate, and attributes such as type of video, ISP, etc. In [101], the QoE model is defined as a weighted sum of several main factors. The weights could be adjusted for different scenarios.

Intuitively, the larger the bit rate, the better the video quality. The relationship between video quality and bit rate could be modeled as $q(t) = f(R[t]) = a \cdot \log(R[t]) + b$ [102] . The coefficients a, b could be adjusted according to specific video type and playback device for stored videos. On the other hand, the variance of video quality across segments influences the user experience as well. The tradeoff between the average quality and variance is a key factor to be taken into consideration.

The key factors of our QoE model is listed below for UE i.

- *Average video quality* $m_i[K]$: it represents the video quality level averaged over the entire video playback period [101], defined as: $m_i[K] = \frac{1}{K}\sum_{k=1}^{K} q(R_i[k])$.

- *Variance of video quality* $\text{Var}_i[K]$: it accounts for the quality variation from segment to segment, given by $\text{Var}_i[K] = \frac{1}{K}\sum_{k=1}^{K}(q(R_i[k]) - m_i[K])^2$. As the average video quality, the variance also has a considerable impact on the QoE [101].

- *Rebuffering ratio* $\text{Reb}_i[K]$: rebuffering occurs when there is underflow at the playback buffer. The rebuffering ratio is defined as the total rebuffering time over the total video duration $L_i = K_i \times l$, i.e.,

$$\text{Reb}_i = \frac{1}{L_i}\sum_{k=1}^{K} \max\left\{0, \pi_i[k_i] + \frac{R_i[k]l}{C_i[k]} - B_i[k-1]\right\}. \tag{4.4}$$

  This factor affects the QoE even more significantly than variance [103].

- *Startup delay* T_i^s: it represents the time between user requests a video and the playback begins. Normally, a certain length of buffer occupancy need to be accumulated before playback starts [101]. It depends on the transmission rate and how the video is encoded.

As different user might focus on different factors, we use a weighted sum to ensure flexibility of this model. For segment k_i, user i's QoE is defined as

$$\begin{aligned} Q[k_i] = q(R_i[k_i]) + \theta \cdot (q(R_i[k_i]) - m_i[K_i])^2 + \\ \frac{\lambda}{K_i l} \max\left\{0, \pi_i[k_i] + \frac{R_i[k_i] l}{\bar{C}_i[k_i]} - B_i[k_i - 1]\right\}. \end{aligned} \tag{4.5}$$

in which $\theta < 0$ and $\lambda < 0$ are tunable weights, and $m_i[K_i]$ is the average video quality. For the entire playback process, the QoE of user i can be defined as

$$Q_i = \sum_{k_i=1}^{K_i} Q[k_i] + \eta \cdot T_i^s \tag{4.6}$$

in which $\eta < 0$ is a tunable weight, and T_s is the startup delay. This model can be flexibly tuned for different users and application scenarios with different parameter sets $\{\theta, \lambda, \eta\}$. Furthermore, if the viewing process is emphasized instead of the startup phase, the overall QoE can be defined as $Q_i = \sum_{k_i=1}^{K_i} Q[k_i]$.

To consider fairness among users, we introduce a concave utility function $U_\alpha(\cdot)$ defined as [104]

$$U_\alpha(x) = \begin{cases} \log(x), & \text{if } \alpha = 1 \\ \frac{x^{1-\alpha}}{1-\alpha}, & \text{otherwise.} \end{cases} \tag{4.7}$$

For instance, when $\alpha = 1$, maximizing the utility sum ensures proportional fairness. We defines the fairness QoE as $Q^{fair}(k_i) = U_\alpha(Q(k_i))$ and the QoE through the playing process $Q_i = \sum_{k_i=1}^{K_i} Q^{fair}(k_i)$.

4.3 Problem Formulation

To achieve the goal of QoE maximization, the challenge is that the BS and video UEs are operating at different timescales. At each time t, the BS adapt to the variation of network states, e.g., updated CSI. On the other hand, the video users adapt the bit rate of the next video segment after downloading the present one. In this section, we first formulate an offline problem and then provide an online transformation with reduced complexity. The decomposition of the online problem is then presented and the decomposed problems will be solved in Section 4.4.

4.3.1 The Offline Optimization Problem

The offline optimization problem is formulated based on the assumption that we know all the information of the video process. The optimization variables related to the BS are wireless resources: $v_{im}(t)$ and $p_{im}(t)$ for UE i on subcarrier m. Video rate adaption is executed each time when the UE finishes downloading a segment. The data-rate $R_i[k_i]$ can only be chosen from a given set $\mathbb{R}_i$ defined by the video encoder (or server). The *offline* QoE maximization problem, denoted by **Prob-Offline**, is formulated as follows.

$$\max_{\{p_{im}(t),v_{im}(t),R_i[k_i]\}} \Lambda = \sum_{i=1}^{N}\sum_{k_i=1}^{K_i} Q^{fair}[k_i] \tag{4.8}$$

$$\text{s.t.: } \sum_{i=1}^{N} v_{im}(t) \leq 1, \ \forall m, t \tag{4.9}$$

$$\sum_{i=1}^{N}\sum_{m=1}^{M} p_{im}(t) \leq P, \ \forall t \tag{4.10}$$

$$R_i[k_i] \in \mathbb{R}_i, \ \forall i \tag{4.11}$$

$$B_i[k_i] \in [0, B_{i,max}], \ \forall i, k_i. \tag{4.12}$$

In terms of $p_{im}(t)$ and $v_{im}(t)$, the optimization problem is convex. For rate adaption, it is an integer programming with a limited solution set (for example, most Youtube videos offer 3 to 6 resolutions). The optimal value could be achieved with dynamic programming (DP).

To deal with variables $R_i[k_i]$, we relax the constraint to allow them to take any values (rather then chosen from a give set $\mathbb{R}_i$), to obtain an approximation problem. Notice that the video rate and quality can be mapped with function $q_i(\cdot)$. Therefore, the quality q_i also belongs to a set of scalar values Θ_i (as $R_i[k_i]$ is chosen from $\mathbb{R}_i$). Furthermore, we can select the optimal quality and then derive the corresponding rate using $q^{-1}(\cdot)$ and round it to the closest rate in set $\mathbb{R}$. Here, we abuse the notation of q_i, but the reader can easily differentiate the $q(\cdot)$ and q_i as the quality function and the scalar value of quality. As $q_i(\cdot)$ is monotonically increasing, we have

$q_i \in [q_{i,min}, q_{i,max}]$ in which $q_{i,min}$ and $q_{i,max}$ can be calculated by substituting the minimum and maximum rate into $q_i(\cdot)$, respectively. The mapping is unique. The approximation problem can be written as

$$\max_{\{p_{im}(t), v_{im}(t), q_i[k_i]\}} \Lambda^{appr} = \sum_{i=1}^{N} \sum_{k_i=1}^{K_i} U_\alpha \left(q_i[k_i]\right. \tag{4.13}$$

$$+ \theta \cdot (q_i[k_i] - m_i[K_i])^2$$

$$\left. + \frac{\lambda}{K_i l} \max\left\{0, \pi_i[k_i] + \frac{q^{-1}(q_i[k_i])l}{\bar{C}_i[k_i]} - B_i[k_i - 1]\right\}\right)$$

$$\text{s.t.: } q_{i,min} \le q_i[k_i] \le q_{i,max} \tag{4.14}$$

$$(4.9) \sim (4.12).$$

Theorem 4.1. *The approximation problem defined in* (4.13) *is a convex optimization problem.*

The proof is given in Appendix A. With Theorem 4.1, we can solve this problem with the KKT conditions to acquire the optimal quality and then round the rate down to the closest feasible rate. However, solving this problem is based on the knowledge of the entire (and future) playback process and network information), e.g., the mean video quality $m_i[K_i]$ over the entire playback process K_i. It is an offline problem which may not be practical in some cases.

4.3.2 Online Optimization Formulation

Following Prob-Offline, an online version **Prob-Online** is derived in this section. Notice that the only term that involves future information is the overall mean quality $m_i[K_i]$. We first propose the formation of Prob-Online with an approximation to this term and then prove the asymptotic convergence property of Prob-Online to Prob-Offline.

For a single user, we define the online QoE as follows.

$$Q_i^{online}[k_i] = U_\alpha(q(R_i[k_i]) + \theta \cdot (q(R_i[k_i]) - \hat{m}_i[k_i - 1])^2$$

$$+ \ \lambda \cdot \text{Reb}_i[k_i]). \tag{4.15}$$

in which $\hat{m}_i[k_i]$ is updated as

$$\hat{m}_i[k_i] = \hat{m}_i[k_i - 1] + \frac{\zeta_i}{k_i + \zeta_i}(q(R_i^*[k_i]) - \hat{m}_i[k_i - 1]). \tag{4.16}$$

In (4.16), $q(R_i^*[k_i])$ is the video quality corresponding to the optimal rate $R_i^*[k_i]$, ζ_i is a tunable parameter for different users. This way, we rewrite the problem from over the entire time window $\mathbb{T}$ to the problem that can be solved at each time slot using past and present information.

Lemma 1. *The $\hat{m}_i[k]$ in* (4.16) *approximates the average of the optimal quality with k goes to infinity.*

The proof is given in Appendix B. Lemma 1 is on the convergence property of $\hat{m}_i[k]$, which we use to replace the term of overall average quality $m_i[K_i]$. It lays the foundation for the proof of convergence of the online algorithm.

Lemma 2. *Prob-Online is a convex optimization problem.*

The proof for lemma 2 is similar to theorem 4.1 and is omitted for brevity. Based on Lemmas 1 and 2, we can take a step further to claim that the solution to the online problem converges to the offline problem solution asymptotically.

Theorem 4.2. *The solution of Prob-Online asymptotically converges to the solution of Prob-Offline.*

The proof is given in Appendix C. With Theorem 4.2, we can derive the solution for Prob-Online with past and present information. More important, the solution converges to the offline optimal solution with the increase of time.

With the Lemmas and Theorems, we can solve the online problem to acquire the optimal solution $\{p_{im}^*(t), v_{im}^*(t), R_i^*[k_i]\}$ for each time slot. However, the user rate adaption may not be synchronized, and more important, the user rate adaptation is executed at a different timescale from BS resource allocation. In addition, the number of video UEs that are actually transmitting packets is varying over time (i.e., due to the request interval). To address all these challenges, we further decompose the optimization problem into two sub-problems: a BS resource allocation problem and a video rate adaptation problem, which are solved in the next section.

4.4 Solution Algorithms and Analysis

4.4.1 Prob-Online Analysis

We first rewrite the online formulation by adding the equality constraints on the capacity of each user.

$$\max_{\{p_{im}(t),v_{im}(t),R_i[k_i]\}} \Lambda^{online} = \sum_{i=1}^{N} Q_i^{online}$$
$$C_i(t) = \sum_{m=1}^{M} r_{im}(t), \forall i \in \mathbb{N}, \forall t \in \mathbb{T} \tag{4.17}$$
$$(4.9) \sim (4.12).$$

In the above formulation, the BS operation, i.e., resource allocation, is coupled with UEs' rate adaptation in the term average capacity $\bar{C}_i[k_i]$. At each time slot $s_i[k_i]$, the controller will try to optimize the QoE by estimating the capacity for the next segment $\bar{C}_i[k_i+1]$. On the other hand, the BS controller will also optimize the QoE by allocate resource to UEs at each time slot t, which updates $C_i(t)$. With asynchronous operations of the two parties, it is natural to decompose the problem to BS and UE subproblem, to decouple their operations.

At the UE side, rate adaption is executed based on the estimation of $\bar{C}_i[k_i + 1]$ at time $s_i[k_i]$ after downloading segment k_i. Most estimation algorithms are based on the history data of capacity. The value of $\bar{C}_i[k_i + 1]$ is influenced by the resource allocation before time k_i. On the other hand, the BS allocates resources to each UE at a smaller timescale than rate adaption. Therefore, at each resource allocation time step, the video rate has already been chosen and remains fixed for a period of time. Based on this observation, we present a primal decomposition approach based on [105].

4.4.2 UE Rate Adaption

The rate adaption at the UE is executed when the previous segment is downloaded. The assigned transmission rate to the UE during the downloading process is determined by the environment conditions sensed by BS. To choose the rate for the next segment, the capacity is mainly an estimation based on the previous segment. It makes sense that we optimize the QoE at each UE by rate adaption with a given estimation of capacity $\bar{C}_i[k_i+1]$.

At $s_i[k_i-1]$, UE i aims to maximize its QoE by choosing $R_i[k_i]$, based on $B_i[k_i-1]$ and history information. We formulate the UE i side rate adaptation problem as

$$\max_{R_i[k_i]} \ I_i^U(k_i)\cdot \hat{Q}_i^{online}[k_i] \tag{4.18}$$

$$\text{s.t.:} \ R_i[k_i]\in \mathbb{R}_i \tag{4.19}$$

$$B_i[k]\in[0,B_{i,max}], \forall k\in[s_i[k_i-1], s_i[k_i]], \tag{4.20}$$

where $\hat{Q}_i^{online}[k_i]$ is defined as in (4.15) with estimated $\bar{C}_i[k_i]$. The indication function $I_i^U(k_i)$ is equal to 1 when the buffer is not full and 0 otherwise. By the time when the buffer is full, the video UE would pause `Get` for several seconds depends on the mechanism. Rebuffering time is updated as in (4.3).

The average download capacity is estimated based on history data. From the application layer, the UE can only acquire an estimation of the average capacity by dividing $R_i[k_i]l$ with time difference between sending request and completing downloading the segment. With information from the TCP layer, we can have a better estimation by narrowing down the downloading period between the time of receiving the first packet and the last packet. However, it is still hard to accurately predict the future downloading capacity due to network dynamics in the future. We can acquire an estimation by simply using the exponential average over the previous capacity. Then solve the optimization by brute-force search in the rate space $\mathbb{R}_i$, which is small (e.g., 3 to 6 different resolutions/rates). In this chapter, we call this simple scheme as **DORA** [106].

Inspired by the work [42], which measures the cellular network capacity and proposes an estimation model based on Poisson process, we consider the downloading capacity as a random variable. Furthermore, by optimization over several future steps with estimated future information, we can increase the robustness of rate adaption based on the theory of stochastic model predictive control (SMPC). In this way, the optimization do not rely on accurate estimations of future information that are hard to acquire.

Assume that the average capacity $\bar{C}_i[k_i]$ is a random process based on distribution $\Xi(\cdot)$ with mean $\tilde{C}_i[k_i-1]$. At each rate adaptation time $s_i[k_i-1]$, we will first update the average capacity $\bar{C}_i[k_i-1]$ with the measurement of this segment transmission. The exponential window moving average (EWMA) method is used to update the mean as $\tilde{C}_i[k_i-1] = \xi\tilde{C}_i[k_i-2] + (1-\xi)\bar{C}_i[k_i-1]$ with exponential weights $\xi \in (0,1)$. Suppose the prediction horizon here is z. The z predictions over the prediction horizon are drawn with Monte Carlo sampling based on the distribution. By solving the optimization problem over the z steps ahead, we can obtain control moves as follows.

$$\vec{R}_i := \{R_i[k_i], R_i[k_i+1], ..., R_i[k_i+z-1]\}. \tag{4.21}$$

The first control result, $R_i[k_i]$, will be taken as the choice for the next segment. In this chapter, we adopt dynamic programming (DP) to compute the overall control moves $\vec{R}_i$. The rough idea is to store the intermediate optimal QoE score of each prediction step and then update it at each step. Due to limited size of the bitrate set $\mathbb{R}$ and small prediction horizon, the time complexity of the DP algorithm, $O(|\mathbb{R}|\cdot z)$, is acceptable in this context. By explicitly considering the uncertainty of estimations, this algorithm provides us a robust rate adaption solution. The new optimization problem is formulated as

$$\max_{R_i[k_i],...,R_i[k_i+z-1]\}} \sum_{j=0}^{z-1} \hat{Q}_i^{online}[k_i+j] \tag{4.22}$$

$$\text{s.t.: } R_i[k_j] \in \mathbb{R}_i, j \in \{k_i, ..., k_i+z-1\} \tag{4.23}$$

$$B_i[k_i] \in [0, B_{i,max}], \forall k_i, \tag{4.24}$$

Algorithm 2: UE Video Rate Adaption Algorithm

```
1  Initialize the mean of $\Xi(\cdot)$ based on history;
2  for $k_i = 1, 2, ..., K_i$ do
3      Calculate the average capacity $\bar{C}_i[k_i - 1]$ based on the downloading process of $k_i - 1$;
4      Update the mean of $\Xi(\cdot)$ with EWMA;
5      Generate $z$ steps of estimation values $\hat{C}_i[k_i + j], j = 0, 1, ..., z - 1$ based on distribution
       $\Xi(\cdot)$;
6      Initialize a vector to store the QoE maximization result for each bit rate, $\vec{Q}_{|\mathbb{R}| \times 1} = \vec{0}$, for
       the DP;
7      for $j = 0, 1, ..., z - 1$ do
8          Use the DP to update $\vec{Q}[j]$;
9      end
10     Derive the optimal series of choices $\vec{R}_i$ from $\vec{Q}[z - 1]$. Apply the first bit rate choice for
       video segment $k_i$;
11 end
```

where $\hat{m}_i[k_i + j]$ and $\hat{B}_i[k_i + j]$ are updated as in (4.16) and (4.4), respectively. The procedure is presented in Algorithm 2.

4.4.3 Base Station Side Optimization

Compared to the UE rate adaption algorithm, the optimized resource allocation at the BS is a master problem that decides the capacity of each UE i at given conditions and chosen data rate $R_i[k_i]$. The UE will obtain resources from the BS in every time slot t, which is much smaller than the timescale of rate adaption (microseconds vs. seconds). Moreover, for each time slot, the data rate of each UE has been selected already. Therefore, in (4.15), the first two terms are constant from the BS perspective. Since $\lambda < 0$, we only need to minimize the rebuffering time. The problem is now transformed to minimizing the total rebuffering time of all UEs by effective resource allocation at the BS. The object function is given by

$$\begin{aligned} \text{Reb}_{BS}(t) = \sum_{i=1}^{N} \max \{ & t - s_i[k_i - 1] - B_i[k_i - 1] \\ & -I_{BS,i}(t) \cdot l, 0 \}, \text{ for } t \in (s_i[k_i - 1], s_i[k_i]], \end{aligned} \tag{4.25}$$

where function $I_{BS,i}(t)$ indicates whether segment k_i has been fully downloaded, defined as

$$I_{BS,i}(t) = \begin{cases} 1, \text{ if } \sum_{\mu=k_i-1}^{t} \sum_{m=1}^{M} r_{im}(\mu) \geq R_i[k_i]l \\ 0, \text{ if } \sum_{\mu=k_i-1}^{t} \sum_{m=1}^{M} r_{im}(\mu) < R_i[k_i]l. \end{cases} \tag{4.26}$$

In (4.25), $t - s_i[k_i - 1]$ is the buffer occupancy consumed since the last time a segment is downloaded, while the third term accounts for the buffer occupancy at that time. If we can guarantee the average capacity $\bar{C}[k_i]$ be larger than the ratio $\frac{R_i[k_i]l}{B[k_i-1]}$, then the target function is minimized. This condition for each UE is hard to achieve due to limited resources at the BS. We can reformulate the BS optimization problem as

$$\max_{\{p_{im}(t), v_{im}(t)\}} \quad \Phi(p_{im}(t), v_{im}(t)) \tag{4.27}$$

$$\text{s. t.:} \sum_{i=1}^{N} v_{im}(t) \leq 1, \ \forall m, t \tag{4.28}$$

$$\sum_{i=1}^{N} \sum_{m=1}^{M} p_{im}(t) \leq P, \ \forall t, \tag{4.29}$$

where

$$\Phi(p_{im}(t), v_{im}(t)) = \sum_{i=1}^{N} \left\{ I_i(t) \frac{1}{\rho_i(t) + \sigma} \sum_{m=1}^{M} r_{im}(t) \right\},$$

$I_i(t)$ is an indication function on whether user i is in a request interval (and thus no resource is needed), and σ is a small scalar constant that prevents the denominator to be zero. In problem (4.27), $\rho_i(t)$ is the user i buffer occupancy state maintained at the BS. Each time a user requests the next video segment, it also feeds back its buffer occupancy state to the BS. Then the BS sets $\rho_i(t)$ to the reported buffer occupancy, i.e., $\rho_i(t) = B_i[t]$. Over the next time slots, $\rho_i[t]$ evolves as follows to emulate the playback process at user i.

$$\rho_i(t) = \begin{cases} \max\{0, \rho_i(t-1)-1\}, & s_i[k_i-1] \leq t < s_i[k_i] \\ \max\{0, \rho_i(t-1)-1\}+l, & t = s_i[k_i], \end{cases}$$

$$k_i = 1, 2, ..., K_i, \tag{4.30}$$

until the the next user i feeback is received. This way, the BS maintains the buffer state of each UE at a minimum control overhead. Problem (4.27) is to maximize a weighted sum of the downlink rates of all UEs at each time t, while each weight is inversely proportional to the playback buffer occupancy at the corresponding UE.

Theorem 4.3. *The problem defined in* (4.27) *is convex.*

With Theorem 4.3, we can solve the problem with a convex optimization solver. The algorithm considers both request interval and robust rate adaption is termed **DORA-RI**.

4.5 Simulation Study

4.5.1 Simulation Scenario and Algorithm Configuration

In this section, the performance of the proposed algorithms is evaluated with Python multi-threading simulation. For the physical layer, the total bandwidth is $W = 5$ MHz and consists of $M = 32$ subcarriers, each with $\kappa = 160$ KHz. The energy constraint of the BS is $P = 10$ W. We generate the channel gain over unit noise energy with the Rayleigh channel model for which the expectation is 5 dB. The time frame for resource allocation is $\tau = 5$ ms. We assume the BS acquires CSI with contamination of -60 dB W/Hz. Since the request interval mainly depends on the network conditions, e.g., the congestion level, it could be as large as 10 s. In this chapter, we simulate the request interval as a uniformly distributed process in the range of 50 ms to 500 ms. The fairness function is chosen as the natural logarithm $U_\alpha(\cdot) = \ln(\cdot)$.

Each video lasts for 2 minutes and is partitioned into 1 s segments and coded into five levels of rates, i.e., $\mathbb{R}$ = [100 kbps, 300 kbps, 500 kbps, 900 kbps, 1500 kbps, 2000 kbps], which is consistent with the 240p, 360p, 480p, 720p,[1] and 1080p formats for general genres [107]. For the QoE model, we use constant α_i and β_i for all users. The quality model α_i and β_i are fitted with the data from [103] and assumed to be the same for all the users. We set $\theta = 0.2$, $\lambda = 2.5$, and $\eta = 20$ according to the guidelines in [101]. The distribution of the download capacity is set according to a normal distribution with mean $\hat{C}_i[k_i]$ and the variance is 10% of the mean. The prediction horizon z is set to 7.

[1]Note that 900 kbps and 1500 kbps are the rates for 720p.

Table 4.2: Three variations of the proposed scheme

	Rate prediction algorithm	Request interval
DORA-RI	SMPC	Considered
DORA-MPC	MPC	Considered
DORA-no-RI	SMPC	Not considered

In order to evaluate the general performance and improvement over the state-of-art techniques, the proposed algorithm DORA-RI is first compared with the original DORA proposed in [106] and a proportionally fair network resource allocation with water-filling algorithm (PFWF-RM) scheme [108, 104]. The purpose is to demonstrate the achievable improvement over these two baseline schemes.

In addition, we would like to gain insights into the the proposed algorithm. Each component of DORA-RI are isolated out to test their impact. The proposed scheme DORA-RI is compared with two variations:

1. DORA-MPC, which uses a deterministic model predictive control (MPC) algorithm for bit rate adaption. All the other parts of this scheme are the same as DORA-RI.

2. DORA-no-RI, which only considers the request interval at the BS but does not adopt SMPC. All the other parts are the same as DORA-RI.

The three variations are summarized in Table 4.2. In this comparison, we aim to examine the impact of each component of DORA-RI on its performance.

4.5.2 Simulation Results and Discussions

Comparison over the benchmark and original schemes

Fig. 4.5 presents the mean QoEs values achieved by the proposed DORA-RI, DORA, and PFWF-RM. The experiments are repeated 20 times for each algorithm and the average values are presented. The decreasing trend of QoE over increased number of users is intuitive. The reason lies on the fact that the average resource each user can have is diminishing. In the worst case, DORA-RI can still achieve $1.7\times$ and $1.3\times$ QoE gains over PFWF-RM and DORA, respectively. It is clear that the enhancement achieved by utilizing the request interval of each

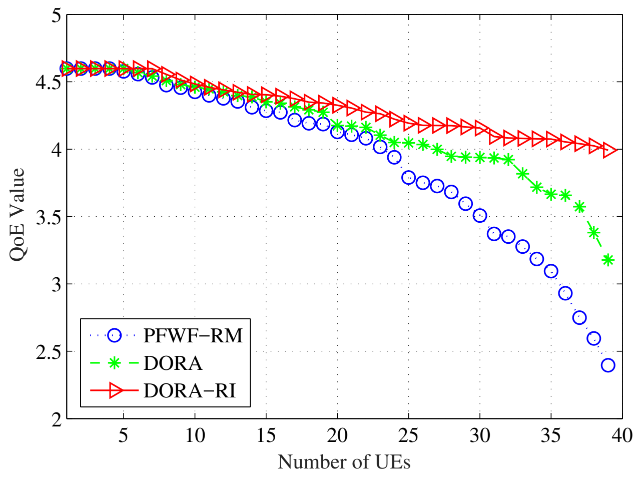

Figure 4.5: Comparison of QoE values for DORA-RI, DORA, and PFWF-RM.

user and by making more robust decisions based on the noisy future. We can achieve much better performance than the original version DORA proposed in [106].

In order to better reveal the reason for the QoE gain, the average rebuffering time ratio results of the three schemes are presented in Fig. 4.6. Again, it is reasonable that the rebuffering ratio is increasing with increased number of UEs. Each of them has a decreasing portion of the total resource. However, DORA-RI can keep the rebuffering time ratio low over the entire range, compared with other two schemes. Especially when the resource is scarce for each user to smoothly support the transmission of video data. By saving the valuable resource form UEs that do not need them during the request interval, we can achieve much less stalling time, which in turn contributes to the high QoE score. Moreover, prediction of the future can help the algorithm to make better decision to use a lower rate but to achieve smoother playback. Therefore, by smartly choosing smaller rates and more efficiently allocating resources, DORA-RI can achieve a $1/10$ rebuffering time ratio, which means much smoother playback and pleasant user experience.

Comparison of different components

Next, we compare the performance of DORA-RI with DORA-MPC which uses MPC for rate adaption instead of SMPC, and DORA-no-RI that only optimizes rate adaption with no request interval consideration. The detail are shown in Table 4.2. In Fig. 4.7, the average QoE values

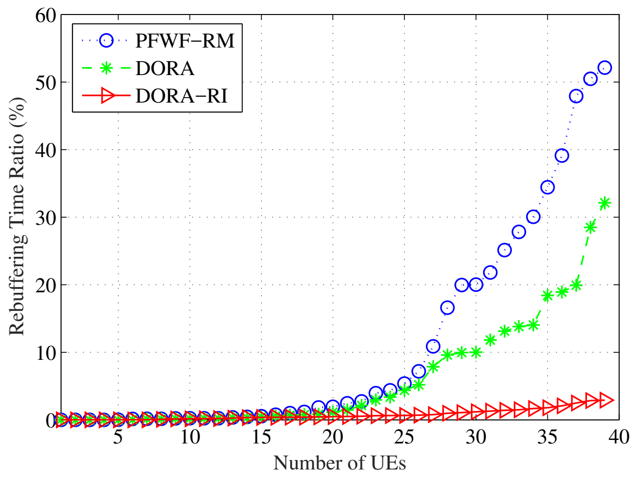

Figure 4.6: Comparison of rebuffering ratio for DORA-RI, DORA and PFWF-RM.

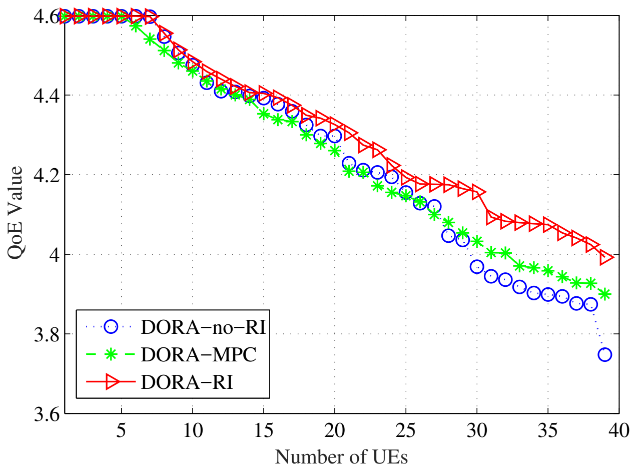

Figure 4.7: Comparison of QoE score for DORA-RI, DORA-MPC and DORA-no-RI.

achieved by each scheme are presented. DORA-RI achieves a 2 percent gain over DORA-MPC and 8 percent gain over DORA-no-RI. Notice that the gain is under the influence of the logarithm utility function (4.7). The real gain in QoE values are 10% and 30% over DORA-MPC and DORA-no-RI, respectively. By considering the request interval, we can achieve a 30 percent gain and even $1.8\times$ gain in the worst case. In addition, SMPC can provide a better performance over deterministic MPC by considering the stochastic dynamics of the network disturbances.

Fig. 4.8 illustrates how the average rebuffering time ratio is influenced by each component. It is obviously that all the three schemes outperform the two baseline schemes (i.e., DORA and PFWF-RM) comparing to Fig. 4.5. DORA-RI achieves a 45 percent smaller rebuffering time

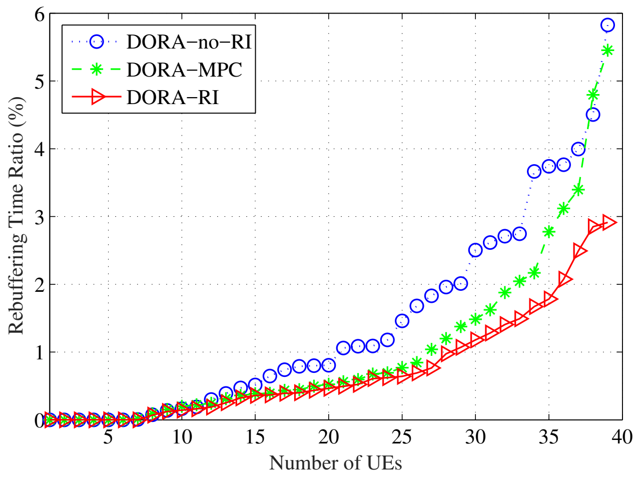

Figure 4.8: Comparison of rebuffering ratio for DORA-RI, DORA-MPC and DORA-no-RI.

ratio than DORA-MPC in the worst case. This benefit is introduced by taking uncertainty into consideration while conducting the optimization. In addition, the consideration of request interval does enhance the rebuffering performance. However, we notice that when the resource gets really scarce, e.g., when the number of UEs becomes larger than 35, the performance of DORA-no-RI and DORA-MPC get closer. This is because the deterministic MPC lacks the ability to properly handle the more random request intervals when the network gets congested. It actually justifies the necessity of incorporating the SMPC.

In Fig. 4.9, the average standard deviation (STD) of bit rate over one playback process is presented. Here, we aim to understand how the bit rate varies during the process. Counter-intuitively, the STD is not increasing as the number of UEs is increased. We found that initially, there is sufficient resources such that each user could always choose the largest bit rate, leading to minimal STD. When the number of UEs gets high, the resource for each user is decreasing, which leaves them less choice on bit rates. Therefore, the STD also gets smaller. In the middle range, however, the STD is relatively larger. This is because the resource is sufficient to alter the capacity largely but not enough to satisfy the largest bit rate. In other words, it is harder to accurately predict future capacity in this range. We can see that DORA-RI still achieves the lowest STD in video rates compared to the other two schemes.

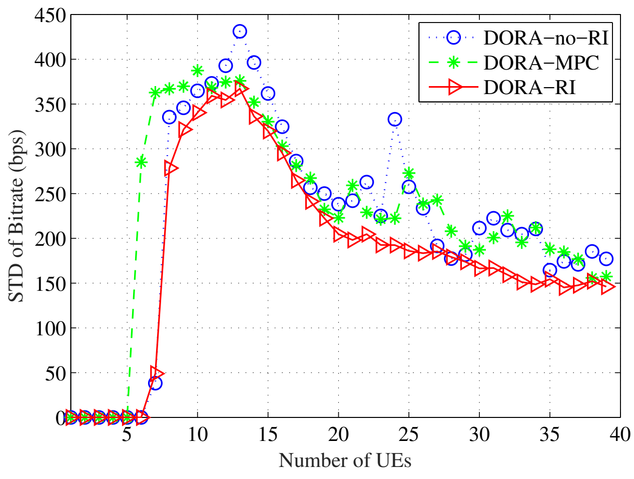

Figure 4.9: Comparison of data-rate standard deviation for DORA-RI, DORA-MPC and DORA-no-RI

4.6 Related Work

HTTP based video streaming technologies has drawn great attention. Some interesting works are on modeling the new QoE model to support bit rate adaption. For example, Yamagishi [109] formulated a parametric QoE model for DASH based on extensive subject experiments. The authors took audio and video bit rate, video resolution, rebuffering events and length into consideration and derived the coefficients for each factor. Some interesting works based on QoE video streaming can be found [110][111]

Bit rate adaption strategy is an important problem in DASH. Many existing techniques could be generally categorized into: (i) buffer based (BB) techniques, (ii) capacity based (CB) schemes, and (iii) integrated techniques. Some state-of-art methods have been proposed. In FESTIVE [112], the authors focused on improving the stability and fairness of multiple users that share a bottleneck link. PANDA [113] adopted a TCP congestion control like method to adjust video segment rate, but required certain overhead for probing. In [114], the authors considered rate adaption with adjustment of a threshold. The authors in [115] proposed a regression method to predict the future capacity and a classical PID based controller for rate adaption. In [101], the authors proposed an MPC based approach for rate adaption at the user side and a fastMPC method. However, the authors used a different QoE model and did not consider the prediction method for robustness. Markov decision process (MDP) based rate adaption algorithms have been proposed in [116] [117]. In [116], the authors proposed a solution, termed mDASH, that was based on MDP for DASH data rate adaption. Decision of the next segment data rate was made by taking factors into consideration, such as buffered video time, and history bandwidth and data rate. The work in [117] was focused on the vehicular environment. For MDP based algorithms, the high computational complexity is an obstacle for realtime applications. However, techniques such as Microsoft SmoothStreaming [118] have been shown to perform poorly in wireless networks [119]. Most rate adaption methods can only passively adapt to the variation in throughput.

The integration of video streaming and wireless network scheduling is a promising direction to maximize the performance of videos in the wireless environment. Works such as [120, 121, 85, 122, 27, 123] are inspiring. The authors in [124] tackled video transmissions in MU-MIMO networks and [125] investigated the adaptive video streaming and scheduling problem. Both works utilized Lyapunov optimization to achieve good performance with assumption of helper(s) as a centralized entity that can acquire user information. The authors in [126] proposed a jointly optimization framework of scheduling and rate-adaption with a proof of optimality. However, this work did not explicitly consider the resource allocation details (e.g., power, subcarrier, and time assignment) and the QoE model used in this work was more based on a mathematical formation. Lin [127] proposed a cross layer method for scalable video streaming over OFDMA networks. The tradeoff between efficiency and fairness was addressed. In this work, the authors used the traditional PSNR as indication of video quality instead of the modern QoE models, which incorporate more important factors that influence user QoE. The authors of [128] tackled the problem of heterogeneous network streaming on the client side. The network cost constraints were considered and the goal was to achieve high quality streaming and low energy cost on the UE. In [129], on the other hand, the authors proposed a method that utilize both unicast and multicast concurrently to reduce the energy consumption of UEs when streaming video over a cellular network. These works are focused mainly on the UE side to achieve a tradeoff between video quality and energy efficiency.

The resource allocation problem in the OFDM network has been extensively studied in the past decades [130, 80, 81, 83]. Refer to [104] for a comprehensive survey of resource allocation in OFDMA networks. Two main topics: energy efficiency optimization and system throughput optimization, were generally addressed. The original problem is a mixture of integer programming (subcarrier assignment) and linear programming (power allocation), which is NP-hard. Therefore, suboptimal solutions were developed by relaxation of time sharing in one time frame [81, 130, 131, **?**, **?**]. In [81], the authors proved that the suboptimal solution will converge to the optimum asymptotically assuming ergodic noise processes.

4.7 Conclusions

In this chapter, we investigated the problem of resource allocation for delivering multiple videos using DASH over the downlink of an OFDMA network. We first presented an offline formulation based on a novel QoE model. We then derived a more practical online formulation, and developed a distributed solution algorithm, which consisted of an resource allocation algorithm at the BS side and a rate adaptation algorithm at the user side. The proposed scheme was validated with simulations and was shown to outperform several benchmark scheme with considerable gains.

4.8 Proof for Theorem 4.1

Proof. By redefining the QoE maximization problem as in (4.13), the QoE function can be written as

$$\begin{aligned} Q^{appr} =& q_i[k_i] + \theta(q_i[k_i] - m_i[K_i])^2 \\ &+ \frac{\lambda}{K_i l} \max\left\{0, \pi_i[k_i] + \frac{q^{-1}(q_i[k_i])l}{\bar{C}_i[k_i]} - B_i[k_i - 1]\right\}, \end{aligned} \tag{4.31}$$

where $q_i[k_i]$ is a linear function. The quadratic part is a convex function over $q_i[k_i]$. The $\max$ term is convex over $q_i[k_i]$ and convex over $p_{im}(t)$ and $v_{im}(t)$. Since parameters θ and λ are both negative, Q^{appr} is concave for all the variables. The target function $\Lambda^{appr}(N)$ is the summation of Q^{appr} over time and users which means it is concave as well. The constraints are all convex sets. Therefore, this is a convex problem. $\square$

4.9 Proof for Lemma 1

Proof. This Lemma could be presented as follows.

$$\lim_{K\to\infty}\left(\frac{1}{K}\sum_{k_i=1}^{K} q_i(R^*[k_i]) - \hat{m}_i[K]\right) = 0 \tag{4.32}$$

For brevity, we denote $q_i(R^*[k_i])$ by $q_i^*[k_i]$. Rewrite (4.16) and take summation from 1 to K. We have

$$\begin{aligned}&\sum_{k_i=1}^{K}\left(\frac{k_i+\zeta}{\zeta}\right)(\hat{m}_i[k_i]-\hat{m}_i[k_i-1]) \\ =& \sum_{k_i=1}^{K}(q_i^*[k_i]-\hat{m}_i[k_i-1]).\end{aligned} \tag{4.33}$$

Expand the left hand side summation to obtain

$$\begin{aligned}&\frac{1}{\zeta}\left(K\hat{m}_i[K]-\sum_{k_i=1}^{K}\hat{m}_i[k_i-1]\right)-(\hat{m}_i[K]-\hat{m}_i[1]) \\ =& \sum_{k_i=1}^{K}(q_i^*[k_i]-\hat{m}_i[K]+\hat{m}_i[K]-\hat{m}_i[k_i-1]).\end{aligned}$$

To obtain the form (4.32), we first divide it by K and then take limit on both sides over K. It follows that

$$\begin{aligned}&\lim_{K\to\infty}\frac{K\hat{m}_i[K]-\sum_{k_i=1}^{K}\hat{m}_i[k_i-1]}{\zeta K}-\lim_{K\to\infty}\frac{\hat{m}_i[K]-\hat{m}_i[1]}{K} \\ =& \lim_{K\to\infty}\sum_{k_i=1}^{K}(q_i^*[k_i]-\hat{m}_i[K]+\hat{m}_i[K]-\hat{m}_i[k_i-1]).\end{aligned}$$

It's obvious that the second term goes to 0 due to finite $\hat{m}_i[K]$ and $\hat{m}_i[1]$. By splitting the right-hand-side into two parts and rearranging terms, we have:

$$
\begin{aligned}
&\frac{1-\zeta}{\zeta}\lim_{K\to\infty}\left(K\hat{m}_i[K] - \sum_{k_i=1}^{K}\hat{m}_i[k_i-1]\right)\\
= &\lim_{K\to\infty}\frac{1}{K}\sum_{k_i=1}(q_i^*[k_i] - \hat{m}_i[K]).
\end{aligned}
$$

The left-hand-side is the limit we want to show to be 0. Note that (4.16) can be viewed as a stochastic approximation update equation for $\hat{m}_i$. Therefore, the convergence of right-hand-side can be proven by applying Theorem 1.1 of Chapter 6 in [132]. □

4.10 Proof for Theorem 4.2

Proof. The convergence proof could be transformed to show that the Prob-Online objective value converges to the Prob-Offline objective value. Specifically, we aim to prove

$$
\lim_{t\to\infty}\Lambda(\mathbf{S}^*) - \Lambda(\tilde{\mathbf{S}}) = 0, \tag{4.34}
$$

where $\mathbf{S}^* = \{\mathbf{q}^*(t), \mathbf{v}^*(t), \mathbf{p}^*(t)\}$ is the online solution and $\tilde{\mathbf{S}} = \{\tilde{\mathbf{q}}(t), \tilde{\mathbf{v}}(t), \tilde{\mathbf{p}}(t)\}$ is the offline solution.

Since Prob-Online is convex, and based on Lemma 2, we can derive the KKT condition as follows.

$$
\begin{cases}
\mathbb{I}_N\left(\frac{\mathrm{d}\Lambda(\mathbf{S_i}^*)}{\mathrm{d}\mathbf{S}} + \alpha_i^*(t) - \gamma_{i,min}^*(t) + \gamma_{i,max}^*(t)\right)\\
\qquad + \beta_{i,m}^*(t) = 0\\
\alpha_i^*(t)(v_{im}^* - 1) = 0\\
\beta_{i,m}^*(p_{im}^* - 1) = 0\\
\gamma_{i,min}^*(q_{i,min} - q_i^*) = 0\\
\gamma_{i,max}^*(q_i^* - q_{i,max}) = 0\\
\alpha_i^*(t), \beta_{im}^*(t), \gamma_{i,min}^*(t), \gamma_{i,max}^*(t) \geq 0,\\
\qquad \forall i \in \mathbb{N}, \forall m \in \mathbb{M},
\end{cases}
\tag{4.35}
$$

where $\mathbb{I}_N$ is the indicator that the variables belong to different users. Lagrange multipliers $\alpha_i^*(t)$, $\beta_{i,m}^*(t)$, $\gamma_{i,min}^*(t)$, and $\gamma_{i,max}^*(t)$ are the dual points that the KKT conditions are satisfied and the optimal value is achieved.

We next construct the help function $\mathbf{H}(\tilde{\mathbf{S}})$ that is differentiable and concave. The definition is

$$\begin{aligned}\mathbf{H}(\tilde{\mathbf{S}}) =& \Lambda(\tilde{\mathbf{S}}) - \alpha_i^*(t)(v_{im}^* - 1) - \beta_{i,m}^*(p_{im}^* - 1) \\ &+ \gamma_{i,min}^*(q_i^* - q_{i,min}) - \gamma_{i,max}^*(q_i^* - q_{i,max}).\end{aligned} \tag{4.36}$$

We have $\mathbf{H}(\tilde{\mathbf{S}}) \geq \Lambda(\tilde{\mathbf{S}})$ due to the constraints in problem (4.13). In addition, we can acquire the following inequality by the concavity and differentiability of $\mathbf{H}(\tilde{\mathbf{S}})$.

$$\mathbf{H}(\tilde{\mathbf{S}}) \leq \mathbf{H}(\mathbf{S}^*) + \frac{\mathrm{d}\mathbf{H}(\mathbf{S}^*)}{\mathrm{d}\mathbf{S}}(\mathbf{S}^* - \tilde{\mathbf{S}}). \tag{4.37}$$

By bringing (4.36) and the KKT conditions (4.35), we obtain the following inequality.

$$\Lambda(\tilde{\mathbf{S}}) \leq \Lambda(\mathbf{S}^*) + 2\theta \sum_{i=1}^{N} \sum_{t=0}^{T} (q_i^*(t) - \hat{m}_i) * (q_i^*(t) - \tilde{q}_i(t). \tag{4.38}$$

In Lemma 1, we have proved that $\lim_{K\to\infty} \frac{1}{K} \sum_{k_i=1}(q_i^*[k_i] - \hat{m}_i[K])$. Here we abuse the notification of K_i and T, which both represent the total playback time. Then we have

$$\lim_{T\to\infty} \frac{1}{T} \sum_{k_i=1} \Lambda(\tilde{\mathbf{S}}) \leq \frac{1}{T} \lim_{T\to\infty} \Lambda(\mathbf{S}^*). \tag{4.39}$$

Since $\tilde{\mathrm{S}}$ is the optimal offline solution, $\Lambda(\tilde{\mathbf{S}})$ is the optimal value for Prob-Offline. It follows that

$$\Lambda(\tilde{\mathbf{S}}) \geq \Lambda(\tilde{\mathbf{S}}). \tag{4.40}$$

Combining (4.39) and (4.40), we conclude that the theorem holds true. $\square$

4.11 Proof for Theorem 4.3

Proof. First of all, we prove the concavity of the rate function, which can be rewritten as $r_{im}(t) = v(t)\kappa \log_2\left(1 + \frac{p(t)g^2(t)}{v(t)\kappa}\right)$ for brevity. For two feasible solutions (v_2, p_2) and (v_3, p_3), suppose there exists a feasible solution $(v_1, p_1) = \epsilon(v_2, p_2) + (1-\epsilon)(v_3, p_3)$, where $0 \le \epsilon \le 1$. By the definition of concavity, we need to show that $r_{im}(v_1, p_1) \ge \epsilon r_{im}(v_2, p_2) + (1-\epsilon) r_{im}(v_3, p_3)$. There are three possible cases for v_2 and v_3 that needs to be analyzed.

- Case I: when $\{v_2 > 0, v_3 > 0\}$. Then we have $v_1 > 0$. Because $\log_2\left(1 + p_1 g_{im}^2\right)$ is a concave function of p_1, its *perspective* $v_1 \nu \log_2\left(1 + \frac{p_1 g_{im}^2}{v_1 \nu}\right)$ is concave given that $v_1 > 0$ [133]. Thus, concavity holds true for this case.

- Case II: when $\{v_2 > 0, v_3 = 0\}$. Then we have $v_1 = \epsilon v_2$ and $p_1 = \epsilon p_2 + (1-\epsilon)p_3$. It follows that

$$\begin{aligned} r_{i,m}(v_1, p_1) &= \epsilon v_2 \kappa \log_2\left(1 + \frac{(\epsilon p_2 + (1-\epsilon)p_3)g_{im}^2}{\epsilon v_2 \kappa}\right) \\ &\ge \epsilon v_2 \log_2\left(1 + \frac{p_2 g_{im}^2}{v_2 \kappa}\right). \end{aligned}$$

- Case III: when $\{v_2 = 0, v_3 = 0\}$. This is a trivial case that the equality holds for $v_1 = 0$.

With the concavity of $r_{im}(t)$, it is convenient to show that the $\sum_{s=1}^{S} r_{im}(t)$ is concave since it is a nonnegative combination of concave functions $r_{im}(t)$. The concavity of the cost function $\Phi(p_{im}(t), v_{im}(t))$ can be argued for the same reason.

In addition, the utility constraints define a convex set Υ. By the definition of utility function, it's convenient to show that for any r_1, $r_2 \in \Upsilon$, $\epsilon r_1 + (1-\epsilon) r_2 \in \Upsilon$ for any ϵ with $0 \le \epsilon \le 1$. Both constraints $\sum_{i=1}^{N}(t) v_{im}(t) \le 1$ and $\sum_{i=1}^{N}(t) \sum_{m=1}^{M} p_{im}(t) \le P$ also define convex sets. They are the *intersection* of *half-spaces*. Intersection preserves the convexity of the sets. Thus the constraints are convex.

We conclude that Problem (4.27) is convex. $\square$

Chapter 5

Future Work

As demonstrated in the previous chapters, the complexity of the entire wireless system is increasing. In the meantime, more and more components are being added into the system for further performance enhancement, which will result in an even more complicated system. From the congestion control perspective, the requirement of adaptive learning and evolving would be an important aspect of future algorithms. Also, the dramatically increasing traffic of video streaming needs more efficient and smarter algorithms to adaptively adapt the data rate and/or jointly control the resource of the BS. Although we have made some interesting progress in model free congestion control, it's still at the early stage of research and application.

The fast development of the deep learning/deep reinforcement learning techniques have benefited many areas, such as computer graphics, computer vision, and human-computer interaction. For deep reinforcement learning, it has been successfully applied in Go and video games in which it can achieve better performance than human. With the proof that it can be used in the complicated scenario of fully observed information, its applications has been expanded. In the computer networking domain, however, most problems are partially observable and normally involve multi-agent cooperation or competition. How to fully utilize the power of DRL in such scenarios is still an open problem. Due to the promising properties of DRL and the complexity of the networking system, I plan to further apply DRL to solve sevearl other existing networking problems.

The detailed future research directions are as follow.

1. **Machine Learning Aided MmWave Networks.** MmWave networks are characterized by high data rate and unreliable connections. It poses a tremendous challenge to congestion control on both the sender side and at the base station or access point. To achieve high transmission efficiency and robustness, the transmission control algorithm should adaptively learn the transmission content and blocking pattern of the mmWave link. I plan to apply the DRL approach to tackle these problems and try to achieve the potential performance gain as brought about by the recent progress of DRL.

2. **Machine Learning Aided Video Streaming.** The recent progress on video streaming has proved that the DASH protocol can potentially adjust to the oscillation of capacity in wireless networks, with a smart data-rate adapting algorithm applied. In addition, with the domination of video traffic in the Internet and wireless networks, the problem of how to better accommodate video streaming in 4G-LTE network and the next generation networks becomes more important than ever. I plan to use the DRL to jointly handle the data-rate adapting as well as resource allocation to further improve the QoE of streaming videos.

3. **Learning and Controlling Efficiency Enhancement.** In our application of DRL, the learning process is time consuming and the control action generation is computationally intense. Although TCP-Drinc achieves a better performance over the benchmark algorithms on both throughput and RTT in our study of a relatively small network, I believe we can still further improve its performance in larger scale networks with more complicated algorithms. With the recent progress on model compression and transfer learning, I plan to further improve the learning and controlling efficiency in our problem to make it more practical.

References

[1] Cisco, “Cisco visual networking index: Global mobile data traffic forecast update, 20162021,” *White Paper*, [online] Available: https://www.cisco.com/c/en/us/solutions/collateral/service-provider/visual-networking-index-vni/mobile-white-paper-c11-520862.html, 2017.

[2] Y. Zhao, S. Mao, J. O. Neel, and J. H. Reed, “Performance evaluation of cognitive radios: Metrics, utility functions, and methodology,” *Proc. IEEE*, vol. 97, no. 4, pp. 642–659, Apr. 2009.

[3] M. Chen, V. C. Leung, S. Mao, and M. Li, “Cross-layer and path priority scheduling based real-time video communications over wireless sensor networks,” in *Vehicular Technology Conference, 2008. VTC Spring 2008. IEEE.* IEEE, 2008, pp. 2873–2877.

[4] S. Mao, X. Cheng, Y. T. Hou, H. D. Sherali, and J. H. Reed, “On joint routing and server selection for md video streaming in ad hoc networks,” *IEEE Transactions on Wireless Communications*, vol. 6, no. 1, 2007.

[5] Q. Zhao and B. Sadler, “A survey of dynamic spectrum access,” *IEEE Signal Process. Mag.*, vol. 24, no. 3, pp. 79–89, May 2007.

[6] D. Hu and S. Mao, “Cooperative relay in cognitive radio networks: Decode-and-forward or amplify-and-forward?” in *Global Telecommunications Conference (GLOBECOM 2010), 2010 IEEE.* IEEE, 2010, pp. 1–5.

[7] Sandvine, “Global internet phenomena report,” *White Paper*, [online] Available: https://www.sandvine.com/trends/global-internet-phenomena/, 2017.

[8] V. Mnih, K. Kavukcuoglu, D. Silver, A. A. Rusu, J. Veness, M. G. Bellemare, A. Graves, M. Riedmiller, A. K. Fidjeland, G. Ostrovski *et al.*, "Human-level control through deep reinforcement learning," *Nature*, vol. 518, no. 7540, p. 529, 2015.

[9] D. Silver, J. Schrittwieser, K. Simonyan, I. Antonoglou, A. Huang, A. Guez, T. Hubert, L. Baker, M. Lai, A. Bolton *et al.*, "Mastering the game of go without human knowledge," *Nature*, vol. 550, no. 7676, p. 354, 2017.

[10] M. Kuure-Kinsey and B. W. Bequette, "Multiple model predictive control strategy for disturbance rejection," *Ind. Eng. Chemistry Research*, vol. 49, no. 17, pp. 7983–7989, July 2010.

[11] W. Wang, X. Wang, and S. Mao, "Deep convolutional neural networks for indoor localization with CSI images," *IEEE Transactions on Network Science and Engineering*, vol. 5.

[12] X. Wang, X. Wang, and S. Mao, "RF sensing for Internet of Things: A general deep learning framework," *IEEE Communications*, vol. 56, no. 9, pp. 62–69, Sept. 2018.

[13] X. Wang, S. Mao, and M. Gong, "An overview of 3GPP cellular vehicle-to-everything standards," *ACM GetMobile: Mobile Computing and Communications Review*, vol. 21, no. 3, pp. 19–25, Sept. 2017.

[14] X. Wang, L. Gao, and S. Mao, "BiLoc: Bi-modality deep learning for indoor localization with 5GHz commodity Wi-Fi," *IEEE Access Journal*, vol. 5, no. 1, pp. 4209–4220, Mar. 2017.

[15] X. Wang, C. Yang, and S. Mao, "Tensorbeat: Tensor decomposition for monitoring multi-person breathing beats with commodity WiFi," *ACM Transactions on Intelligent Systems and Technology*, vol. 9, no. 1, pp. 8:1–8:27, Sept. 2017.

[16] X. Wang, S. Mao, and M. Gong, "A survey of lte wi-fi coexistence in unlicensed bands," *ACM GetMobile: Mobile Computing and Communications Review*, vol. 20, no. 3, pp. 17–23, July 2016.

[17] X. Wang, L. Gao, and S. Mao, “Csi phase fingerprinting for indoor localization with a deep learning approach,” *IEEE Internet of Things Journal*, vol. 3, no. 6, pp. 1113–1123, Dec. 2016.

[18] X. Wang, L. Gao, S. Mao, and S. Pandey, “Csi-based fingerprinting for indoor localization: A deep learning approach,” *IEEE Transactions on Vehicular Technology*, vol. 66, no. 1, pp. 763–776, Jan. 2017.

[19] X. Wang, L. Gao, and S. Mao, “PhaseFi: Phase fingerprinting for indoor localization with a deep learning approach,” in *Proc. IEEE GLOBECOM 2015*, San Diego, CA, Dec. 2015, pp. 1–6.

[20] M. Feng, S. Mao, and T. Jiang, “Joint duplex mode selection, channel allocation, and power control for full-duplex cognitive femtocell networks,” *Elsevier Digital Communications and Networks Journal*, vol. 1, no. 1, pp. 30–44, Feb. 2015.

[21] M. Feng and S. Mao, “Harvest the potential of massive mimo with multi-layer technologies,” *IEEE Network*, vol. 30, no. 5, pp. 40–45, Sept./Oct. 2016.

[22] M. X. Gong, S. F. Midkiff, and S. Mao, “A cross-layer approach to channel assignment in wireless ad hoc networks,” *ACM/Springer Mobile Networks and Applications Journal*, vol. 12, no. 1, pp. 43–56, Feb. 2007.

[23] M. Feng, S. Mao, and T. Jiang, “Joint duplex mode selection, channel allocation, and power control for full-duplex cognitive femtocell networks,” *Elsevier Digital Communications and Networks Journal*, vol. 1, no. 1, pp. 30–44, Feb. 2015.

[24] A. Kumar and K. G. Shin, “Managing TCP connections in dynamic spectrum access based wireless LANs,” in *Proc. IEEE SECON 2010*, Boston, MA, June 2010, pp. 1–9.

[25] K. R. Chowdhury, M. Di Felice, and I. F. Akyildiz, “TP-CRAHN: A transport protocol for cognitive radio ad-hoc networks,” in *Proc. IEEE INFOCOM 2009*, Rio de Janeiro, Brazil, Apr. 2009, pp. 2482–2490.

[26] C. Luo, F. R. Yu, H. Ji, and V. C. Leung, “Cross-layer design for TCP performance improvement in cognitive radio networks,” *IEEE Trans. Veh. Technol.*, vol. 59, no. 5, pp. 2485–2495, 2010.

[27] M. Feng, T. Jiang, D. Chen, and S. Mao, “Cooperative small cell networks: High capacity for hotspots with interference mitigation,” *IEEE Wireless Communications*, vol. 21, no. 6, pp. 108–116, Dec. 2014.

[28] D. Hu, S. Mao, and J. H. Reed, “On video multicast in cognitive radio networks,” in *INFOCOM 2009, IEEE.* IEEE, 2009, pp. 2222–2230.

[29] X. Chen, H. Zhai, J. Wang, and Y. Fang, “A survey on improving TCP performance over wireless networks,” in *Resource Management in Wireless Networking*, M. Cardeiand, I. Cardei, and D.-Z. Du, Eds. Kluwer Academic Publishers, 2005, pp. 657–695.

[30] H. Salameh, M. Krunz, and D. Manzi, “Spectrum bonding and aggregation with guard-band awareness in cognitive radio networks,” *IEEE Trans. Mobile Comput.*, vol. 13, no. 3, pp. 569–581, Mar. 2014.

[31] V. Misra, W.-B. Gong, and D. Towsley, “Fluid-based analysis of a network of AQM routers supporting TCP flows with an application to RED,” in *ACM SIGCOMM Comput. Commun. Rev.*, vol. 30, no. 4, Oct. 2000, pp. 151–160.

[32] T. Lakshman, A. Neidhardt, and T. Ott, “The drop from front strategy in TCP and in TCP over ATM,” in *Proc. IEEE INFOCOM 1996*, San Francisco, CA, Mar. 1996, pp. 1242–1250.

[33] S. Kunniyur and R. Srikant, “End-to-end congestion control schemes: Utility functions, random losses and ECN marks,” *IEEE/ACM Trans. Netw.*, vol. 11, no. 5, pp. 689–702, 2003.

[34] C. Hollot, V. Misra, D. Towsley, and W.-B. Gong, “On designing improved controllers for AQM routers supporting TCP flows,” in *Proc. IEEE INFOCOM 2001*, Anchorage, AK, Apr. 2001, pp. 1726–1734.

[35] P. Ignaciuk and M. Karbowańczyk, “Active queue management with discrete sliding modes in TCP networks,” *Bull. Pol. Ac.: Tech.*, vol. 62, no. 4, pp. 701–711, Dec. 2014.

[36] D. Cox and L. Dependence, “A review,” in *Statistics: An Appraisal*, H. David and H. David, Eds. Ames, IA: The Iowa State University Press, 1984, pp. 55–74.

[37] V. Jacobson, “Congestion avoidance and control,” *ACM SIGCOMM Comput. Commun. Rev.*, vol. 18, no. 4, pp. 314–329, 1988.

[38] S. Floyd, A. Gurtov, and A. Gurtov, “The NewReno modification to TCP’s fast recovery algorithm,” Apr. 2004, IETF RFC 3782.

[39] L. S. Brakmo, S. W. O’Malley, and L. L. Peterson, “TCP Vegas: New techniques for congestion detection and avoidance,” *ACM SIGCOMM Comput. Commun. Rev.*, vol. 24, no. 4, pp. 24–35, Oct. 1994.

[40] S. Ha, I. Rhee, and L. Xu, “CUBIC: a new TCP-friendly high-speed TCP variant,” *ACM SIGOPS Operating Systems Review*, vol. 42, no. 5, pp. 64–74, July 2008.

[41] K. Tan, J. Song, Q. Zhang, and M. Sridharan, “A compound TCP approach for high-speed and long distance networks,” in *Proc. IEEE INFOCOM 2006*, Barcelona, Spain, Apr. 2006, pp. 1–12.

[42] K. Winstein, A. Sivaraman, and H. Balakrishnan, “Stochastic forecasts achieve high throughput and low delay over cellular networks,” in *Proc. NSDI 2013*, Lombard, IL, Apr. 2013, pp. 459–471.

[43] Y. Zaki, T. Pötsch, J. Chen, L. Subramanian, and C. Görg, “Adaptive congestion control for unpredictable cellular networks,” in *ACM SIGCOMM Comput. Commun. Rev.*, vol. 45, no. 4, Oct. 2015, pp. 509–522.

[44] S. Floyd, “TCP and explicit congestion notification,” *ACM SIGCOMM Comput. Commun. Rev.*, vol. 24, no. 5, pp. 8–23, Oct. 1994.

[45] C. Hollot, V. Misra, D. Towsley, and W.-B. Gong, "A control theoretic analysis of RED," in *Proc. IEEE INFOCOM 2001*, Anchorage, AK, Apr. 2001, pp. 1510–1519.

[46] S. Floyd and V. Jacobson, "Random early detection gateways for congestion avoidance," *IEEE/ACM Trans. Netw.*, vol. 1, no. 4, pp. 397–413, Aug. 1993.

[47] X.-H. Zhang, K.-S. Zou, Z.-Q. Chen, and Z.-D. Deng, "Stability analysis of AQM algorithm based on generalized predictive control," in *Advanced Intelligent Computing Theories and Applications*, ser. LNCS. Springer, 2008, vol. 5226, pp. 1242–1249.

[48] P. Wang, H. Chen, X. Yang, and Y. Ma, "Design and analysis of a model predictive controller for active queue management," *Elsevier ISA transactions*, vol. 51, no. 1, pp. 120–131, Jan. 2012.

[49] K. Chavan, R. G. Kumar, M. N. Belur, and A. Karandikar, "Robust active queue management for wireless networks," *IEEE Trans. Control Syst. Technol.*, vol. 19, no. 6, pp. 1630–1638, 2011.

[50] K. Nichols and V. Jacobson, "Controlling queue delay," *ACM Commun.*, vol. 55, no. 7, pp. 42–50, May 2012.

[51] Y. Wang, S. Mao, and R. Nelms, "Distributed online algorithm for optimal real-time energy distribution in the smart grid," *IEEE Internet of Things Journal*, vol. 1, no. 1, pp. 70–80, Feb. 2014.

[52] D. Hu and S. Mao, "On medium grain scalable video streaming over femtocell cognitive radio networks," *IEEE Journal on Selected Areas in Communications*, vol. 30, no. 3, pp. 641–651, Apr. 2012.

[53] S. Mao, S. S. Panwar, and Y. T. Hou, "On optimal traffic partitioning for multipath transport," in *Proc. IEEE INFOCOM 2005*, Miami, FL, Mar. 2005, pp. 2325–2336.

[54] M. Chen, J. Yang, Y. Hao, S. Mao, and K. Hwang, "A 5G cognitive system for healthcare," *MDPI Big Data and Cognitive Computing Journal*, vol. 1, no. 1, pp. 2–16, Mar. 2017.

[55] Y. Sun, M. Peng, Y. Zhou, Y. Huang, and S. Mao, "Application of machine learning in wireless networks: Key techniques and open issues," *arXiv preprint, arXiv:1809.08707*, 2018, accessed on: Dec. 2018.

[56] M. Feng and S. Mao, "Dealing with limited backhaul capacity in millimeter wave systems: A deep reinforcement learning approach," *IEEE Commun.*, to appear.

[57] X. Chen, H. Zhang, C. Wu, S. Mao, Y. Ji, and M. Bennis, "Optimized computation offloading performance in virtual edge computing systems via deep reinforcement learning," *IEEE Internet of Things J.*, to appear.

[58] Y. Sun, M. Peng, and S. Mao, "Deep reinforcement learning based mode selection and resource management for green fog radio access networks," *IEEE Internet of Things J.*, to appear.

[59] Z. Chang, L. Lei, Z. Zhou, S. Mao, and T. Ristaniemi, "Learn to cache: Machine learning for network edge caching in the big data era," *IEEE Wireless Commun.*, vol. 25, no. 3, pp. 28–35, June 2018.

[60] M. Alizadeh, A. Greenberg, D. A. Maltz, J. Padhye, P. Patel, B. Prabhakar, S. Sengupta, and M. Sridharan, "Data center tcp (dctcp)," in *ACM SIGCOMM computer communication review*, vol. 40, no. 4. ACM, 2010, pp. 63–74.

[61] M. Dong, Q. Li, D. Zarchy, P. B. Godfrey, and M. Schapira, "Pcc: Re-architecting congestion control for consistent high performance." in *NSDI*, vol. 1, no. 2.3, 2015, p. 2.

[62] W. Jiang, F. Ren, R. Shu, Y. Wu, and C. Lin, "Sliding mode congestion control for data center ethernet networks," *Computers, IEEE Transactions on*, vol. 64, no. 9, pp. 2675–2690, 2015.

[63] K. Xiao, S. Mao, and J. Tugnait, "Congestion control for infrastructure-based CRNs: A multiple model predictive control approach," in *Proc. IEEE GLOBECOM 2016*, Washington DC, Dec. 2016.

[64] ——, “MAQ: A multiple model predictive congestion control scheme for cognitive radio networks,” *IEEE Trans. Wireless Commun.*, vol. 16, no. 4, pp. 2614–2626, Apr. 2017.

[65] K. Winstein and H. Balakrishnan, “Tcp ex machina: computer-generated congestion control,” *ACM SIGCOMM Computer Communication Review*, vol. 43, no. 4, pp. 123–134, 2013.

[66] A. Sivaraman, K. Winstein, P. Thaker, and H. Balakrishnan, “An experimental study of the learnability of congestion control,” in *ACM SIGCOMM Computer Communication Review*, vol. 44, no. 4. ACM, 2014, pp. 479–490.

[67] Z. Xu, J. Tang, J. Meng, W. Zhang, Y. Wang, C. H. Liu, and D. Yang, “Experience-driven networking: A deep reinforcement learning based approach,” *arXiv preprint arXiv:1801.05757*, 2018.

[68] W. Li, F. Zhou, K. R. Chowdhury, and W. M. Meleis, “QTCP: Adaptive congestion control with reinforcement learning,” *IEEE Trans. Netw. Sci. Eng.*, in press.

[69] K. Jacobsson, L. L. Andrew, A. Tang, K. H. Johansson, H. Hjalmarsson, and S. H. Low, “Ack-clocking dynamics: modelling the interaction between windows and the network,” in *INFOCOM 2008. The 27th Conference on Computer Communications. IEEE.* IEEE, 2008.

[70] C. Jin, D. X. Wei, and S. H. Low, “Fast tcp: motivation, architecture, algorithms, performance,” in *INFOCOM 2004. Twenty-third AnnualJoint Conference of the IEEE Computer and Communications Societies*, vol. 4. IEEE, 2004, pp. 2490–2501.

[71] D. X. Wei, C. Jin, S. H. Low, and S. Hegde, “Fast tcp: motivation, architecture, algorithms, performance,” *IEEE/ACM transactions on Networking*, vol. 14, no. 6, pp. 1246–1259, 2006.

[72] J. N. Foerster, Y. M. Assael, N. de Freitas, and S. Whiteson, “Learning to communicate to solve riddles with deep distributed recurrent Q-networks,” *arXiv preprint, arXiv:1602.02672*, 2016, accessed on: Dec. 2018.

[73] J. Foerster *et al.*, “Stabilising experience replay for deep multi-agent reinforcement learning,” *arXiv preprint, arXiv:1702.08887*, 2017, accessed on: Dec. 2018.

[74] S. Omidshafiei, J. Pazis, C. Amato, J. P. How, and J. Vian, “Deep decentralized multi-task multi-agent reinforcement learning under partial observability,” *arXiv preprint, arXiv:1703.06182*, 2017, accessed on: Dec. 2018.

[75] M. Hausknecht and P. Stone, “Deep recurrent Q-learning for partially observable MDPs,” *CoRR, abs/1507.06527*, vol. 7, no. 1, 2015.

[76] M. Abadi *et al.*, “Tensorflow: A system for large-scale machine learning,” in *Proc. USENIX OSDI’16*, Savannah, GA, Nov. 2016, pp. 265–283.

[77] C. Caini and R. Firrincieli, “TCP Hybla: A TCP enhancement for heterogeneous networks,” *Int. J. Satellite Commun. Netw.*, vol. 22, no. 5, pp. 547–566, Sept. 2004.

[78] S. Liu, T. Başar, and R. Srikant, “TCP-Illinois: A loss-and delay-based congestion control algorithm for high-speed networks,” *Elsevier Performance Evaluation*, vol. 65, no. 6-7, pp. 417–440, June 2008.

[79] G. F. Riley and T. R. Henderson, “The ns-3 network simulator,” in *Modeling and tools for network simulation.* Springer, 2010, pp. 15–34.

[80] Z. Mao and X. Wang, “Efficient optimal and suboptimal radio resource allocation in OFDMA system,” *IEEE Trans. Wireless Commun.*, vol. 7, no. 2, pp. 440–445, Feb. 2008.

[81] X. Wang and G. B. Giannakis, “Resource allocation for wireless multiuser OFDM networks,” *IEEE Trans. Infor. Theory*, vol. 57, no. 7, pp. 4359–4372, July 2011.

[82] M. X. Gong, S. Midkiff, and S. Mao, “Design principles for distributed channel assignment in wireless ad hoc networks,” in *Communications, 2005. ICC 2005. 2005 IEEE International Conference on*, vol. 5. IEEE, 2005, pp. 3401–3406.

[83] Z. Ren, S. Chen, B. Hu, and W. Ma, “Energy-efficient resource allocation in downlink OFDM wireless systems with proportional rate constraints,” *IEEE Trans. Veh. Technol.*, vol. 63, no. 5, pp. 2139–2150, Mar. 2014.

[84] Y. Wang, S. Mao, and R. M. Nelms, “Distributed online algorithm for optimal real-time energy distribution in the smart grid,” *IEEE Internet of Things Journal*, vol. 1, no. 1, pp. 70–80, 2014.

[85] M. Chen, V. C. M. Leung, S. Mao, and M. Li, “Energy-efficient itinerary planning for mobile agents in wireless sensor networks,” in *Proc. IEEE ICC 2009*, Dresden, Germany, June 2009, pp. 1–5.

[86] Y. Xu and S. Mao, “User association in massive MIMO HetNets,” *IEEE Systems Journal*, vol. 11, no. 1, pp. 7–19, Mar. 2017.

[87] M. X. Gong, S. F. Midkiff, and S. Mao, “On-demand routing and channel assignment in multi-channel mobile ad hoc networks,” *Elsevier Ad Hoc Networks Journal*, vol. 7, no. 1, pp. 63–78, Jan. 2009.

[88] M. Feng, S. Mao, and T. Jiang, “Joint duplex mode selection, channel allocation, and power control for full-duplex cognitive femtocell networks,” *Digital Communications and Networks*, vol. 1, no. 1, pp. 30–44, 2015.

[89] M. Feng, T. Jiang, D. Chen, and S. Mao, “Cooperative small cell networks: High capacity for hotspots with interference mitigation,” *IEEE Wireless Communications*, vol. 21, no. 6, pp. 108–116, 2014.

[90] S. Mao and S. S. Panwar, “A survey of envelope processes and their applications in quality of service provisioning,” *IEEE Communications Surveys & Tutorials*, vol. 8, no. 3, pp. 2–20, 2006.

[91] M. Feng, S. Mao, and T. Jiang, “Dynamic base station sleep control and RF chain activation for energy efficient millimeter wave cellular systems,” *IEEE Transactions on Vehicular Technology*, vol. 67, no. 10, pp. 9911–9921, Oct. 2018.

[92] ——, "Joint frame design, resource allocation and user association for massive mimo heterogeneous networks with wireless backhaul," *IEEE Transactions on Wireless Communications*, vol. 17, no. 3, pp. 1937–1950, Mar. 2018.

[93] M. Feng and S. Mao, "Interference management and user association for nested array-based massive mimo hetnets," *IEEE Transactions on Vehicular Technology*, vol. 67, no. 1, pp. 454–466, Jan. 2018.

[94] S. Mao, S. S. Panwar, and Y. T. Hou, "On minimizing end-to-end delay with optimal traffic partitioning," *IEEE Transactions on Vehicular Technology*, vol. 55, no. 2, pp. 681–690, Mar. 2006.

[95] M. Chen, V. C. Leung, S. Mao, and T. Kwon, "Receiver-oriented load-balancing and reliable routing in wireless sensor networks," *Wireless Communications and Mobile Computing*, vol. 9, no. 3, pp. 405–416, 2009.

[96] DASH Industry Forum, "The dash.js project," [online] Available: https://github.com/Dash-Industry-Forum/dash.js/wiki.

[97] A. Balachandran, V. Sekar, A. Akella, S. Seshan, I. Stoica, and H. Zhang, "Developing a predictive model of quality of experience for internet video," in *Proc. ACM SIGCOMM'13*, Hong Kong, China, Aug. 2013, pp. 339–350.

[98] A. Khan, L. Sun, and E. Ifeachor, "Content clustering based video quality prediction model for mpeg4 video streaming over wireless networks," in *Proc. IEEE ICC'09*, Dresden, Germany, June 2009, pp. 1–5.

[99] J. You, U. Reiter, M. M. Hannuksela, M. Gabbouj, and A. Perkis, "Perceptual-based quality assessment for audio–visual services: A survey," *Sig. Process.: Image Commun.*, vol. 25, no. 7, pp. 482–501, 2010.

[100] F. Dobrian, V. Sekar, A. Awan, I. Stoica, D. Joseph, A. Ganjam, J. Zhan, and H. Zhang, "Understanding the impact of video quality on user engagement," in *ACM SIGCOMM Comput. Commun. Rev.*, vol. 41, no. 4. ACM, 2011, pp. 362–373.

[101] X. Yin, A. Jindal, V. Sekar, and B. Sinopoli, "A control-theoretic approach for dynamic adaptive video streaming over HTTP," in *Proc. ACM SIGCOMM'15*, London, UK, Aug. 2015, pp. 325–338.

[102] C. Chen, X. Zhu, G. de Veciana, A. C. Bovik, and R. W. Heath, "Rate adaptation and admission control for video transmission with subjective quality constraints," *IEEE J. Sel. Topics Sig. Process.*, vol. 9, no. 1, pp. 22–36, Feb. 2015.

[103] C. Chen, L. K. Choi, G. de Veciana, C. Caramanis, R. W. Heath, and A. C. Bovik, "A dynamic system model of time-varying subjective quality of video streams over HTTP," in *Proc. IEEE ICASSP'13*, Vancouver, Canada, May 2013, pp. 3602–3606.

[104] F. Shams, G. Bacci, and M. Luise, "A survey on resource allocation techniques in OFDMA networks," *Elsevier Comput. Netw.*, vol. 65, no. 2, pp. 129–150, June 2014.

[105] D. P. Palomar and M. Chiang, "A tutorial on decomposition methods for network utility maximization," *IEEE J. Sel. Areas Commun.*, vol. 24, no. 8, pp. 1439–1451, Aug. 2006.

[106] K. Xiao, S. Mao, and J. Tugnait, "QoE-driven resource allocation for DASH over OFDMA networks," in *Proc. IEEE GLOBECOM'16*, Washington, DC, USA, Dec. 2016, pp. 1–6.

[107] S. Lederer, C. Müller, and C. Timmerer, "Dynamic adaptive streaming over HTTP dataset," in *Proc. ACM Multimedia'12*, Nara, Japan, Oct./Nov. 2012, pp. 89–94.

[108] H. J. Kushner and P. A. Whiting, "Convergence of proportional-fair sharing algorithms under general conditions," *IEEE Trans. Wireless Commun.*, vol. 3, no. 4, pp. 1250–1259, July 2004.

[109] K. Yamagishi and T. Hayashi, "Parametric quality-estimation model for adaptive-bitrate streaming services," *IEEE Trans. Multimedia*, vol. 19, no. 7, pp. 1545–1557, July 2017.

[110] M. Feng, Z. He, and S. Mao, "Qoe driven video streaming over cognitive radio networks for multi-user with single channel access," *IEEE ComSoc MMTC Communications-Frontiers*, vol. 12, no. 2, pp. 7–11, Mar. 2017.

[111] M. Feng, S. Mao, and T. Jiang, “Enhancing the performance of future wireless networks with software defined networking,” *Springer Frontiers of Information Technology and Electronic Engineering Journal*, vol. 17, no. 7, pp. 606–619, July 2016.

[112] J. Jiang, V. Sekar, and H. Zhang, “Improving fairness, efficiency, and stability in HTTP-based adaptive video streaming with festive,” *IEEE/ACM Trans. Netw.*, vol. 22, no. 1, pp. 326–340, Jan. 2014.

[113] Z. Li, X. Zhu, J. Gahm, R. Pan, H. Hu, A. C. Begen, and D. Oran, “Probe and adapt: Rate adaptation for HTTP video streaming at scale,” *IEEE J. Sel. Areas Commun.*, vol. 32, no. 4, pp. 719–733, Apr. 2014.

[114] T.-Y. Huang, R. Johari, N. McKeown, M. Trunnell, and M. Watson, “A buffer-based approach to rate adaptation: Evidence from a large video streaming service,” in *Proc. ACM SIGCOMM’14*, Chicago, IL, Aug. 2014, pp. 187–198.

[115] G. Tian and Y. Liu, “Towards agile and smooth video adaptation in dynamic HTTP streaming,” in *Proc. CoNEXT’12*, Nice, France, Dec. 2012, pp. 109–120.

[116] C. Zhou, C.-W. Lin, and Z. Guo, “mDASH: A Markov decision-based rate adaptation approach for dynamic HTTP streaming,” *IEEE Trans. Multimedia*, vol. 18, no. 4, pp. 738–751, Apr. 2016.

[117] A. Bokani, M. Hassan, S. Kanhere, and X. Zhu, “Optimizing http-based adaptive streaming in vehicular environment using markov decision process,” *IEEE Trans. Multimedia*, vol. 17, no. 12, pp. 2297–2309, Dec. 2015.

[118] Microsoft, “Smooth streaming protocol,” [online] Available: https://msdn.microsoft.com/en-us/library/ff469518.aspx, Sept. 2017.

[119] S. Akhshabi, A. C. Begen, and C. Dovrolis, “An experimental evaluation of rate-adaptation algorithms in adaptive streaming over HTTP,” in *Proc. ACM MMSys’11*, San Jose, CA, Feb. 2011, pp. 157–168.

[120] D. Hu and S. Mao, “Streaming scalable videos over multi-hop cognitive radio networks,” *IEEE Transactions on Wireless Communications*, vol. 9, no. 11, pp. 3501–3511, Nov. 2010.

[121] Y. Huang, S. Mao, and S. F. Midkiff, “A control-theoretic approach to rate control for streaming videos,” *IEEE Transactions on Multimedia*, vol. 11, no. 6, pp. 1072–1081, Oct. 2009.

[122] M. Gong, S. F. Midkiff, and S. Mao, “Design principles for distributed channel assignment in wireless ad hoc networks,” in *Proc. IEEE ICC 2005*, Seoul, Korea, May 2005, pp. 3401–3406.

[123] I. K. Son and S. Mao, “Design and optimization of a tiered wireless access network,” in *Proc. IEEE INFOCOM 2010*, San Diego, CA, Mar. 2010, pp. 1–9.

[124] D. Bethanabhotla, G. Caire, and M. J. Neely, “Adaptive video streaming in MU-MIMO networks,” arXiv:1401.6476, [online] Available: https://arxiv.org/abs/1401.6476, Jan. 2014.

[125] ——, “Adaptive video streaming for wireless networks with multiple users and helpers,” *IEEE Trans. Commun.*, vol. 63, no. 1, pp. 268–285, Jan. 2015.

[126] V. Joseph and G. de Veciana, “NOVA: QoE-driven optimization of DASH-based video delivery in networks,” in *Proc. IEEE INFOCOM’14*, Toronto, Canada, Apr./May 2014, pp. 82–90.

[127] K. Lin and S. Dumitrescu, “Cross-layer resource allocation for scalable video over OFDMA wireless networks: Trade-off between quality fairness and efficiency,” *IEEE Trans. Multimedia*, vol. 19, no. 7, pp. 1654–1669, July 2017.

[128] Y. Go, O. C. Kwon, and H. Song, “An energy-efficient http adaptive video streaming with networking cost constraint over heterogeneous wireless networks,” *IEEE Trans. Multimedia*, vol. 17, no. 9, pp. 1646–1657, Sept. 2015.

[129] S. Almowuena, M. M. Rahman, C.-H. Hsu, A. A. Hassan, and M. Hefeeda, "Energy-aware and bandwidth-efficient hybrid video streaming over mobile networks," *IEEE Trans. Multimedia*, vol. 18, no. 1, pp. 102–115, Jan. 2016.

[130] J. Huang, V. G. Subramanian, R. Agrawal, and R. A. Berry, "Downlink scheduling and resource allocation for OFDM systems," *IEEE Trans. Wireless Commun.*, vol. 8, no. 1, pp. 288–296, Jan. 2009.

[131] S. Mao, Y. Wang, S. Lin, and S. S. Panwar, "Video transport over ad-hoc networks with path diversity," *ACM Mobile Computing and Communications Review*, vol. 7, no. 1, pp. 59–61, Jan. 2003.

[132] J. Harold, G. Kushner, and G. Yin, *Stochastic approximation and recursive algorithm and applications*, 2nd ed. New York, NY: Springer-Verlag, 2003.

[133] S. Boyd and L. Vandenberghe, *Convex Optimization*. Cambridge, UK: Cambridge University Press, 2004.